

## PROPOSITIONS

accompanying the thesis

Nonlinear Transformation of Wave Spectra in the Nearshore Zone

by

Yasser Eldeberky

Delft, 29 October 1996

1. For reasons of computational efficiency, phase-averaged energy based models are preferred over phase-resolving models in computations of random waves in extensive areas.
2. The influence of depth-induced breaking on the evolution of the wave spectrum can be modeled (in case of single-peaked spectra) by spectrally distributing the total local rate of energy dissipation in proportion to the spectral levels.
3. The nonlinearly generated low-frequency waves due to incident random waves are significantly damped in the surf zone. This effect is associated with depth-induced breaking of the short waves.
4. The biphasic evolution in shallow-water waves can be parametrized in terms of local parameters such as the Ursell number.
5. For computational efficiency in practical applications, the average effect of triad wave interactions on the wave spectrum can be modeled using a lumped presentation of the interaction integral, in which the values of the integrand are scaled with those of the self-interactions, supplemented with an empirical parametrization of the biphasic evolution.
6. The statistical description of nonlinear random waves is a subject about which numerous misunderstandings can remain even after repeated explanations.
7. In extreme events in the southern North Sea, the wave heights are mainly depth controlled and the significant wave height is of order 0.4 times the water depth.
8. International exchange of researchers is beneficial to science and thus it should be encouraged.
9. Heuristic approaches can be beneficial to practical applications as much as the fundamental approaches.
10. For great discoveries, intuition is as important as intelligence.

## STELLINGEN

behorende bij het proefschrift

### Nonlinear Transformation of Wave Spectra in the Nearshore Zone

door

Yasser Eldeberky

Delft, 29 oktober 1996

1. Voor berekeningen van onregelmatige golfvelden in uitgestrekte gebieden wordt uit overwegingen van rekefficiëntie de voorkeur gegeven aan fase-gemiddelde modellen boven deterministische modellen.
2. In gevallen van enkeltoppige spectra kan de invloed van diepte-geïnduceerde breking op de ontwikkeling van het spectrum gemodelleerd worden door het totale gedissipeerde vermogen spectraal te verdelen in verhouding tot de spectrale niveaus.
3. De niet-lineair opgewekte lange golven in een invallend veld van onregelmatige korte golven worden significant gedempt in de brandingszone. Dit effect is geassocieerd met de diepte-geïnduceerde breking van de korte golven.
4. De ontwikkeling van de bifasen in ondiep-water golven kan worden geparаметeriseerd in termen van lokale parameters zoals het getal van Ursell.
5. Ten behoeve van rekefficiëntie kan het gemiddelde effect van drie-golfwisselwerkingen op het golfspectrum voor praktische toepassingen gemodelleerd worden door de waarden van alle interacties te schalen met die van de zelf-interacties, en door gebruik te maken van een empirische parameterisatie van de bifasen.
6. De statistische beschrijving van niet-lineaire onregelmatige golven is een onderwerp waarover zelfs na herhaalde uitleg tal van misverstanden kunnen blijven bestaan.
7. Tijdens extreme omstandigheden zijn de golfhoogten in de zuidelijke Noordzee overwegend bepaald door de diepte en is de significante golfhoogte in de orde van 0,4 keer de lokale waterdiepte.
8. Internationale uitwisseling van onderzoekers is goed voor de wetenschap en moet daarom worden gestimuleerd.
9. Heuristische benaderingen kunnen voor praktische toepassingen even waardevol zijn als fundamentele.
10. Voor grote ontdekkingen is intuïtie even belangrijk als intelligentie.

**TR diss  
2825**

670101  
3191094  
TR diss 2825



# Nonlinear Transformation of Wave Spectra in the Nearshore Zone

PROEFSCHRIFT

ter verkrijging van de graad van doctor  
aan de Technische Universiteit Delft,  
op gezag van de Rector Magnificus Prof. ir. K.F. Wakker,  
in het openbaar te verdedigen ten overstaan van een commissie,  
door het College van Dekanen aangewezen,  
op dinsdag 29 oktober 1996 te 16.00 uur

door

Yasser ELDEBERKY  
master of science in hydraulic engineering, IHE Delft  
geboren te Elgiza-Cairo, Egypte

Dit proefschrift is goedgekeurd door de promotor:

Prof.dr.ir. J.A. Battjes

Samenstelling promotiecommissie:

Rector Magnificus

Prof.dr.ir. J.A. Battjes,

Prof.dr.ir. J.A. Pinkster,

Prof.dr.ir. G.S. Stelling,

Prof.dr. M. Stiassnie,

Prof.dr.ir. M.J.F. Stive,

Dr.ir. N. Booij,

Dr. P.A. Madsen,

voorzitter

Technische Universiteit Delft, promotor.

Technische Universiteit Delft.

Technische Universiteit Delft.

Technion Institute of Technology (Israël).

Technische Universiteit Delft.

Technische Universiteit Delft.

Danish Hydraulic Institute (Denemarken).

CIP-GEGEVENS KONINKLIJKE BIBLIOTHEEK, DEN HAAG

Eldeberky, Yasser

Nonlinear Transformation of Wave Spectra in the Nearshore Zone/

Yasser Eldeberky

Thesis Delft University of Technology. Also published in the series 'Communications on Hydraulic and Geotechnical Engineering' (ISSN 0169-6548), Report No 96-4 - With ref.

- With summary in Dutch.

ISBN 90-9009757-0

NUGI 816

Subject headings: Nonlinear transformation / Wave Spectra / Nearshore Zone.

Copyright © 1996 by Y. Eldeberky

All right reserved.

No part of the material protected by this copyright notice may be reproduced or utilised in any form or by any means, electronic or mechanical, including photocopying, recording or by any information storage and retrieval system, without permission of the copyright owner.

*To my wife Sahar  
and  
my sons Karim and Basel*



## Acknowledgements

The research presented in this thesis was funded jointly by the National Institute for Coastal and Marine Management (RIKZ) and the Road and Hydraulic Engineering Division (DWW) of the Dutch Department of Public Works (Rijkswaterstaat). The work has been carried out at the Delft University of Technology while the author was in a study leave from Helwan University, Cairo, Egypt.

I want to express my gratitude to my supervisor Prof. Jurjen A. Battjes for introducing me to this field of research in a very stimulating way while I was a graduate student at Delft in 1990. His guidance and insight are highly appreciated.

In the course of my four years as a Research Fellow at the Delft University of Technology I have been fortunate to interact with a large number of people, from The Netherlands and abroad, who have in part influenced the work presented in this thesis. To mention one name usually means to forget a few of others. Thus I wish to thank all colleagues and friends who have positively contributed to this work.

Special thanks to my dear wife Sahar for her consistent love and support during the long process of my postgraduate research. I am very grateful for having Sahar and my sons Karim and Basel to share my life with. The encouragement that my parents and my parents in law always gave me is especially appreciated.

*Yasser Eldeberky*

*October 29, 1996 Delft, The Netherlands*





## Abstract

Growing demands to both utilize and preserve our coastal zones cause a need for better understanding of the underlying coastal dynamics as well as the capabilities to model these processes. This study deals with the nonlinear transformation of wave spectra in the shallow nearshore regions, in particular those due to nonlinear triad wave interactions and wave breaking. The study aims at increasing the knowledge and the physical insight in the mechanism of these processes, and incorporating this knowledge in numerical shallow-water wave models.

Bispectral analysis of shallow-water waves is performed to investigate aspects of nonlinear dynamics. Among these is the mechanism of phase couplings as waves evolve over a shoaling region. The evolution of the biphase has previously been found to be consistent with visual observation that waves evolve from a slightly peaked, nearly sinusoidal shape in deep water (with biphase equal to zero) to a shape characterized by a steep front face and a gently sloping rear face (with biphase equal to  $-\pi/2$ ). This biphase evolution is also found in present study, based on analyses of detailed data sets; its variation has been parametrized in terms of the Ursell number for use in approximate computational models.

The bispectral analysis is also used to examine the spatial variation in intensity of nonlinear coupling in a random wavefield propagating over and beyond a shallow bar. The observed spatial variations of nonlinearity parameters (such as bicoherence, skewness and asymmetry) indicate strong phase couplings between the primary and its harmonics over the bar owing to nonlinear triad interactions. In the deepening region beyond the bar, the bound harmonics are released and the wavefield is found to be spatially homogeneous without memory of phase locks which existed over the bar. This implies that the

wavefield there can again be fully described by the energy density spectrum without specific additional phase information.

Deterministic complex-amplitude evolution equations based on Boussinesq equations with improved dispersion characteristics are used to simulate harmonic generation in shallow water. An existing model has been extended into the surf zone by incorporating the effect of energy dissipation due to wave breaking. The spectral breaking function distributes the total rate of random-wave energy dissipation in proportion to the local spectral level, based on previous experimental results. The model is used to predict the surface elevations from given complex Fourier amplitudes obtained from measured time records in laboratory experiments at the upwave boundary. The model is also used, together with the assumption of random, independent initial phases, to calculate the evolution of the energy spectrum of random waves. The results are in good agreement with observed surface elevations as well as spectra.

For random-wave predictions in the nearshore, phase-averaged energy based models are preferred. A statistical model for the average effect of triad wave interactions is presented and investigated. The model is based on the Zakharov kinetic equation for resonant three-wave interactions. A narrow frequency filter is introduced to allow for the off-resonant energetic triad interactions. The model is applicable for dispersive waves without restriction to resonant colinear interactions. Numerical simulation of the spectral evolution in shallow-water waves has shown the ability of the model to transfer energy to higher harmonics with intensities dependent on the filter bandwidth. Verification with observations has shown promising results, but the model needs improvement especially the specification of the filter bandwidth. Suggestions for further development and improvement of this approach are given.

Along the line of statistical modeling of triad wave interactions, a parametrized energy formulation is developed in order to minimize the computational efforts. The model is based on the Boussinesq evolution equations, supplemented with an empirical parametrization of the biphase evolution and a lumped presentation of the interaction integral, in which the values of the integrand are scaled with

---

those of the self-interactions. This lumped triad approximation (LTA) model is implemented in a one-dimensional energy balance equation to compute the evolution of the energy spectrum in shallow water. Comparisons with observations have shown good agreement. The computational efficiency and the fair performance of the LTA model favour its use in application for wind-generated waves in coastal regions.

x

## Samenvatting

De toenemende druk op kustzones brengt de behoefte met zich mee aan een beter begrip van hydrodynamische en morfologische kustprocessen en aan het vermogen die te modelleren. Dit onderzoek heeft betrekking op niet-lineaire transformaties van golfspectra in ondiepe kustwateren, in het bijzonder als gevolg van drie-golfwisselwerkingen en de invloed van golfbreking. Het doel van het onderzoek is het verhogen van het inzicht in en de kennis van deze processen, en de ontwikkeling van numerieke modellen voor de berekening ervan.

Bispectrale analyse is uitgevoerd om een aantal niet-lineaire aspecten van de dynamica van ondiep-water golven te onderzoeken, met name met betrekking tot de fasekoppelingen tussen spectrale componenten in een golfveld in afnemende diepte. De ontwikkeling van de bifase was al eerder onderzocht, en kwalitatief in overeenstemming gevonden met de visueel waar te nemen vervorming van het golfprofiel van een licht gepiekte, min of meer sinusvormig profiel in diep water (bifase gelijk aan nul) tot vrijwel een zaagtand profiel met steil voorfront (bifase gelijk aan  $-\pi/2$ ). Deze trend is in het onderhavig onderzoek ook gevonden in een analyse van een verzameling gedetailleerde gegevens, en is geparameteriseerd als functie van een lokaal getal van Ursell voor gebruik in een benaderend rekenmodel.

Bispectrale analyse is eveneens gebruikt voor een onderzoek van de ruimtelijke variaties van de intensiteit van de niet-lineaire koppelingen in een onregelmatig golfveld dat zich voortplant over en voorbij een lokale ondiepte. De waargenomen variaties van niet-lineariteitsparameters zoals bicoherentie, scheefheid en asymmetrie duiden op sterke koppelingen boven de ondiepte tussen de primaire componenten en hun harmonischen, als gevolg van drie-

golfwisselwerkingen. In het diepere gedeelte voorbij de ondiepte worden de aanvankelijk gebonden harmonischen ontkoppeld; het resulterend golfveld wordt ruimtelijk homogeen, zonder "geheugen" voor de specifieke fasekoppelingen die boven de ondiepte hebben bestaan. Het golfveld in dat gebied kan, evenals ervoor, worden beschreven met uitsluitend het energiespectrum, op basis van het conventioneel random-fase model.

Een deterministisch spectraal model voor complexe amplituden, gebaseerd op Boussinesq vergelijkingen met verbeterde dispersie, is gebruikt om opwekking van hogere harmonischen in ondiep water te simuleren. Een bestaand model is uitgebreid met een formulering voor het effect van energiedissipatie door golfbreking. De totale dissipatie is spectraal verdeeld naar evenredigheid met de lokale spectrale dichtheid. Met dit uitgebreide model zijn oppervlakte uitwijkingen in een aantal punten gesimuleerd, uitgaande van gemeten waarden aan de bovenwindse zijde. Ook zijn op basis van de berekende complexe amplituden schattingen gemaakt van de ruimtelijke variatie van de energiespectra. De simulaties zijn in goede overeenstemming met de metingen, zowel voor de energiespectra als voor de oppervlakte-uitwijkingen.

Voor berekening van onregelmatige golven in uitgestrekte gebieden zijn deterministische modellen te rekenintensief en verdienen statistische modellen de voorkeur. Voor dat doel is een formulering gegeven van de gemiddelde spectrale energie-overdracht als gevolg van niet-resonante drie-golfwisselwerkingen, gebaseerd op een soortgelijk model voor resonante wisselwerkingen van Zakharov. Hiertoe is een frekwentie-filter van kleine maar eindige breedte gebruikt. Het model geldt nominaal voor ééndimensionale niet-dispersieve golven. Numerieke simulaties van de ontwikkeling van energiespectra in ondiep water hebben aangetoond dat dit model weliswaar kwalitatief de juiste trends voorspelt, met name overdracht van energie van de spectrale piek naar de hogere harmonischen, maar de geschikte bepaling van de te gebruiken filterbandbreedte moet nader worden onderzocht. Hiervoor wordt een concrete suggestie gegeven.

---

Ten einde de vereiste rekencapaciteit nog meer terug te brengen is een geparameteriseerde formulering ontwikkeld voor de gemiddelde energie-overdracht als gevolg van drie-golf-wisselwerkingen. Deze is gebaseerd op de deterministische Boussinesq-vergelijkingen voor complexe amplituden en is uit praktische overwegingen in geparameteriseerde vorm uitgedrukt, waarbij de drie-golfwisselwerkingen evenredig zijn gesteld aan de zelf-zelf wisselwerkingen en waarbij tevens gebruik is gemaakt van de eerder gegeven Ursell-afhankelijke parameterisatie van de bifasen. Dit "Lumped Triad Approximation" (LTA) model is in een één-dimensionaal numeriek model voor de golfenergiebalans ingebouwd. De rekenuitkomsten van dit model zijn in redelijk goede overeenkomst met meetwaarden. De geringe rekenintensiteit en de redelijke prestaties van het model zijn een indicatie van het potentieel van het model voor toepassingen in kustgebieden.





## Contents

Acknowledgements .....	v
Abstract .....	vii
Samenvatting (Abstract in Dutch) .....	xi
Contents .....	xv
 1. Introduction .....	 1
1.1 General .....	1
1.2 Literature review .....	2
1.3 Study objectives .....	12
1.4 Outline .....	13
 2. Phenomenological description of harmonic generation .....	 15
2.1 Linear and nonlinear transformations .....	15
2.2 Nonlinear triad wave interactions .....	17
2.3 Qualitative features of nonlinear wave transformation in the nearshore .....	 19
2.4 The role of wave breaking .....	24
 3. Bispectral analysis of shallow-water waves .....	 27
3.1 Introduction .....	27
3.2 The bispectrum .....	27
3.3 Skewness and asymmetry .....	31
3.4 Bispectral evolution of shoaling waves .....	33
3.5 Nonlinear coupling in waves passing over a bar .....	42
3.5.1 Introduction .....	42
3.5.2 Analysis of experimental data .....	43
3.5.3 Analysis of numerical-model results .....	52

---

3.6	The evolution of the biphasic . . . . .	57
3.7	Summary and conclusions . . . . .	60
4.	Deterministic modeling of wave evolution in shallow water . . . . .	65
4.1	Introduction . . . . .	65
4.2	Eulerian equations of motion . . . . .	65
4.3	Time-domain Boussinesq equations . . . . .	67
4.3.1	Introduction . . . . .	67
4.3.2	Boussinesq-type equations . . . . .	68
4.4	Spectral Boussinesq equations . . . . .	71
4.4.1	Evolution equations . . . . .	71
4.4.2	Nonlinear correction to the linear phase speed . . . . .	76
4.5	Spectral Boussinesq modeling of random breaking wave . . . . .	77
4.5.1	Wave energy dissipation due to breaking . . . . .	78
4.5.2	Evolution equation for random breaking waves . . . . .	82
4.6	Model to data comparison . . . . .	83
4.6.1	Model implementation . . . . .	83
4.6.2	Verification of the evolution equation for nonbreaking waves . . . . .	84
4.6.3	Verification of the evolution equation for breaking waves . . . . .	90
4.7	Summary and conclusions . . . . .	103
5.	Random-wave modeling of wave evolution in shallow water . . . . .	107
5.1	Introduction . . . . .	107
5.2	Hamiltonian equations of motion . . . . .	108
5.3	The evolution equations . . . . .	112
5.4	Statistical description of random waves . . . . .	113
5.5	The hierarchy of moment equations . . . . .	115
5.6	Kinetic wave equation . . . . .	118
5.7	Summary and conclusions . . . . .	122

---

6.	Energy formulation for triad wave interactions . . . . .	125
6.1	Introduction . . . . .	125
6.2	Kinetic equation for off-resonant triad interactions . . . . .	125
6.2.1	Formulation for the energy spectrum of the canonical variable . . . . .	125
6.2.2	Formulation for the energy spectrum of the sea surface elevation . . . . .	128
6.2.3	Nondimensional representation . . . . .	130
6.3	Numerical investigation of energy transfer rate . . . . .	132
6.3.1	Aim of investigation . . . . .	132
6.3.2	Discretization of the interaction integral . . . . .	133
6.3.3	Numerical grid . . . . .	134
6.3.4	Results of calculations and analysis . . . . .	135
6.4	Spectral evolution . . . . .	145
6.4.1	Model formulation and implementation . . . . .	145
6.4.2	Simulation of spectral evolution . . . . .	149
6.4.3	Remedy to the nonconservative approximation . . . . .	153
6.4.4	Sensitivity to the filter bandwidth . . . . .	156
6.5	Discussion . . . . .	159
6.6	Summary and conclusions . . . . .	160
7.	Parametrized energy formulation for triad interactions . . . . .	163
7.1	Introduction . . . . .	163
7.2	Evolution equations for the complex amplitudes . . . . .	163
7.3	Evolution equation for the spectral energy . . . . .	166
7.4	Evolution equation for the bispectrum . . . . .	168
7.5	Model to data comparisons . . . . .	172
7.5.1	Evolution model . . . . .	172
7.5.2	Numerical simulations and comparisons . . . . .	173
7.6	Summary and conclusions . . . . .	179

8.	Conclusions and recommendations . . . . .	181
8.1	General . . . . .	181
8.2	Bispectral analysis . . . . .	182
8.3	Deterministic modeling of nonlinear shallow-water waves .	183
8.4	Statistical modeling of nonlinear shallow-water waves . . . .	184
8.5	Recommendations for future research . . . . .	186
	References . . . . .	189
	Curriculum Vitae . . . . .	201

# Chapter 1

## 1. Introduction

### 1.1 General

Wave transformations in the nearshore region result in a visually spectacular and scientifically and technically important phenomenon. The dissipation of wave energy by breaking and subsequent fluid motion in the surf zone are both significant from the engineering point of view. They are of great importance concerning natural or man-induced morphological developments, coastal structures and the transport and dispersion of dissolved and suspended matter in coastal regions.

Waves in the nearshore regions are profoundly modified by bottom topography. In shallow water, linear and nonlinear dynamical processes change the characteristics of the wavefield. Refraction, shoaling, nonlinear interactions and breaking are typical manifestations of these transformations. The understanding of these physical processes has been improved in recent years and a number of attempts have been made to incorporate this knowledge in numerical wave models.

Observations of shoaling wavefields indicate that waves evolve from a slightly peaked, nearly sinusoidal shape in deep water to a shape characterized by sharp crests, flat troughs and relatively steep shoreward faces. These profile distortions, that occur just before wave breaking, are typical manifestation of the nonlinear effects in the nearshore region. These nonlinear effects together with dissipation of wave energy by breaking represent the dominant physical mechanisms in the evolution of waves in the nearshore. Thus a good understanding of the nonlinear aspects of shallow-water waves including the effects of breaking, and modeling these effects are both of direct interest.

The wave energy spectrum, which contains information about many statistical properties of the wavefield, has long been considered as an appropriate design tool in engineering application. Thus, knowledge of the wave spectrum in the shoaling region and in the surf zone is of great importance to coastal engineering. The wave spectrum in the nearshore region is significantly modified due to both nonlinear effects as well as wave breaking. These transformations are the main concern of this study.

## 1.2 Literature review

The propagation of nonlinear shallow-water waves has been investigated by numerous researchers during the last few decades. Investigations have been carried out to gain insight in the nonlinear dynamics involved in the nearshore wave evolution, and to incorporate this knowledge in numerical wave models.

Relevant literature related to nonlinear shallow-water waves is reviewed below. A distinction is made between literature dealing with the physical aspects and literature concerned with the modeling aspects.

### *Physical aspects*

Generation of high-frequency waves, due to nonlinearity in a wavefield propagating over a shallow region, has long been known both observationally and theoretically.

Johnson et al. (1951) observed that over natural reefs the energy was transmitted as a multiple crest system. Jolas (1960) conducted experiments with a simple incident wave over a submerged shelf and observed higher harmonics of the primary on the transmission side when the water depth above the shelf was shallow enough. Dattatri et al. (1978) observed rather complex forms of the transmitted waves over submerged breakwaters, which indicated the presence of higher harmonics. Kojima et al. (1990) reported their experimental

results with immersed plates, emphasizing the phenomenon of harmonic generation and of wave decomposition. Rey et al. (1992) have reported experiments for wave propagation over a submerged self. They noted that nonlinear effects at the obstacle introduce asymmetry and skewness to the initially symmetric wave profile, and generate a hierarchy of shorter superharmonic free waves propagating away from the obstacle.

Beji and Battjes (1993) have performed laboratory experiments to elucidate the phenomenon of high-frequency energy generation observed in the energy spectra of waves traveling over a submerged shallow bar. The dominant physical mechanism is found to be the amplification of bound harmonics in the shoaling region, and their release in the deeper region, resulting in the decomposition of the wavefield.

Field observations in the nearshore regions with-bar-trough type bathymetries indicated significant changes in the wave spectrum. Byrne (1969), Dingemans (1989) and Young (1989) reported generation of higher harmonics during the wave passage over shallow regions.

Phillips (1960) showed theoretically that a second-order Stokes wave is the result of a nonlinear interaction between two primary wavetrains which forces a harmonic. He showed that these nonlinear triad interactions, i.e., two waves interacting to give rise to a third, are near-resonant. Laboratory experiments conducted by Longuet-Higgins and Smith (1966) and Phillips (1967) confirmed Phillips' theory.

Hasselmann et al. (1963) used the bispectrum to investigate the skewness of surface waves, i.e., lack of symmetry with respect to the horizontal. The bispectrum is formally defined as the Fourier transform of the second-order covariance function. The imaginary part of the bispectrum is related to wave asymmetry, i.e., lack of symmetry with respect to the vertical (Masuda and Kuo, 1981a; Elgar and Guza, 1985b). Thus, the lack of horizontal and vertical symmetry can be examined simultaneously using the bispectral analysis.

Elgar and Guza (1985b) used the bispectral analysis to examine the skewness and asymmetry of shoaling nonbreaking surface gravity waves. In deep water they observed phase-coupling between the primary waves in the energetic part of the spectrum and the first harmonic, consistent with Stokes-type nonlinearities, similar to those observed by Hasselmann et al. (1963). They noted that further shoaling gradually leads to more intense triad interactions involving higher harmonics, and an evolution of the phase relations consistent with the wave profile that is pitched shoreward relative to a vertical axis. They also observed that shoreward propagating low-frequency energy has a significant coupling to higher-frequency modes within the spectral peak, which is suggestive of a difference interaction between primary frequencies; a similar interaction was also noted by Hasselmann et al. (1963). Moreover Elgar and Guza (1985b) observed that the low-frequency wave was  $180^\circ$  out of phase with the wave group, a value consistent with the classical concept of bound waves (Longuet-Higgins and Stewart, 1962; 1964).

Along with the cross spectral energy transfers, shallow-water nonlinearity leads to phase evolution of various frequency components. These phase modifications result in phase speeds substantially different from those predicted by the linear Stokes theory. In the field observations of Yefimov et al. (1972), high-frequency waves had phase speeds between the free-wave speed and the speed of the spectral peak, suggestive of presence of free and forced components in these data. Numerous other investigators have also noted a discrepancy between linear theory and observed phase speed in shallow water (Büsching, 1978; Elgar and Guza, 1985a). Specifically, they have noted that the celerity was roughly constant for all wind-wave frequencies.

Field and laboratory observations of velocity measurements indicated that the onshore velocity associated with the wave crest is stronger and of shorter duration than the offshore velocity associated with the wave trough (Huntley and Bowen, 1975; Flick et al., 1981; Herbers et al., 1992). The horizontal asymmetry of the cross-shore flow, which is a reflection of the wave shape, is known as the velocity skewness.



Recently Doering and Bowen (1995) investigated the spatial variation of velocity skewness and asymmetry for shoaling and breaking surface gravity waves. They utilized a simple analytical solution for harmonic growth in the special case of a monochromatic primary wavetrain (Elgar and Guza, 1986). They proposed and tested a simple parametrization for bispectral evolution, that is based on the Ursell number. They found that the parametrization provides a reasonable prediction of velocity skewness and asymmetry due to wave shoaling.

Elgar et al. (1992) have examined the sensitivity of nonlinear interactions to the directional distributions of incident waves in laboratory experiments. They found that the shape of the directional spectrum of the incident wavefield has only a minor effect on the magnitudes of nonlinear energy transfers during shoaling. The principal effect of directionality is found to be in the directions, not the amplitudes, of the nonlinearly generated waves, implying the importance of triad interactions between noncolinear as well as colinear waves.

The effect of wave breaking on the spectral evolution in random waves in the presence of harmonic generation has been investigated experimentally by several authors. Battjes and Beji (1992) performed experiments for nonbreaking and breaking waves over a submerged bar using single-peaked incident wave spectra (see also Beji and Battjes, 1993). The wave steepness was varied as well as the spectral shape; both a narrow, swell-type spectrum and a broader, wind-sea-type spectrum with a Jonswap (Joint North Sea Wave Project) high-frequency tail were used. In their experiments, significant spectral changes occurred, both for breaking and steep but nonbreaking waves. However, the spectral shape (not the overall energy content) evolved in a like manner for the two cases.

Mase and Kirby (1992) have performed laboratory experiments to elucidate the shoaling and breaking of random waves over a plane beach profile. They observed that in very shallow water the high-frequency energy is more influenced by breaking compared with the primary spectral peak. Their analysis suggested a spectral breaking function that consists of two parts: the first part represents proportional energy decay for all frequency components, the second

part is proportional to the square of the frequency.

Smith and Vincent (1992) have measured shoaling and decay of two coexisting wave systems on a beach in a wave flume. They observed that the high-frequency wave system decays faster in the presence of low-frequency waves than in their absence. They mentioned several mechanisms as possible explanations, among which is a shoaling analogue of the mechanism proposed by Banner and Phillips (1974) in which the high-frequency waves experience the underlying low-frequency waves in terms of a large-scale flow that enhances breaking of shorter waves. Later Vincent et al. (1994) have analyzed laboratory data on irregular waves with single-peaked spectra shoaling and breaking on a 1:30 slope. They concluded that within the surf zone the spectral distribution of dissipation due to breaking is proportional to the energy densities and is not otherwise dependent on frequency. This is consistent with the results of Beji and Battjes (1993).

### *Modeling aspects*

Analytical solutions to the governing equations of motion are usually obtained by expanding the dependent variables in a power series and by assuming that the bottom slope is a small quantity of higher order than that to which the expansion is carried. Classical wave theories based on this approach include Stokes waves and cnoidal waves. The Stokes theory formally requires that wave nonlinearity is much smaller than the dispersivity; in the shoaling region this criterion is satisfied only for infinitesimal waves. The Boussinesq equations (Boussinesq, 1872) are valid in the shoaling region where both nonlinearity and dispersivity are of the same order. For unidirectional wave propagation Boussinesq equations reduce to the Korteweg-deVries (KdV) equation (Korteweg and de Vries, 1895), to which the cnoidal wave is an exact analytical solution. These exact analytical solutions to the Boussinesq and KdV equations are waves of permanent form. However, the waves in the shoaling region undergo substantial deformation, a process characterized by gradual peaking of the wave crest, flattening of the trough, and steepening of the front faces.

Clearly, solutions for waves of permanent form to describe the wave evolution are unrealistic. Thus, models are required to describe wave evolution in the shoaling region.

Two classes of models for wave propagation can be distinguished, differing mainly in their formulations and the field of applications. In the first, phase-averaged, class of models the governing equations are formulated in terms of wave energy (or action) density. These models describe the average properties of the wavefield. Their computational efficiency makes them feasible for wind wave prediction on the open sea in relatively extensive areas (dimensions many times the wavelength). The second, phase-resolving, class of models comprises equations describing the instantaneous state of motion, either in the time-domain or in the frequency-domain (with amplitudes and phases). These models are computationally demanding compared with those of the first class and are therefore restricted to smaller domains.

Phase-resolving models, such as Boussinesq equations, incorporate nonlinear shallow-water effects. Peregrine (1967) formulated Boussinesq equations for shallow-water wave propagation over varying bottom. A major limitation of these equations is that they are only applicable to relatively shallow-water depths because of their weak dispersion characteristics.

Several attempts have been made to improve the dispersion in Boussinesq-type equations in order to extend their range of applicability into deeper water. Witting (1984) developed a one-dimensional Boussinesq-type equation from the depth-integrated flow equations. He used a Taylor series expansion of the velocity about the bottom, and selected the coefficients of this expansion such that the resulting dispersion relation best matched that of exact linear theory for a wide range of water depths. Madsen et al. (1991) introduced additional terms in the momentum equation to recapture the excellent dispersion characteristics of Witting (1984). Nwogu (1993), using the inviscid Euler equations, developed a set of extended Boussinesq equations by choosing an arbitrary depth  $z_\alpha$  where the velocity variables are taken. The resulting dispersion relation was then expressed in terms of this arbitrary depth, and thus best-fitted to the dispersion

relation of the exact linear theory from deep to shallow water. Schäffer and Madsen (1995) used higher order Padé expansion in  $kh$  of the Stokes linear dispersion relation for waves on arbitrary depth to derive a new set of Boussinesq equations. Their equations are valid even for wavelengths as small as the water depth. Merckelbach (1995) presented another set of Boussinesq equations with higher-accuracy dispersion.

Beji and Battjes (1994) used a variant of Madsen and Sørensen's (1992) extended Boussinesq equations to model the nonlinear evolution of unidirectional nonbreaking waves over a bar. Their equations are expressed in depth-averaged velocity. The observed phenomena of bound harmonics generation in the shoaling region and their release beyond the bar were well predicted by their time-domain computations using this model.

Elgar et al. (1990) used a Boussinesq-based model to predict the velocity skewness through the shoaling region. They obtained accurate estimates of the velocity skewness. However, the model is not applicable for breaking waves. Bosboom (1995) used a spectral Boussinesq model for breaking waves (Eldeberky and Battjes, 1996) to predict the velocity skewness of waves in the shoaling region and the surf zone. The model predictions were in fair agreement with observations.

The KdV equation is essentially a reduction of the Boussinesq equation assuming unidirectional propagation (i.e., no reflection). The KdV equation is a wave equation expressed in only one dependent variable (surface elevation). Svendsen (1976) formulated a KdV equation for variable depth. The extension of KdV equation to deeper water by adding more dispersion has not been considered in the literature as has been done for Boussinesq equations.

To study the nonlinear energy transfers between spectral wave components, spectral evolution equations are commonly used. Several authors have derived spectral evolution equations for shallow-water waves from KdV or Boussinesq equations. The KdV equation is easier to transform into the frequency-domain since it has only one variable (surface elevation) in one equation. Bryant (1973)

and Mei (1989) derived evolution equations from KdV-type equations for a horizontal bottom.

Freilich and Guza (1984) derived evolution equations for the Fourier amplitude and phase from Peregrine's equation (1967). They noted that triad interactions across the energetic part of the wind-wave spectrum provide the mechanism for cross spectral energy transfers and modal phase modifications as the waves propagate shoreward through the shoaling region. Based on comparisons of energy spectra, coherence and relative phase between model predictions and data, they concluded that the spectral evolution equations accurately predict Fourier coefficients of the wavefield through the shoaling region (their study did not include breaking waves).

Liu et al. (1985) used time-domain Boussinesq equations to derive evolution equations for spectral wave components in a slowly varying, two-dimensional domain using the parabolic approximation. Their model is an extension of the Freilich and Guza (1984) model to two horizontal dimensions. The model is used to compute the evolution of a monochromatic wave with its harmonics. Application of this model to an entire spectrum of wind waves required an extensive computational effort.

Elgar and Guza (1986) used the one-dimensional nonlinear Boussinesq model of Freilich and Guza (1984) to model the bispectral evolution in shoaling nonbreaking waves. They noted that model predictions of bispectrum, sea-surface-elevation skewness and asymmetry match field observations. They found that the bispectral evolution is insensitive to mild bottom slopes; that is, model runs over a horizontal bottom and over mildly sloping bottoms resulted in a similar bispectral structure. They also concluded that the gross trends in the nonlinear evolution of the bispectrum, skewness and asymmetry do not depend critically on the initial phase coupling. They further found a simple analytical solution for harmonic growth in the special case of a monochromatic primary wavetrain, in which the relative phase is dependent on the relative depth as well as the propagation distance.

Madsen and Sørensen (1993) derived evolution equations for the complex Fourier amplitudes based on their time-domain extended Boussinesq equations. They used the evolution equations to study triad wave interactions in shallow water. Comparisons of model predictions with observations and direct time-domain solutions showed good agreement.

Agnon et al. (1993) derived a one-dimensional nonlinear shoaling model for time periodic, spatially varying waves. In the limit of shallow water, the quadratic interaction model converges to the Boussinesq model. Extension to two-dimensional domain for small angle of incidence is made by Kaihatu and Kirby (1995) using the parabolic approximation.

Nwogu (1994) has used his extended time-domain Boussinesq model to investigate the effect of near-resonant triad interactions on the transformation of directional wave spectra in shallow water. He derived expressions from the Boussinesq equations for the magnitude of the second-order waves induced by bidirectional, bichromatic waves. He observed that the growth of sub- and superharmonics of the primary waves is near-resonant for unidirectional waves in shallow water. However in a multidirectional sea in shallow water, the second-order interactions are near-resonant for the higher harmonics but non-resonant for the lower harmonics.

Phase-averaged spectral energy models are feasible for application in the open ocean (e.g., WAM Development and Implementation Group, 1988). The state-of-the-art wind wave propagation models are based on the spectral energy balance equation with various source/sink terms representing generation by wind, nonlinear quadruplet wave interactions or wave-current interactions, dissipation by bottom friction and whitecapping (deep-water breaking). Reference is made to Komen et al. (1994) for a detailed description of the theoretical background and derived models for oceanic and shelf sea applications.

Recently attempts have been made to extend spectral energy oceanic models into the shallower water and even to the surf zone (e.g., Resio, 1988; Holthuijsen

et al., 1993). In shallow water, the cross-spectral energy transfers become increasingly important, therefore a representation for the average effects of nonlinear triad interactions is highly desired.

Abreu et al. (1992) made the first step and developed a statistical model for the nonlinear evolution of the frequency-directional spectrum, suitable as a source term in a spectral energy balance. The model is based on the nondispersive, nonlinear shallow-water equations and an asymptotic closure (Newell and Aucoin, 1971) for directionally spread, nondispersive waves. In their formulation only triads containing waves travelling in the same direction (i.e., with colinear wavenumber vectors) are considered resonant. In practical application, the restriction to nondispersive waves is a grave one, because it implies a continued, resonant, one-way transfer to the higher harmonics, in contrast to the case of (weakly) dispersive waves for which the transfer is non-resonant and back-and-forth, because of the mismatch in the phase speed. This restriction is easily violated in practical application. The consequence of this is an unwanted behavior of the high-frequency part of the spectrum (dispersive waves).

In the surf zone, energy dissipation due to depth-induced wave breaking becomes a dominant process. A few theoretical models exist for the prediction of the total rate of breaking-induced energy dissipation in random waves (e.g., Battjes and Janssen, 1978; Thornton and Guza, 1983).

For application of time-domain Boussinesq equations to the surf zone, Schäffer et al. (1993) suggested a breaking criterion based on a surface roller approach. The effect of the roller is included in the vertical distribution of the horizontal velocity, which leads to an additional convective momentum term.

Recently several attempts have been made to develop a spectral formulation for energy dissipation by wave breaking. Liu (1990) presented a spectral parabolic equation supplemented with a breaking dissipation term. He extended the energy dissipation function for linear waves of Dally et al. (1985) to nonlinear shallow-water waves. His breaking dissipation term is a complex function with

magnitude proportional to the wave amplitude. The imaginary part of the complex dissipation function, which influences the phase of each harmonic and, consequently, the surface profile inside the surf zone, is chosen to have the same value as the real part. The consequences were that the free-surface profiles were entirely wrong compared with the measurements, although the wave heights were correctly predicted.

Mase and Kirby (1992) have presented a hybrid frequency-domain KdV equation for random wave transformation. In their equation the damping coefficient which accounts for breaking dissipation was estimated from observations of spectral densities over a sloping beach. It was formulated as a summation of two terms; the first term represents proportional energy decay for all frequency components, the second term is proportional to the square of the frequency (see, also, Kirby et al., 1992). The model results were in agreement with the observations used in the analysis.

Eldeberky and Battjes (1996) have formulated a spectral dissipation function both for energy models and complex amplitude models, in which the total rate of random-wave energy dissipation is distributed in proportion to the local spectral level (based on observations of Beji and Battjes, 1993). The spectral breaking term is implemented in the evolution equations of an extended Boussinesq model. The model predictions for the wave spectrum as well as the wave profile were in good agreement with observations in shallow water.

### 1.3 Study objectives

The aim of the study presented in this thesis is twofold. In the first place, to gain more understanding of the dynamics of nonlinear shallow-water waves, in particular the generation of higher harmonics due to triad wave interactions and the influence of wave breaking.

For random wave predictions in extensive areas, phase-averaged, spectral energy based models are appropriate. The significant role of triad wave



interactions in the nearshore area has made the development of a predictive energy-based spectral model for the generation and dissipation of the harmonics in breaking waves highly desired. The second goal of this study is therefore to develop a statistical model for nonlinear triad wave interactions and a spectral formulation for depth-induced wave breaking.

#### **1.4 Outline**

The layout of this thesis is as follows. In chapter 2, a phenomenological description of harmonic generation is given as an introductory documentation to the phenomenon of nonlinear triad interactions. Bispectral analyses of observations of shallow-water waves are presented in chapter 3. In chapter 4, a deterministic spectral Boussinesq model is extended into the surf zone by the inclusion of a dissipation term to account for wave breaking and used to simulate harmonic generation in shallow water.

Random wave modeling of nonlinear triad wave interactions is considered in chapter 5, in which a Hamiltonian formulation for nonlinear shallow-water waves is considered. An energy formulation for triad interactions based on the Zakharov kinetic equation is presented and investigated in chapter 6. In chapter 7, a computationally efficient, parametrized energy formulation based on Boussinesq equations representing harmonic generation is developed and verified. Conclusions and suggestions for future research are finally presented in chapter 8.



## Chapter 2

### 2. Phenomenological description of harmonic generation

Harmonic generation in shallow-water waves is described in this chapter from a phenomenological point of view. The description and interpretations presented here are based partly on review of existing literature and partly on knowledge gained during the course of this study.

The arrangement of this chapter is as follows. Section 1 contrasts the role of the linear and nonlinear transformations in shallow-water waves and the influence of the dispersion characteristics in the mechanism of nonlinear interactions. Some elementary principles of nonlinear triad wave interactions are given in section 2. In section 3, qualitative features of nonlinear wave transformation in shallow water are presented. The role of wave breaking is finally considered in section 4.

Some of the comments and interpretations given in this chapter are fairly general for which no explicit references are given. For specific points, some references are cited occasionally.

#### 2.1 Linear and nonlinear transformations

As ocean surface gravity waves propagate toward the shore in shoaling waters, they undergo substantial evolution from their deep-water state. In the shoaling waters, linear and nonlinear processes act simultaneously to transform the wave characteristics. Changing bottom topography causes refraction and shoaling of the wavefield, which result in spatial variations in the amplitudes and directions.

Although linear theory predicts the observed increasing wave amplitudes and narrowing directional distributions of swell and sea waves in a qualitative sense, nonlinear effects are important. Nonlinear evolution can alter the spectral (frequency-direction) characteristics of the wavefield as well as the wave profiles. Initially symmetric wave profiles and oscillatory velocities become asymmetric and skewed. In addition, phase speeds substantially differ from those predicted by the linear dispersion relationship.

As waves travel from deep to shallow water, the dispersion characteristics of the wavefield play an important role in the mechanism of the nonlinear wave interactions. Three regions of different dispersion characteristics can be distinguished. In deep water (relative depth  $kh \gg O(1)$ , where  $k$  is a characteristic wavenumber and  $h$  the water depth), the wavefield undergoes strong frequency dispersion. Strong frequency dispersion is the dependency of phase speed  $c$  on frequency  $\omega$  (deep-water waves  $c = g/\omega$ , where  $g$  is the gravitational acceleration). In this region, the dispersion characteristics permit resonant interactions among quartets of waves to occur, resulting in slow cross-spectral energy transfers. Although energy exchanges due to these cubic nonlinearities are very small on wavelength scales, the wave spectrum is substantially modified over hundreds of wavelengths (Hasselmann, 1962).

In very shallow water ( $kh \ll 1$ , a condition approximately satisfied by wind waves within the surf zone), waves are almost nondispersive (shallow-water waves  $c = \sqrt{gh}$ ). Near-resonant interactions among triads of waves occur, resulting in rapid spectral evolution.

In intermediate depths ( $kh = O(1)$ ), between the deep-water region with strongly dispersive waves and the shallow-water region with nondispersive waves, waves are weakly dispersive ( $c = (g/\omega) \tanh kh$ ) and undergo substantial changes caused by the off-resonant energetic triad interactions. Triad interactions drive rapid spectral evolution over several (rather than hundreds of) wavelengths.

## 2.2 Nonlinear triad wave interactions

In the shoaling region, the short evolution distance and moderate dispersion suggest that second-order (quadratic) nonlinearities involving triads of waves are important. Triad interactions occur among waves with frequencies and wavenumbers such that

$$f_1 \pm f_2 = f_3 \quad (2.1)$$

and

$$k_1 \pm k_2 = k_3 \quad (2.2)$$

where  $f$  and  $k$  are the scalar frequency and vector wavenumber, respectively.

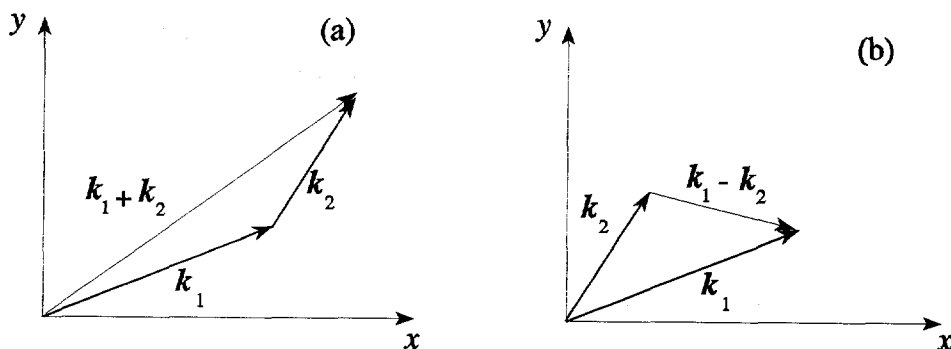


**Figure 2.1** Wavenumber vectors of triad interactions (a): sum interaction, (b): difference interaction

The wave components  $(f_1, k_1)$  and  $(f_2, k_2)$  each satisfy the linear dispersion relation

$$\omega^2 = gk \tanh(kh) \quad (2.3)$$

in which  $k$  is the wavenumber magnitude. The physical meaning of (2.1) and (2.2) is that the sum (or difference) interaction between wave components 1 and 2 forces motions with the scalar-sum (or difference) frequency and the vector-sum (or difference) wavenumber (Fig. 2.1). If component 3 satisfies the linear dispersion relation (2.3) then the interaction is resonant (Armstrong et al., 1962) implying a continued one-way transfer of energy to component 3. Note that for gravity surface waves this is only possible in very shallow water where the waves are nondispersive. In fact theories for weakly nonlinear wind-generated surface gravity waves show that the nonlinear triad interactions do not support resonances (e.g. Phillips, 1960; Hasselman, 1962). If component 3 does not satisfy the linear dispersion relation (2.3) then the interaction is non-resonant (in intermediate depths where waves are weakly dispersive) and the transfer is back-and-forth because of the mismatch in the phase speed.

The intensity of the triad interactions is mainly controlled by the phase mismatch. The difference between the so-called bound wavenumber given by  $|k_1 \pm k_2|$  and the free wavenumber obtained from the linear dispersion relation  $|k(f_3)|$  represents the wavenumber mismatch:

$$\Delta_k = |k_1 \pm k_2| - |k(f_3)| \quad (2.4)$$

The normalized wavenumber mismatch

$$\delta_k = \Delta_k / |k(f_3)| \quad (2.5)$$

is a measure of the departure from exact resonance. Its magnitude determines the intensity of energy exchanges between the interacting waves. Zero mismatch (nondispersive shallow-water waves) represents the limiting case in the interaction process, in which the interacting waves remain intact and in phase (resonant interaction) during evolution. Thus, the magnitude of energy transfer is maximum and a continued one-way transfer takes place to the harmonics over relatively short evolution distance.

When the mismatch  $\delta_k \ll 1$  (weakly dispersive shoaling waves), phase relations between the interacting waves vary slightly over a wavelength. Consequently the magnitudes and the sign of energy transfers between the interacting waves vary slowly over a wavelength, allowing significant net energy transfers over several wavelengths. Large values of the mismatch (strongly dispersive deep-water waves), imply that phase relations between interacting waves vary rapidly over a wavelength, not allowing for significant energy transfers.

It is common practice to distinguish between the sum and difference interactions. In shallow water, the sum interactions between the primary waves at the energetic part of the spectrum (with peak frequency  $f_p$ ) lead to the generation of harmonics around a frequency  $2f_p$  (first harmonic of the primary). Eventually, the sum interactions between the primary waves near  $f_p$  and the first harmonics at  $2f_p$  give rise to harmonics near  $3f_p$ . The difference interactions between primary waves within the energetic part of the spectrum lead to the generation of bound long waves.

### 2.3 Qualitative features of nonlinear wave transformation in the nearshore

In the shoaling regions, nonlinearity significantly transforms the characteristics of the wave spectra as well as the wave profiles. It drives cross-spectral transfers of energy and phase modifications leading to distortion of wave profiles. Qualitative descriptions are given below for the influence of nonlinearity on the phase speed, the wave-profiles, the frequency and frequency-direction energy spectra, and the underlying velocity field.

#### *Phase speed*

Free waves propagate with phase speeds determined from the linear dispersion relation (2.3). In shallow water, however, the bound waves generated by the off-resonant energetic interactions are coupled to the primary wave group and thus propagate with phase speeds substantially different from those predicted by the linear dispersion relation (Büsching, 1978). Due to nonlinearity, high-frequency waves have phase speeds between the free-wave speed and the speed

at the spectral peak.

### *Wave profiles*

As waves propagate in a shoaling region, two stages of profile distortion can be distinguished. As they travel in decreasing intermediate depth, they lose their horizontal symmetry and develop sharp crests and flat troughs (Stokes-type) due to the weak nonlinearity. This is a consequence of generation of bound harmonics that are phase locked and in phase with the primary. As they propagate into shallower water, the bound harmonics are gradually amplified. During this stage the wave profiles gradually lose also their vertical symmetry and assume a saw-toothed shape (Fig. 2.2b,c) with crests pitched forward (the harmonics are leading the primary waves). This is implying that the harmonics are forced to a forward phase shift (i.e., propagate faster) with respect to the primary (Flick et al., 1981). These profile distortions are also influenced by the effects of amplitude dispersion (i.e., tendency for a wave crest to propagate faster than the trough, as in  $c = \sqrt{g(h + \zeta)}$  where  $\zeta$  is the surface elevation) because of the finite amplitude effects.

When waves propagate over a submerged shallow bar the phenomenon of harmonic generation manifests itself strongly (Beji and Battjes, 1993). In the shoaling region, bound harmonics are amplified due to the increasing nonlinearity. Over the bar crest, where the waves enter a nearly nondispersive medium, the resonant conditions are nearly satisfied and rapid transfers of energy take place from the primary waves to the harmonics. These transfers coupled with the effects of amplitude dispersion generate the so-called dispersive tail waves propagating at nearly the same phase speed as the primary waves (Fig. 2.2c). These dispersive tail waves can be regarded as free since their phase speeds are mainly determined by the water depth. In the deepening region beyond the bar, the nonlinearity decreases, and the wavefield decomposes into freely propagating shorter components with smaller amplitude (Fig. 2.2d,e).



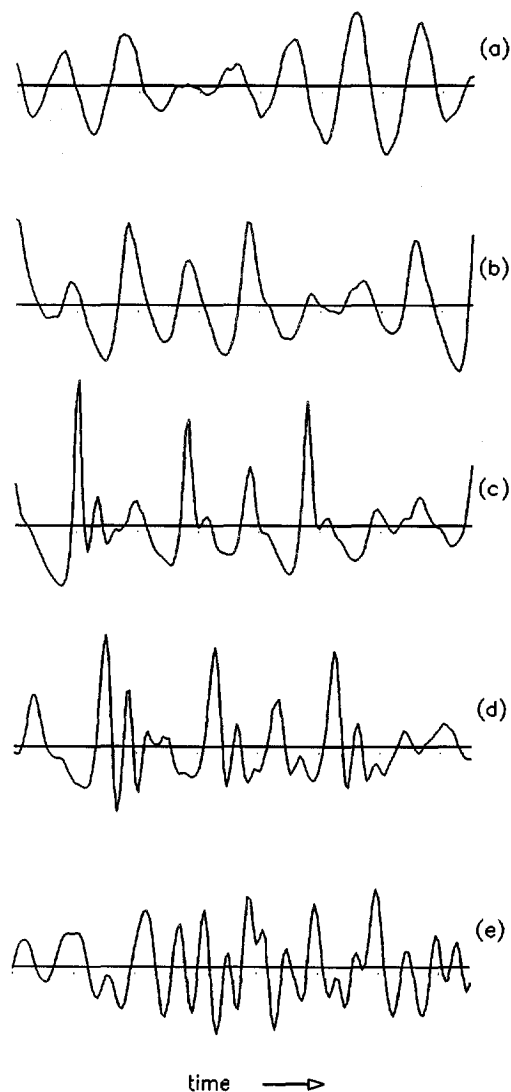


**Figure 2.2** *Sea surface elevation versus time for evolution of random waves over a submerged bar. (a): in deep water, (b) and (c): over the bar crest, (d) and (e) beyond the bar. Measurements taken from Beji and Battjes (1993).*

### Frequency spectra

The evolution of the frequency spectrum of wave energy in shallow water is dominated by the energy transfers between the spectral components. The influences of these transfers on the shape of the spectrum vary with the frequency distribution of the incident deep water spectrum. Narrowband frequency-spectra develop secondary peaks at harmonics of the peak frequency (Fig. 2.3a), while broadband frequency-spectra show an increase in the energy level over a wide range of frequencies higher than the energetic part of the spectrum (Fig. 2.3b).

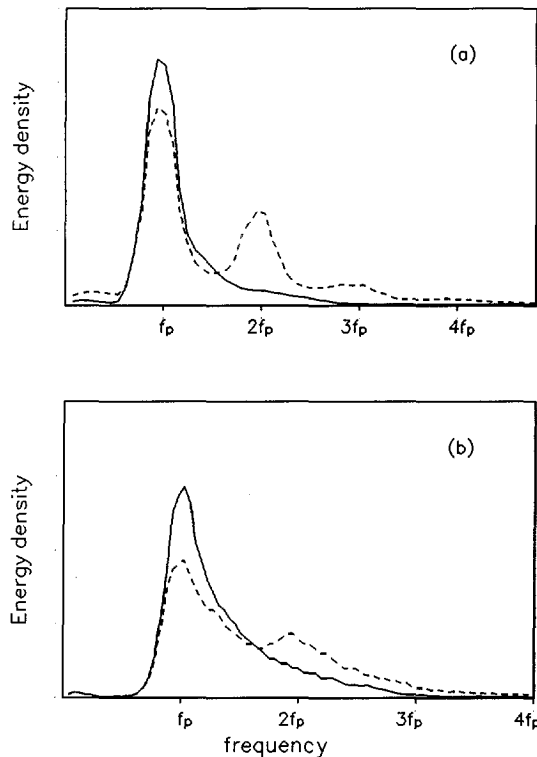


**Figure 2.3** *Energy spectra of sea surface elevation for random waves evolution in shoaling region. Solid lines denote spectra at deep water, dashed lines denote transformed spectra in shallow water. (a): Narrowband spectrum, (b): broadband spectrum. Measurements taken from Arcilla et al. (1994)*

### *Frequency-direction spectra*

The directional properties of the wavefield play a role in the interaction mechanism in which the harmonics are generated. First consider a wavefield with a wide directional distribution in deep water. As waves propagate into shallow water, changing bottom topography tends to narrow the directional distribution owing to refraction. Thus, all wavenumber vectors attain nearly the same direction (i.e., "colinear"). Nonlinear triad interactions between the nearly colinear waves (i.e., waves propagating within the same directional sector) generate higher harmonics which are directionally aligned with the primary directional peak. (Note this does not hold for the long waves resulting from the difference interactions.)

Directionally bi-modal wave spectra (in deep water) behave differently as they transform in shallow water (Freilich et al., 1990). In this case, the wavenumber vectors of the two directional peaks are not (nearly) colinear. The interactions between the primary waves in the two directional peaks (the so-called "noncolinear" interactions) produce a new directional peak (at the vector-sum wavenumber  $k_1 + k_2$ ). Colinear interactions between waves within each primary peak generate also peaks that are directionally aligned with the primary ones. In shoaling directionally bi-modal wave spectra, both colinear and noncolinear triad interactions are important.

### *Near-bottom velocity*

Harmonic generation does not only influence the wave shape, but also the underlying velocity field. Observations of near-bottom velocity show skewed velocity records in regions where there are strong nonlinear couplings. Phase-couplings between the primary waves and their higher harmonics, as a result of sum interactions between the primary waves, lead to oscillatory velocities skewed onshore, i.e., onshore velocities stronger and of shorter duration than offshore velocities. On the other hand, phase coupling between the primary and the bound long wave, as a result of difference interaction between the primary waves, leads to oscillatory velocity skewed offshore, i.e., offshore velocities stronger and of shorter duration than onshore velocities (Doering and Bowen, 1995).

## 2.4 The role of wave breaking

The distortions of the wave profiles in shallow water (asymmetric and skewed profiles) associated with harmonic generation are characteristics of nearly breaking and broken waves. The role of wave breaking in such regions and its influence on the spectral evolution has not yet rigorously been established. Knowledge of the spectral distribution of energy dissipation due to wave breaking is necessary for prediction of wave evolution in the shoaling region and in the surf zone.

Wave breaking can be seen as a two-stage process. The pre-breaking stage is characterized by a sequence of orderly motions dominated by the generation of bound harmonics resulting in wave steepening and profile distortions. The second stage starts with the incipient wave breaking and is characterized by a chaotic appearance, air-entrainment and turbulence. After breaking the wave either recovers its laminar nature and continues to propagate with a smaller amplitude or it turns into a turbulent bore. The first case is observed when waves break over a submerged nearshore bar, the second on a beach where depth decreases monotonically at a rate sufficient to sustain turbulence.

Several attempts have been made to establish a spectral distribution for the energy dissipation due to wave breaking based on analyses of wave spectra in the surf zone. Conclusions based on these analyses seem to significantly depend on the experimental conditions such as the initial spectral shape and the severeness of wave breaking. The method adopted in this study is based on the observations of shallow-water wave breaking in the presence of harmonic generation over a shallow bar (Beji and Battjes, 1993) as well as over a slope (Vincent et al., 1994). They concluded that for single-peaked incident wave spectra, the nonlinear interactions taking place in the course of waves' passage across shallow regions appeared not to be affected by wave breaking. Wave breaking did not substantially affect the dynamics of the nonlinear triad interactions (at least for the energetic part of the spectrum and its higher harmonics).

---

Little is known about the influence of wave breaking on the low-frequency waves. In the surf zone, although wave height is depth limited, the amplitude of the low-frequency waves tends to increase with decreasing depth, reaching a maximum at the shore line generally without breaking of the long waves. This does not necessarily imply that the low-frequency motions are not affected by breaking of the shorter waves. The nonlinearly generated low-frequency motion could be substantially damped in the inner surf zone (Eldeberky and Battjes, 1996).



## Chapter 3

### 3. Bispectral analysis of shallow-water waves

#### 3.1 Introduction

In this chapter, aspects of nonlinear dynamics of waves propagating in shallow water are investigated using the bispectral analysis. Since its introduction, the bispectrum has been used extensively to examine nonlinearity in shoaling surface gravity waves. The purpose of this chapter is to gain more understanding and physical insight in the nonlinear transformation of wave spectra in shallow water with aid of the bispectral analysis.

The organization of this chapter is as follows. The definition of bispectrum is given in section 2. In section 3, the relation between the bispectrum and the skewness and asymmetry are described. Bispectral analysis of shoaling waves over a laboratory beach profile is carried out in section 4. In section 5, the nonlinear couplings in waves passing over a bar region are investigated. The evolution of relative phase in waves propagating over a shallow bar is examined in section 6. A summary and conclusions are finally given in section 7. (Parts of this chapter have been published in slightly different form in Eldeberky and Battjes (1994a).)

#### 3.2 The bispectrum

The bispectrum was introduced by Hasselmann et al. (1963) to examine wave nonlinearity in intermediate water depths. Since its introduction, bispectral analysis has been used by many investigators to study nonlinear phenomena in a wide variety of fields such as seismic action (Haubrich, 1965), fluid

turbulence (Yeh and Van Atta, 1973), plasma fluctuations (Kim and Powers, 1979) and deep-water surface gravity waves (Masudo and Kuo, 1981b). Recently, it has been used extensively to examine nonlinearity in shoaling surface gravity waves (Elgar and Guza, 1985b; Herbers and Guza, 1992).

The sea surface elevation can be represented using spatially varying Fourier components, in which the time variation can be factored out (assuming time periodicity) as follows

$$\zeta(x, t) = \sum_{p=-\infty}^{\infty} C_p(x) \exp[-i(\omega_p t)] \quad (3.1)$$

where  $\omega$  is the radian frequency ( $=2\pi f$ ),  $p$  is the rank of the harmonic,  $C_p$  is the complex Fourier amplitude varying with position  $x$ .

For a Gaussian sea, the sea surface can be represented as a superposition of statistically independent waves in which the phases are random. Consequently the sea surface can be fully described by the continuous energy spectrum, which is defined as the Fourier transform of the second-order correlation function  $R(\tau)$  of the time series,

$$E(\omega) = \frac{1}{2\pi} \int_{-\infty}^{+\infty} R(\tau) \exp(-i\omega\tau) d\tau \quad (3.2)$$

where  $R(\tau)$  is given by

$$R(\tau) = \langle \zeta(t) \zeta(t+\tau) \rangle \quad (3.3)$$

in which  $\tau$  is a time lag, and  $\langle . \rangle$  denotes the expected-value, or average, operator. Note that the spectral energy density function  $E(\omega)$  is defined for positive and negative frequencies.

For discretely sampled data, the discrete energy spectrum  $E_p$  can be represented in terms of Fourier amplitudes,



$$E_p = \langle C_p C_p^* \rangle \quad (3.4)$$

Here  $C_p^*$  is the complex conjugate amplitude of  $C_p$ . The discrete energy spectrum  $E_p$  is related to the continuous one by  $E_p = E(\omega)\Delta\omega$  for  $\omega \cong \omega_p$ , in which  $\Delta\omega = 2\pi\Delta f$  is the angular frequency-band.

The energy spectrum (3.4) is independent of the phases. If the phases of Fourier components are not random and statistically correlated, the sea surface is not Gaussian (Hasselmann et al., 1963). Departure from a Gaussian form cannot be detected by the energy spectrum. Higher-order spectra such as the bispectrum can be used to investigate nonlinearity in shallow-water waves. It is a complex quantity, formally defined as the Fourier transform of the third-order correlation function of the time series:

$$B(\omega_1, \omega_2) = \left[ \frac{1}{2\pi} \right]^2 \int_{-\infty}^{+\infty} \int_{-\infty}^{+\infty} R(\tau_1, \tau_2) \exp[-i(\omega_1 \tau_1 + \omega_2 \tau_2)] d\tau_1 d\tau_2 \quad (3.5)$$

in which

$$R(\tau_1, \tau_2) = \langle \zeta(t) \zeta(t+\tau_1) \zeta(t+\tau_2) \rangle \quad (3.6)$$

The digital (discrete) bispectrum, for discretely sampled data, is (Haubrich, 1965; Kim and Powers, 1979)

$$B_{l,m} = \langle C_l C_m C_{l+m}^* \rangle \quad (3.7)$$

in which  $l$  and  $m$  are the frequency indices. The digital bispectrum for discretely sampled data can be estimated from (3.7) by ensemble averaging. It relates to a triad of waves with frequency indices  $l$ ,  $m$  and  $l+m$ .

The bispectrum  $B_{l,m}$  vanishes if:

- (1) There is no energy present at frequencies  $l$  or  $m$  or  $l+m$  (i.e., zero Fourier amplitude of any component participating in the triad interactions);
- (2) There is no phase relation (coherence) between the waves forming the triad (i.e., statistically independent free waves).

On the other hand, if the wave at  $n=l+m$  is generated through the interaction between  $l$  and  $m$ , then a phase coherence will exist and the expected value of the bispectrum will be nonzero.

The bispectrum can be efficiently computed using symmetry properties, in which it can be uniquely described by its values in a bi-frequency octant. For a digital time series with Nyquist frequency  $f_N$ , the bispectrum is uniquely defined within a triangle in  $(f_1, f_2)$ -space (bi-frequency plan) with vertices at  $(l=0, m=0)$ ,  $(l=f_N, m=0)$ , and  $(l=f_{N/2}, m=f_{N/2})$ . The relation between the continuous bispectrum  $B(\omega_1, \omega_2)$  and the discrete  $B_{l,m}$  is

$$B(\omega_1, \omega_2) = \left[ \frac{1}{\Delta\omega} \right]^2 B_{l,m} \quad (3.8)$$

in which  $\Delta\omega$  is the frequency-band,  $\omega_1 = l\Delta\omega$  and  $\omega_2 = m\Delta\omega$ .

The bispectrum can be used to identify coupled modes, however it does not give a qualitative measure of the intensity of nonlinear interactions since its value depends on the amplitudes of the three waves involved in the interaction. It is convenient to cast the bispectrum into its normalized magnitude and phase, the so-called bicoherence and biphas, given respectively by (Kim and Powers, 1979)

$$b_{l,m}^2 = \frac{|B_{l,m}|^2}{\langle |C_l C_m|^2 \rangle \langle |C_{l+m}|^2 \rangle}, \quad (3.9)$$

$$\beta_{l,m} = \arctan \left[ \frac{\text{Im} \{B_{l,m}\}}{\text{Re} \{B_{l,m}\}} \right] \quad (3.10)$$

Expressing the Fourier coefficient  $C$  in terms of magnitude  $|C|$  and phase  $\phi$ , the biphas is (Kim et al., 1980)

$$\beta_{l,m} = \phi_l + \phi_m - \phi_{l+m} \quad (3.11)$$

In a random wavefield with statistically independent components, the phases are

randomly distributed between  $-\pi$  and  $\pi$ , and thus the biphase-values tend to be scattered between  $-\pi$  and  $\pi$ .

Clearly, the bicoherence is independent of the wave amplitude, unlike the bispectrum. For the bicoherence normalization given by (3.9), the bicoherence value is bounded by zero and 1 (i.e.,  $0 \leq b^2 \leq 1$ ). Zero-value of bicoherence indicates statistically uncorrelated waves. On the other hand, the maximum value of the bicoherence is unity, implying fully coupled waves. For a three-wave system, Kim and Powers (1979) show that  $b^2(l, m)$  represents the fraction of the total energy at the sumfrequency ( $n=l+m$ ) due to the nonlinear interaction.

For a finite-length time series even a truly Gaussian process will have a non-zero bispectrum. A 95% significance level on zero bicoherence is given by Haubrich (1965) as

$$b_{95\%}^2 \geq 6/\text{d.o.f} \quad (3.12)$$

where d.o.f. is the number of degrees of freedom in the bispectral estimates.

Confidence limits on the estimates of bicoherence depend on the true value of bicoherence, but it has been shown that the variance of bicoherence estimates is less than  $2/\text{d.o.f.}$  (Kim and Powers, 1979). Confidence levels for estimates of biphase depend on bicoherence values and the number of degrees of freedom. Biphase estimates for frequency pairs with very low bicoherence are unstable and tend to randomly distributed values between  $-\pi$  and  $\pi$ .

### 3.3 Skewness and asymmetry

The so-called skewness and asymmetry of the sea surface are profile distortions caused by the presence of bound harmonics due to nonlinear interactions. The so-called skewness is the lack of symmetry with respect to the horizontal. Skewed profiles of gravity water waves are characterized by sharp crests and flat troughs (Stokes-type wave), in which the harmonics are phase-locked and

in phase with the primary. The name derives from the fact that the probability density function of these profile is skewed. On the other hand, the asymmetry is the lack of symmetry with respect to the vertical. Asymmetric profiles are usually characterized by steep forward fronts and mild rear faces (nearly saw-toothed shape), in which the harmonics are phase-locked and leading the primary.

The skewness of a random variable ( $\underline{x}$ ) is conventionally defined as its normalized third central moment:

$$S = \frac{\langle (\underline{x} - \mu_x)^3 \rangle}{\sigma_x^3} \quad (3.13)$$

Here,  $\mu_x$  and  $\sigma_x$  are the mean and the standard deviation of  $\underline{x}$ .

The mean square, or the variance of the surface elevation can be recovered from the integral of the energy spectrum, i.e. (using the discrete form)

$$\langle \zeta^2(t) \rangle = \sum_{p=-\infty}^{\infty} E_p \quad (3.14)$$

Hasselmann et al. (1963) showed that the integral over the real part of the bispectrum recovers the mean cube, or third-order moment of the surface elevation

$$\langle \zeta^3(t) \rangle = \sum_{l=-\infty}^{\infty} \sum_{m=-\infty}^{\infty} \text{Re} \{ B_{l,m} \} \quad (3.15)$$

The skewness or the nondimensional mean cube of the surface elevation can be obtained by normalizing (3.15) by the variance to the power 3/2:

$$S = \frac{\langle \zeta^3(t) \rangle}{\langle \zeta^2(t) \rangle^{3/2}} \quad (3.16)$$

Similarly, the asymmetry of the surface elevation can be obtained from the

integral over the imaginary part of the bispectrum after normalization with the variance to the power 3/2:

$$A = \frac{\sum_{l=-\infty}^{\infty} \sum_{m=-\infty}^{\infty} \text{Im} \{B_{l,m}\}}{\langle \xi^2(t) \rangle^{3/2}} \quad (3.17)$$

The skewness and asymmetry represent overall measures of nonlinearity and indicate the departure of the wave profile statistics from the Gaussian distribution. These parameters are used in the analysis of data presented in the following sections.

### 3.4 Bispectral evolution of shoaling waves

Observations of shoaling waves are analyzed to elucidate the phenomenon of harmonic generation in the shoaling region and the surf zone. The objectives of these analyses are to determine the significant interactions that lead to harmonic generation and the influence of wave breaking on the intensity of nonlinear couplings.

#### *Experimental data*

The so-called Delta Flume '93 experiment reported by Arcilla et al. (1994), also Roelvink and Reniers (1995), has yielded time series of surface elevation on a large-scale sandy 2DV beach in a laboratory. Three different wave conditions were used representing slightly erosive, highly erosive, and strongly accretive conditions. These wave conditions resulted in development of a nearshore sand bar.

Surface elevation measurements taken from the Delta Flume experiment of random waves propagating over a barred beach have been employed here to examine nonlinear couplings. The target spectrum was narrow-banded with peak frequency of 0.125 Hz and significant wave height of 0.60 m. The initial bottom geometry was a barred beach profile with deep water depth of 4.1 m.

Time series of surface elevation were obtained at several locations at a 10 Hz sampling rate. The measurement locations and the bottom geometry used here are shown in Fig. 3.1.

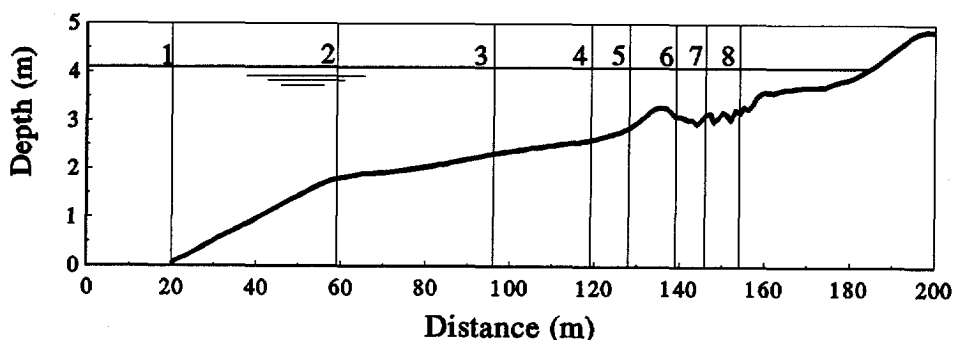


**Figure 3.1** *Bed profile and locations of wave gauges (Arcilla et al., 1994)*

### *Analysis and results*

The surface elevation spectra are shown in Fig. 3.2. In the shoaling regions, strong energy transfers occur from the primary to the higher harmonics. In shallow water over the bar, wave breaking takes place leading to reduction of the total energy.

The bispectra are computed according to equation (3.7), in which the complex Fourier amplitudes  $A_p$  were determined from the time records with a standard FFT-algorithm. The data were processed by dividing the record into equal segments, each of 102.4 seconds duration resulting in a frequency resolution for the raw data of 0.00976 Hz. The bispectral estimates are obtained by ensemble averaging over 28 segments. Therefore the number of degrees of freedom in the estimates is 56.

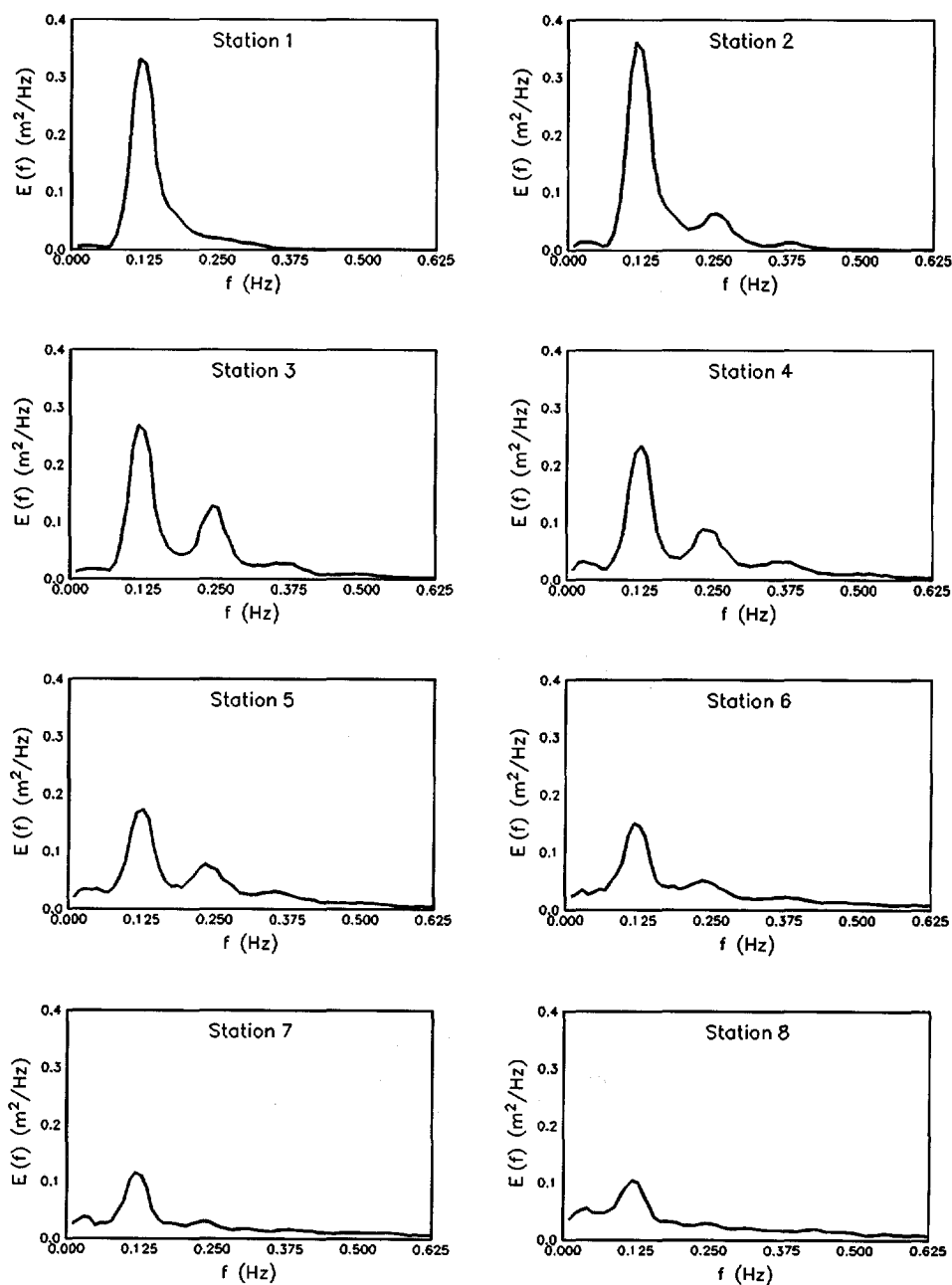
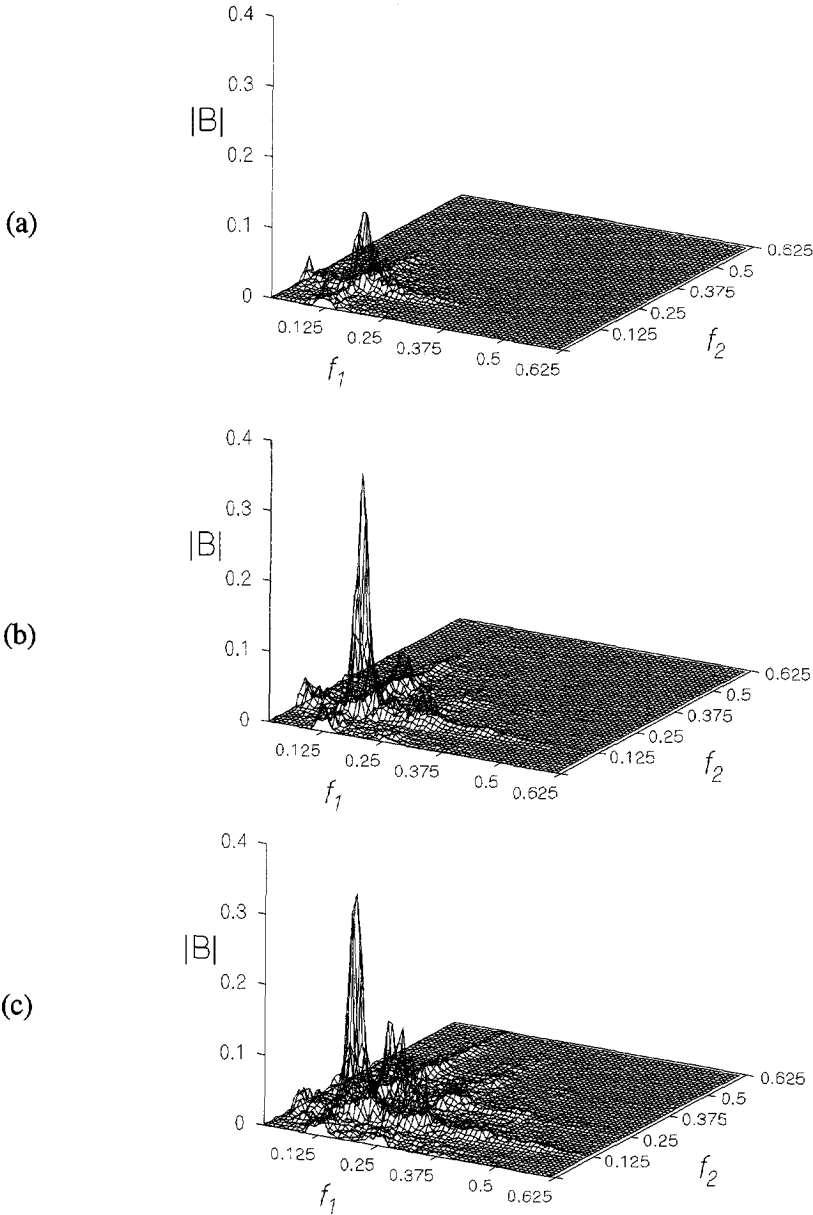
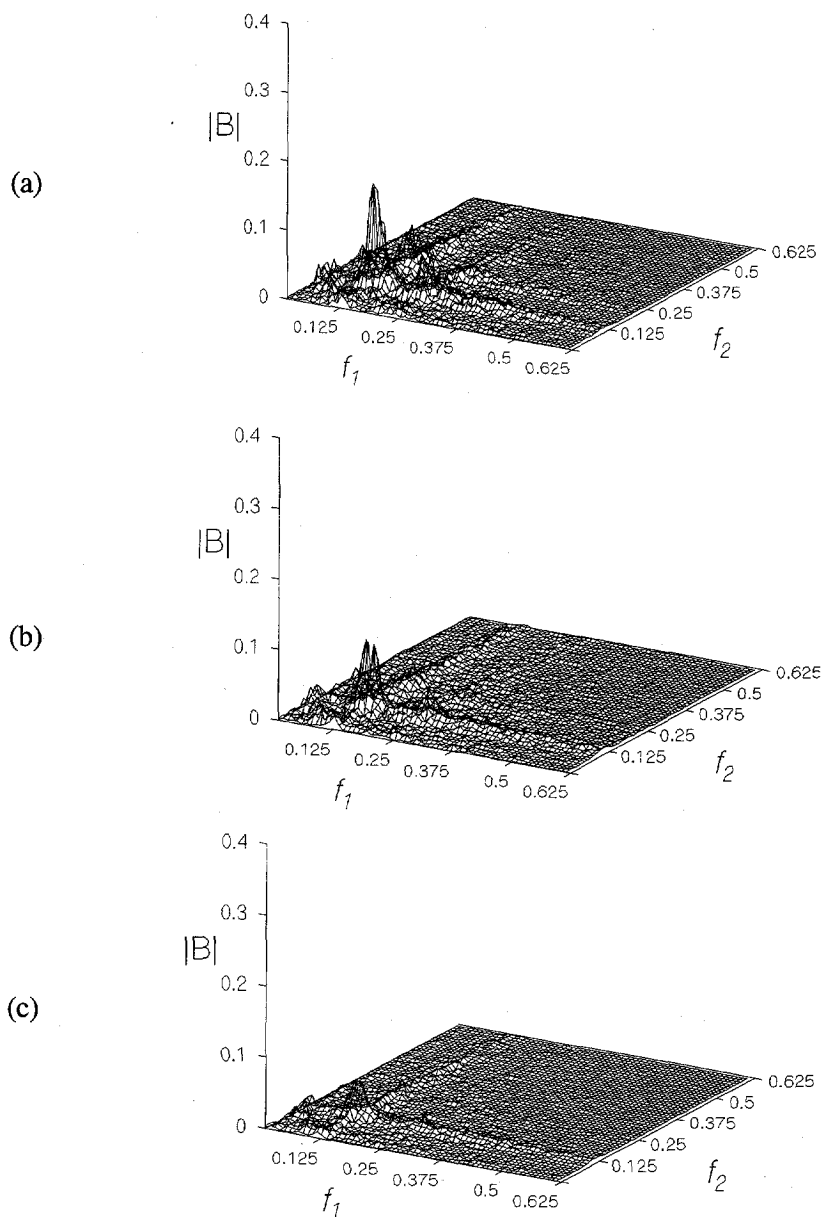


Figure 3.2 Surface elevation spectra. Measurements from Arcilla et al. (1994)



**Figure 3.3** Bispectra at three stations, from top to bottom: panel (a) station 1, (b) station 3, (c) station 4. Frequency  $f$  in Hz. Absolute bispectrum  $|B|$  in  $\text{cm}^3/\text{Hz}^2$ .





**Figure 3.4** *Bispectra at three stations, from top to bottom: panel (a) station 5, (b) station 6, (c) station 7. Frequency  $f$  in Hz. Absolute bispectrum  $|B|$  in  $\text{cm}^3/\text{Hz}^2$ .*

Absolute values of the continuous bispectra (computed using equation 3.8) for six stations are given in Figs. 3.3 and 3.4, where only the positive quadrants ( $f_1, f_2 > 0$ ) are shown. Note that the bispectra are symmetric around the diagonal  $f_1 = f_2$ .

The bispectrum at the upwave boundary is shown in panel (a) in which a weak bispectral peak already exists at (0.125 Hz, 0.125 Hz). This peak indicates the self-interaction of the primary at 0.125 Hz with itself leading to the first harmonic at 0.25 Hz. After propagation 39 m over a decreasing water depth, the bispectrum (Fig. 3.3, panel b) shows amplification of the 'self-interaction' peak of the primary. This peak suggests strong interaction, forcing first harmonics, i.e., second-order Stokes-type nonlinearity. A less pronounced bispectral peak exists at (0.125 Hz, 0.02 Hz). This peak indicates phase-coupling between the primary and the low-frequency waves. Physically, this peak is attributed to the interactions between neighboring primary waves; the resultant wave group forces a long wave at the difference frequency that is phase coupled to the group. Another bispectral peak starts to develop at (0.125 Hz, 0.25 Hz), indicating interaction between the primary and its first harmonic resulting in energy transfer to the second harmonic. This peak is intensified after propagation of an additional 47 m in shoaling waters (panel c) and a new bispectral peak appears at (0.25 Hz, 0.25 Hz) indicating the self-interaction of the first harmonic. Note that the bispectral peak at (0.125 Hz, 0.125 Hz) does not show significant changes compared with the previous location (panel b).

As the wavefield propagates into shallower water, wave breaking takes place leading to energy dissipation. The bispectral peak at (0.125 Hz, 0.125 Hz) is significantly damped compared with the spectral peaks of the other interactions (Fig. 3.4, panel a). Over the bar, most of the bispectral regions show substantial reduction in their intensities (Fig. 3.4, panels b and c) owing to strong wave breaking.

Since the bispectrum depends on the wave amplitude, it is expected that the bispectral values reduce in regions of strong wave breaking due to energy dissipation. Conclusion about the influence of wave breaking on the nonlinear couplings requires a measure of nonlinear coupling that is independent of the wave amplitude. This is the normalized bispectrum, i.e., bicoherence.

Bicoherence functions have been calculated from the records using equation (3.9). These calculations were restricted to those frequency pairs for which the absolute value of the bispectral density exceeded 5% of the maximum value in the same bispectrum in order to suppress noisy and spiky results. Isolines of  $b(f_1, f_2)$  at station 1 and 4 are shown in Fig. 3.5.

The results show a strong increase of the region of significant bicoherence between station 1 and 4. The bicoherence at station 4 shows distinct regions of high intensities at the harmonics of the primary waves. The variations of the maximum squared bicoherence over the beach profile are shown in Fig. 3.6. The bicoherence values for the harmonic interactions increase over the shoaling region; farther shoreward bicoherence values are substantially reduced owing to wave breaking.

The overall nonlinearity parameters, skewness and asymmetry, have been calculated at several locations using equations (3.16) and (3.17). Their variations over the beach profile are shown in Fig. 3.7. The skewness increases significantly in the shoaling region, reaches a maximum value before the bar crest, and decreases beyond the bar mainly due to wave breaking.

The variation of the asymmetry shows a different trend than the variation of the skewness. In most of the shoaling region, the values of the asymmetry remain rather low. They increase rapidly over the bar. Farther beyond the bar, the asymmetry decreases due to wave breaking.

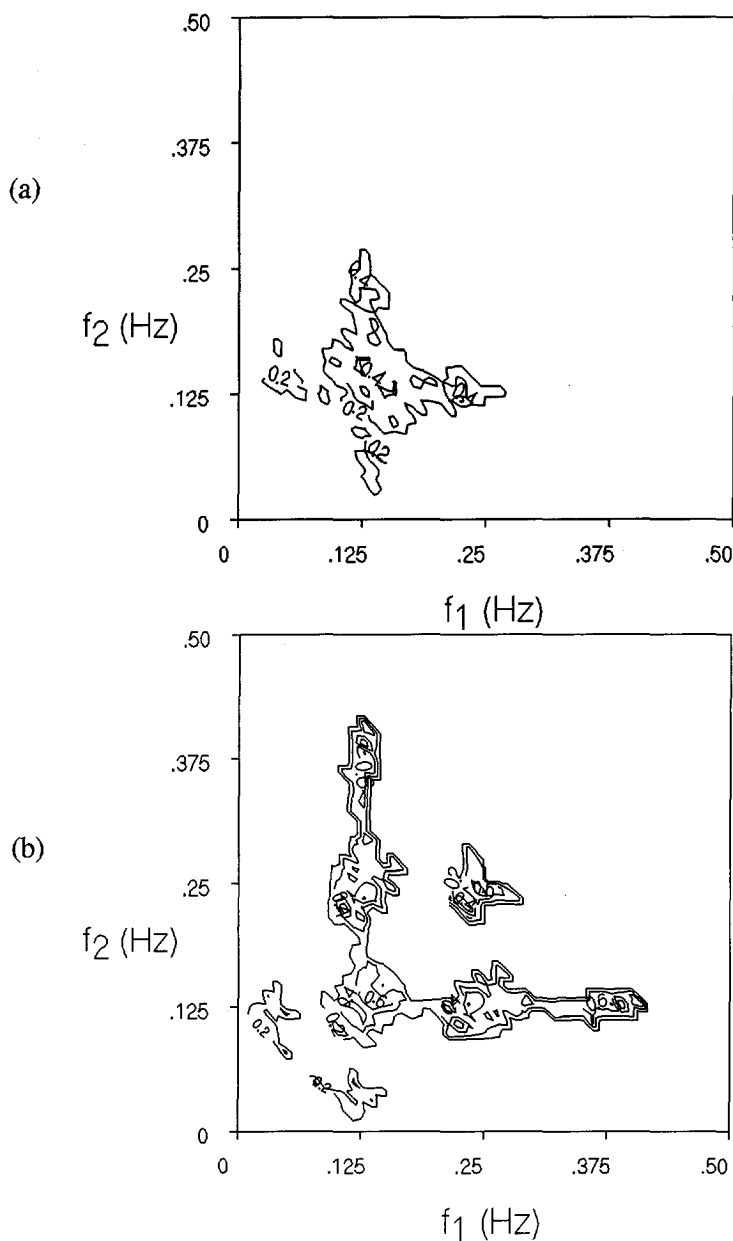


**Figure 3.5** Bicoherence at two stations, from top to bottom: panel (a) station 1, (b) station 4. Frequency  $f$  in Hz. The minimum bicoherence-contour level is 0.2, with additional contours every 0.2.

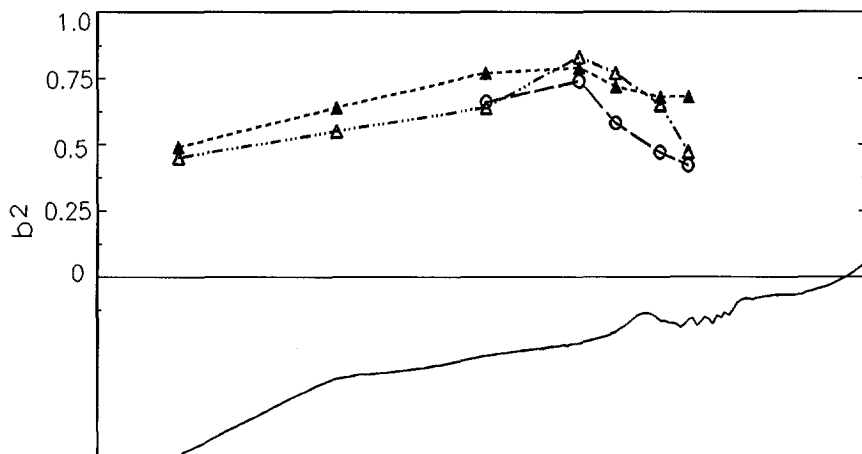


**Figure 3.6** The spatial variations of the maximum bicoherence  $b^2$  of the harmonic interactions for random wave propagation over a beach profile.  $\blacktriangle$ :  $(f_p, f_p)$ ;  $\triangle$ :  $(f_p, 2f_p)$ ;  $\circ$ :  $(2f_p, 2f_p)$

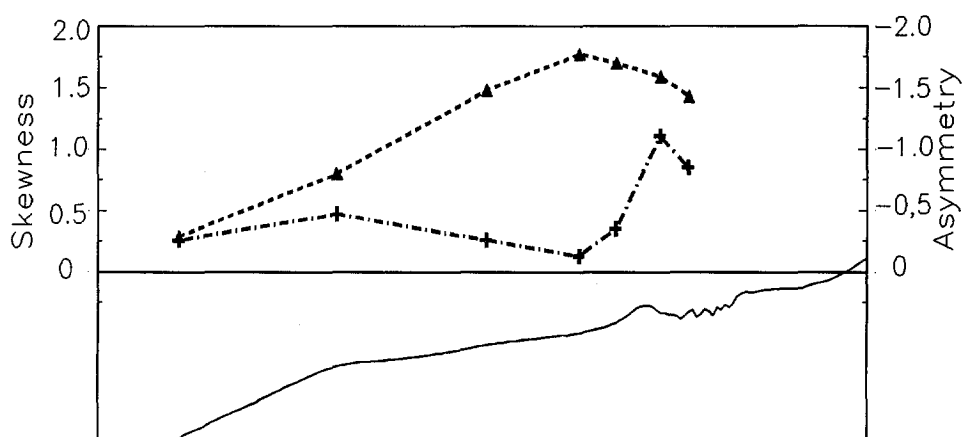


**Figure 3.7** The spatial variations of skewness (dashed line) and asymmetry (dot dashed line) for random wave propagation over a beach profile

*Summary and conclusions*

The bispectral analysis of shoaling breaking waves has shown that in the outer part of the shoaling region, weak nonlinearity and the moderate dispersion characteristics lead to off-resonant energetic triad interactions. In this region bound waves that are locked and in phase with the primary are amplified resulting in skewed wave profiles of Stokes-type. In the inner part of the shoaling region, nonlinearity increases and waves become nearly nondispersive, the near-resonant triad interactions result in amplification of the harmonics and force them into forward phase shifts with respect to the primary. These phase modifications lead to rapid increase in the asymmetry (nearly saw-toothed shape) and a slight reduction in skewness. As waves enter the surf zone, wave breaking substantially weakens the intensity of nonlinear couplings. This is evident from the reduction in the bicoherence levels as well as the skewness and asymmetry values.

### 3.5 Nonlinear coupling in waves passing over a bar

#### 3.5.1 Introduction

Nonlinear coupling between spectral components is examined as the wavefield evolves while passing over a shallow bar followed by a deepening region. The conventional viewpoint is that on the seaside, the harmonics, bound to the primary, are amplified because of the increasing nonlinearity in the shoaling region, and that they are released on the shoreside, at least partially, because of the decreasing nonlinearity in the deepening region. Strictly speaking, however, even in the shoaling region free components are generated as a result of the nonhomogeneity, whereas conversely some degree of phase lock may remain in the deepening region. If the latter were true then the wavefield beyond a bar region is statistically inhomogeneous and thus cannot fully described by the energy density spectrum without the need for additional, site dependent phase information.

A question which deserves attention in this context relates to the possibility of a "memory" in the wavefield on the downwave side of the bar, of what happened over the bar. Such "memory" is equivalent to a persistent phase lock between harmonics. This in turn can imply spatial nonhomogeneity. This possibility is well established for the interaction between a discrete, finite set of wave components in shallow water, in particular a monochromatic wave and its harmonics, where a recurrent pattern of cross-spectral energy transfer back and forth occurs, resulting in spatially periodic amplitude variations. However, these effects are expected to cancel out in case of a continuous spectrum. (Moreover, the nonlinearity will decrease as the waves move into deeper water.) If this is indeed the case, the wavefield shoreward side of the bar would again be statistically homogenous. Knowledge of the energy spectrum on the downwave side without specific additional phase information from "upwave" regions would then be sufficient to characterize the wavefield in a statistical sense.

The description given above of the generation and release of harmonics is qualitative, as is usually the case. Here these phenomena are investigated quantitatively. The approach taken here is essentially experimental, with a numerical extension. Time series of surface elevation at various locations are analyzed in the time-domain and in the frequency-domain to determine the bispectrum, bicoherence, biphas, skewness and asymmetry. The spatial variations of these nonlinearity indicators over and beyond the bar are of special interest, in view of the question raised above.

### **3.5.2 Analysis of experimental data**

#### *Experimental data*

Experiments with random waves reported by Beji and Battjes (1993) have yielded time series of surface elevation at a number of stations over a bar and on either side of it. The bottom profile used in the experiments is shown in Fig. 3.8. A submerged trapezoidal bar was constructed, consisting of an upslope of 1:20 and a 2 m horizontal crest followed by 1:10 downslope. The still-water

depth was 0.10 m over the bar crest, and 0.40 m in the deep-water regions. At the end of the flume opposite to the wave generator, a plane beach with 1:25 slope was present from a previous experiment; it acted merely as a wave absorber. The flume was equipped with a hydraulically driven, piston-type random wave generator. The control signal is provided via a personal computer, which is connected to a converter that supplies the voltage input for the amplifier which in turn sends the amplified signal to the driver.

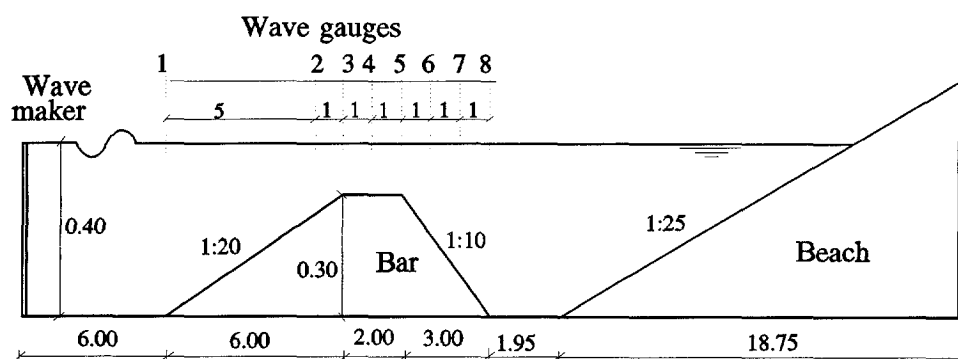


**Figure 3.8** Layout for the experimental setup of Beji and Battjes (1993). All lengths are expressed in meters.

Surface elevations were measured at stations 1 to 8. Station 1 is at the beginning of the upslope side of the bar, station 2 is 5.0 meters from station 1, and stations 3 to 8 are positioned every 1.0 meter. The sampling frequency was 10 Hz, for a total of 9000 data points. The target spectrum for the data used here was narrow-banded with peak frequency of 0.40 Hz and variance of 0.35 cm<sup>2</sup>.

### *Analysis and results*

These measurements have been analyzed to address the questions raised above. The analyses are mainly in the frequency-domain. Energy spectra for these observations (Fig. 3.9) indicate significant transfers of energy from the spectral peak to higher frequencies.



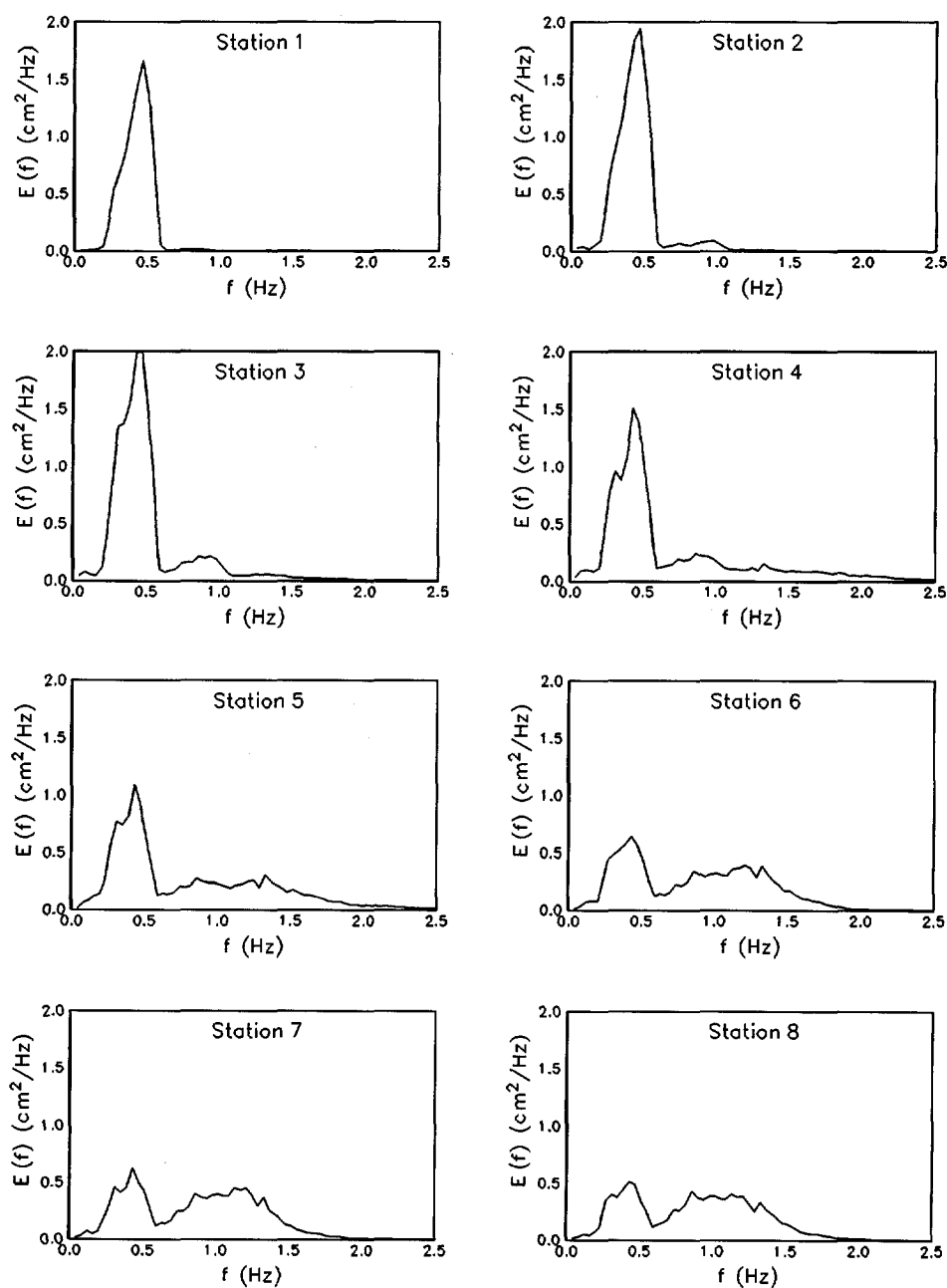


**Figure 3.9** Surface elevation spectra of nonbreaking waves propagating over a bar. Measurements from Beji and Battjes (1993)

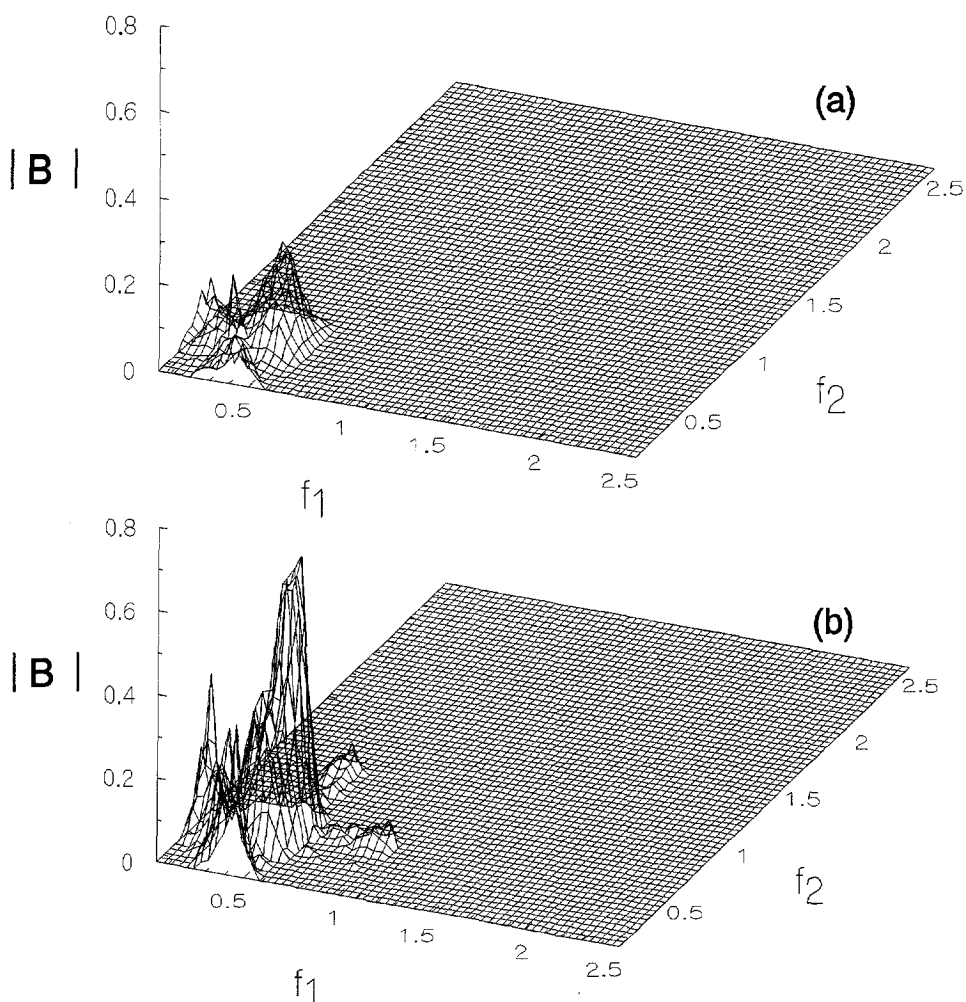


**Figure 3.10a** *Bispectra, panel (a) station 1, (b) station 2. Frequency  $f$  in Hz. Absolute bispectrum  $|B|$  in  $\text{cm}^3/\text{Hz}^2$ .*

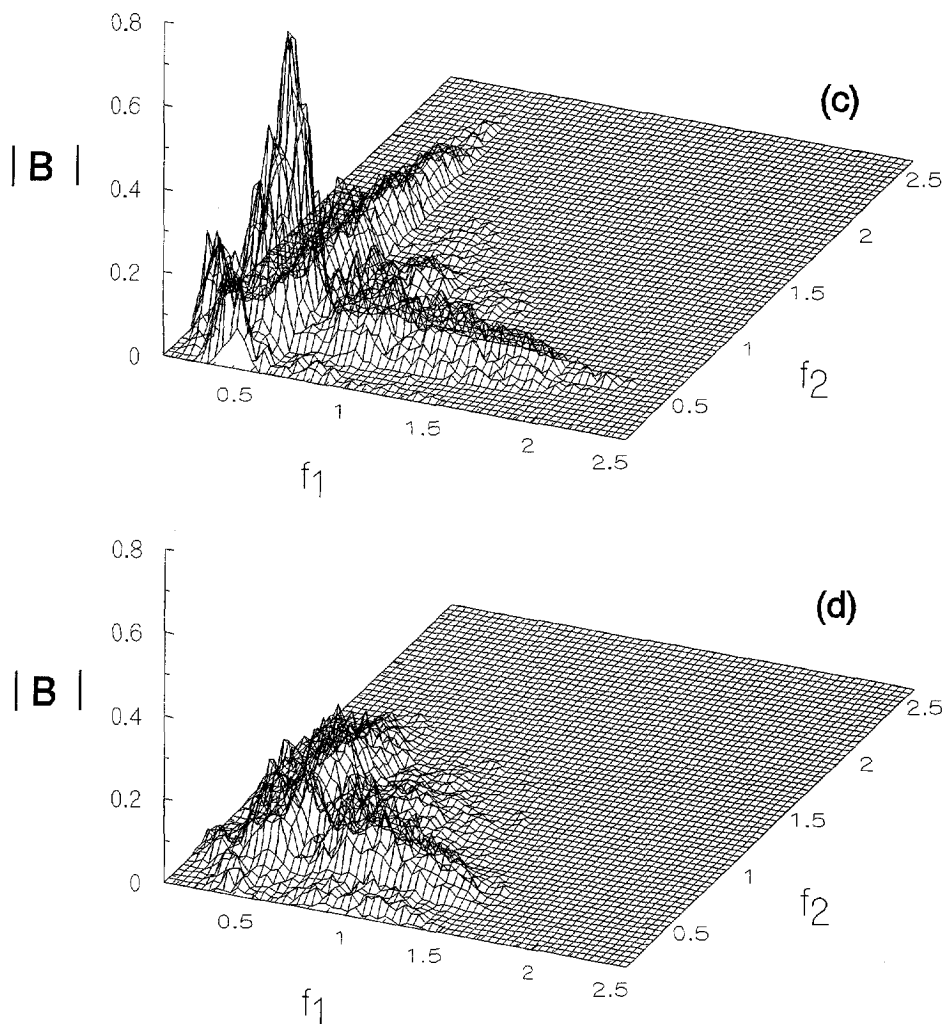


**Figure 3.10b** Bispectra, panel (c) station 4, (d) station 8. Frequency  $f$  in Hz. Absolute bispectrum  $|B|$  in  $\text{cm}^3/\text{Hz}^2$ .

The bispectra have been computed according to equations (3.7) and (3.8) with ensemble averaging over 33 segments, each of 25.6 seconds duration (10 Hz sampling rate). Therefore, the number of degrees of freedom in the estimates is 66. Absolute values of the computed bispectra for four stations are given in Figs. 3.10a, b. They show significant quadratic self-interactions of the primary waves in the regions near the spectral peak, and interactions between these components and their harmonics, with intensity increasing on the upslope to a maximum over the bar crest (panel c) and decreasing again to low values in deep water beyond the bar (panel d).

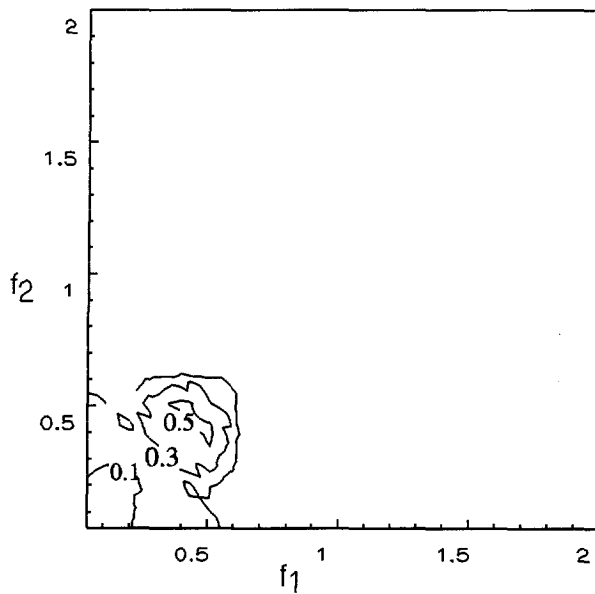


**Figure 3.11a** *Isolines of bicoherence  $b$  at station 1. Frequency  $f$  in Hz.*

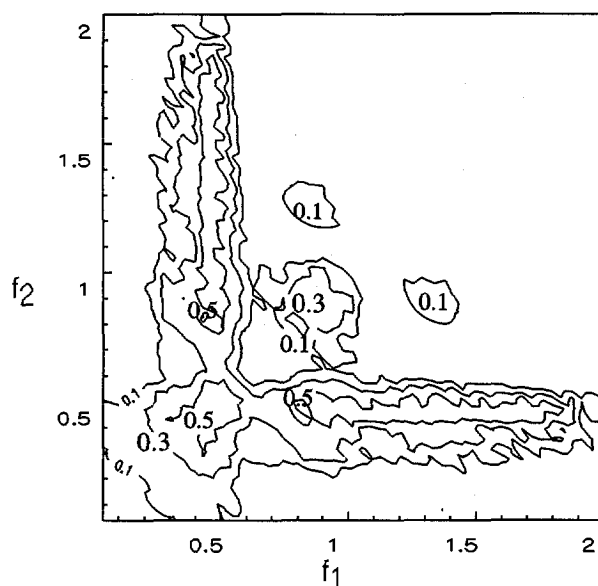


**Figure 3.11b** *Isolines of bicoherence  $b$  at station 4. Frequency  $f$  in Hz.*

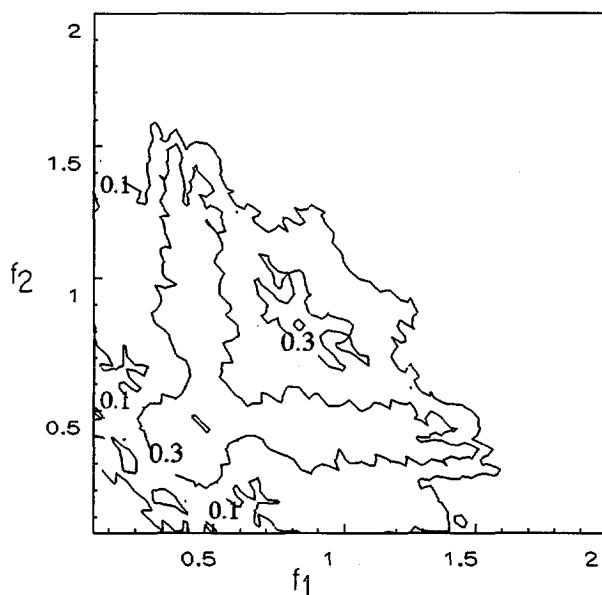


**Figure 3.11c** *Isolines of bicoherence  $b$  at station 8. Frequency  $f$  in Hz.*

Bicoherence functions have been calculated from the records using equation (3.9). Noisy and spiky results have been suppressed by limiting the calculations to those frequency pairs for which the absolute value of the bispectral density exceeded 5% of the maximum value in the same bispectrum. Isolines of the bicoherence  $b(f_1, f_2)$  at stations 1, 4 and 8 are shown in Figs. 3.11a, b and c. These figures indicate a strong increase of the bispectral region with significant values of the bicoherence, which persists even on the leeside of the bar. The bicoherence values vary less with the depth than we had expected. Values of  $b^2_{max}$  are shown in Fig. 3.13. They vary from 0.33 at station 1, through a maximum of 0.53 at station 2, to 0.28 at stations 6 and 8.

The biphas has been computed from the bispectrum using equation (3.10) for selected frequency-pairs. These pairs represent the self-interactions of the primary denoted as  $(f_p, f_p)$ , and the interaction between the primary and the first harmonic denoted as  $(f_p, 2f_p)$ , and with the second harmonic denoted as  $(f_p, 3f_p)$ .

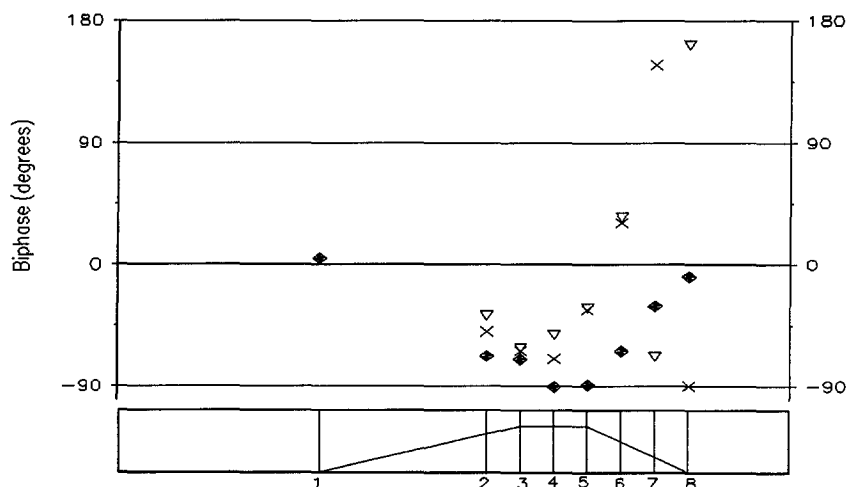


**Figure 3.12**

*Biphase for selected frequency pairs in random wave propagating over a bar. ◆  $(f_p, f_p)$ ; ×  $(f_p, 2f_p)$ ; ▽  $(f_p, 3f_p)$ .*

The variations in the biphase-values over the bar are plotted in Fig. 3.12. At station 1, the biphase of only the  $(f_p, f_p)$  interaction is shown; biphases of the other interactions are not plotted because no energy exists at the higher harmonics. The near-zero value of the biphase at station 1 implies Stokes-type waves with sharp crests and flat troughs. As the waves propagate over the upslope side of the bar, the biphases converge to a value of  $-\pi/2$  over the bar crest implying a wave pitched forward (nearly saw-toothed shape). Over the downslope of the bar the biphase-value of the  $(f_p, f_p)$  interaction evolves back to near zero-values. On the other hand, the biphases of the harmonic interactions tend to be randomly scattered beyond the bar. The evolution of the biphases over and beyond the bar implies that the higher harmonics seem to be released beyond the bar due to decreasing nonlinearity.

The variation of the skewness and asymmetry over the upslope, the bar crest and the downslope is shown in Fig. 3.13. As a check on the bispectral calculation, the skewness obtained directly from the time series (time-average equivalent of equation 3.13) is also shown. The agreement is good. The variations of skewness and asymmetry in Fig. 3.13 indicate a significant increase on the upslope to a maximum over the bar. On the lee side of the bar, the skewness and asymmetry decrease rapidly to near-zero values, comparable to those on the exposed side of the bar. This in turn means absence of significant nonlinear interactions at the downwave side of the bar. We expect that for random waves with a continuous spectrum, this will imply spatial homogeneity.

The spatial coverage of the experimental data (up to station 8) is not enough to check or to illustrate this. Therefore, a numerical "wave flume" has been employed to obtain computed signals in the region beyond that of the measurements (farther downwave). Results are described below.

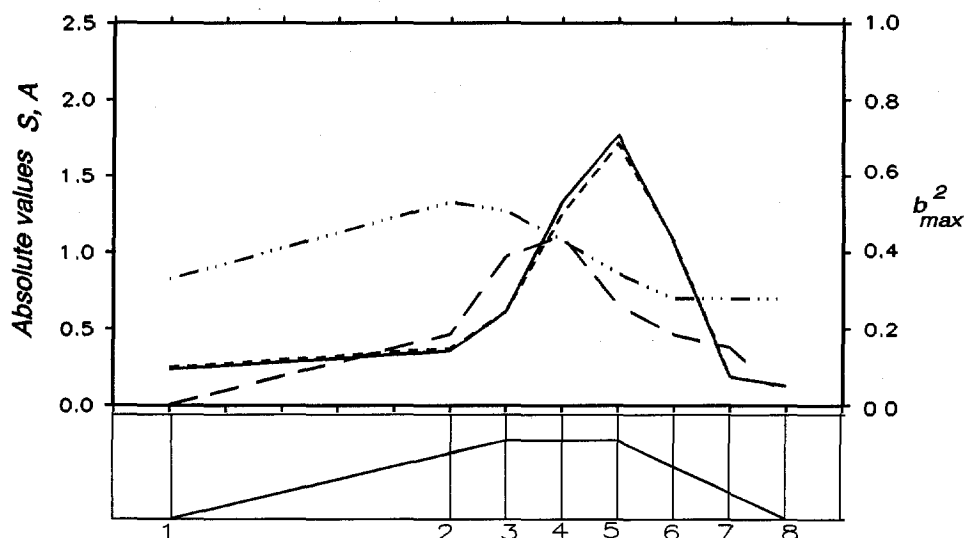


**Figure 3.13** *Spatial variation of indicators of nonlinearity in the physical wave flume. Solid line: skewness from time series; short dash: skewness from bispectra; long dash: asymmetry from bispectra; three-dots and dash: maximum squared bicoherence.*

### 3.5.3 Analysis of numerical-model results

#### *Model formulation*

Numerical simulations were performed using a 1-D extended Boussinesq model (Beji and Battjes, 1994) with improved dispersion characteristics, as in Madsen and Sørensen (1992), describing relatively long, small amplitude waves propagating in water of slowly varying depth. Reference is made to chapter 4 for a detailed description of Boussinesq theory. The model formulation used in the numerical computation is given in chapter 4 by equation (4.16). This set of equations has been integrated numerically using a difference scheme and validated against measurements of wave propagation over a bar as described by Beji and Battjes (1994).



In the computation, the initial condition used is the unperturbed state. The upwave boundary condition at station 1 is specified from the measurements of surface elevation there at each time step. At the outgoing boundary, an absorbing boundary condition has been used to ensure that the disturbances leave the computational domain without reflection.

### Analysis

The model performance in simulating the nonlinear propagation of waves over a bar has been examined as follows. The original physical experiment has been simulated and the numerical output, at the position of the wave gauges, has been analyzed in the frequency-domain to obtain skewness and asymmetry (equations 3.16 and 3.17). The spatial variations of these parameters are compared with those obtained from the analysis of the measurements in the physical experiment (Fig. 3.14).

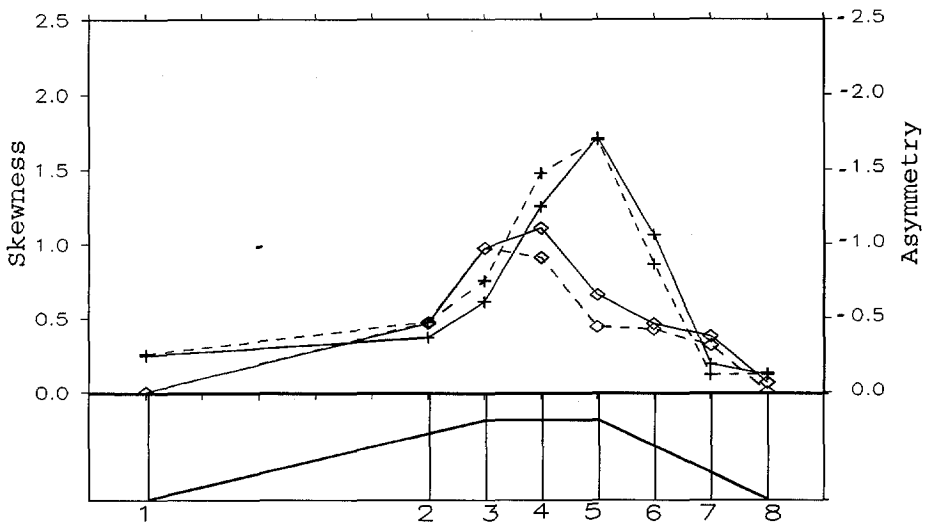


**Figure 3.14** Skewness (+) and asymmetry (◇) obtained from the bispectra: comparisons between results from the physical wave flume (solid lines) and the numerical wave flume (dashed lines).

The comparison shows the ability of the numerical model to reproduce the nonlinear evolution of waves propagating in varying water depth with sufficient accuracy for the present purpose.

#### *Numerical simulation for extended region*

Additional time-domain numerical computations have been performed extending to distances farther downwave in order to examine the homogeneity of the wavefield in that region. The computational domain now extends to station 16 at 11 m farther downwave from the bar; the distances between stations 9 to 13 are 1.0 m and those between stations 14 to 16 are 2.0 m.

Computations are done for two different upwave boundary conditions, corresponding to sinusoidal and irregular waves. The former is to demonstrate the spatial inhomogeneity associated with the interference between a single primary wave and its free harmonics. The latter is to investigate the matter for the case of a continuous spectrum, where the innumerable interferences are expected to cancel, resulting in a homogeneous wavefield. To demonstrate the contrast between the two cases, the nonlinearity parameter (amplitude to depth ratio  $a/h$ ) is kept constant by imposing the same surface elevation variance at the upwave boundary. The computations are performed for the same record duration as in the physical experiment, and the computed signals at stations 1 to 16 have been analyzed in the frequency-domain in the same manner as the experimental records.

Fig. 3.15 shows the spatial variations of the harmonics' amplitudes in case of sinusoidal incident waves. Over the bar, a significant energy transfer takes place into the first, second, and third harmonics. Beyond the bar, the amplitudes do not vary because of absence of nonlinear interactions.

The corresponding variations in the skewness and asymmetry are shown in Fig. 3.16. They indicate a significant increase on the upslope to a maximum over the bar as a result of harmonic generation. On the downslope side of the bar, the skewness and asymmetry decrease rapidly to values between  $\pm 0.5$ . Beyond the bar, although the amplitudes of the harmonics are nearly constant, the skewness

and asymmetry vary significantly as a result of the varying phase lags between the freely propagating component-waves, resulting in a spatially nonhomogeneous wavefield.

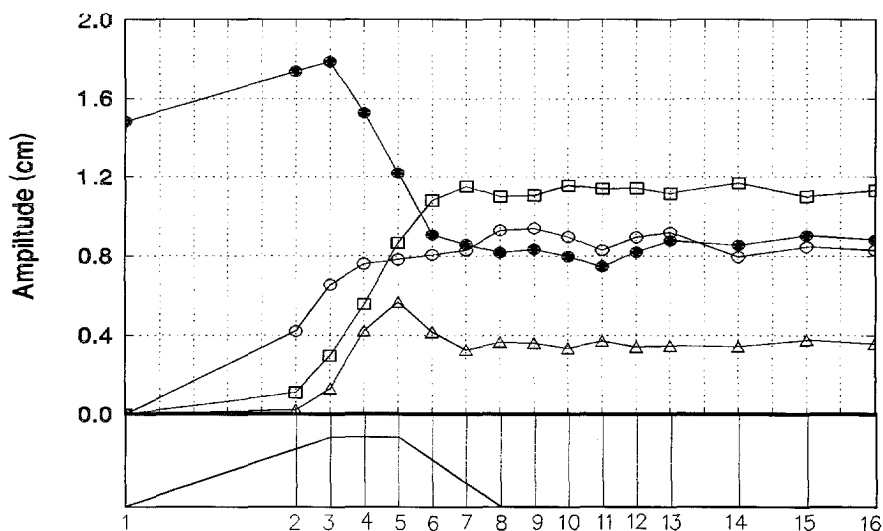


**Figure 3.15** *Spatial variations of the amplitudes of the primary wave and its harmonics primary wave (●), first harmonic (○), second harmonic (□), and third harmonic (△).*

Fig. 3.17 shows the variations of skewness and asymmetry of irregular waves over the upslope, the bar crest, the downslope and farther downwave; the latter is of particular interest here. It shows that over the horizontal region beyond the bar, the skewness and asymmetry remain at near-zero values (less than 0.2), comparable to those on the exposed side of the bar, without any significant spatial variations, in contrast to the case of sinusoidal waves. (For skewness values less than 0.2, Ochi and Wang (1984) found virtually no deviation from the Gaussian probability density of the sea surface elevation.) This implies that there is no memory of the bar location, in contrast to the discrete case. The practical implication of this is that the waves downwave from the bar can again be assumed to have independent, random phases and that the wavefield is spatially homogeneous.

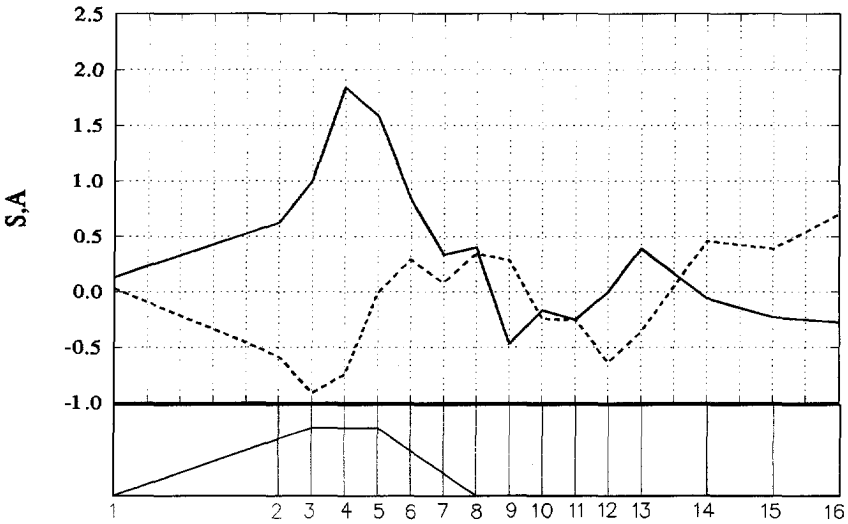


**Figure 3.16** *The spatial variations of skewness (solid line) and asymmetry (dashed line) for sinusoidal incident waves.*

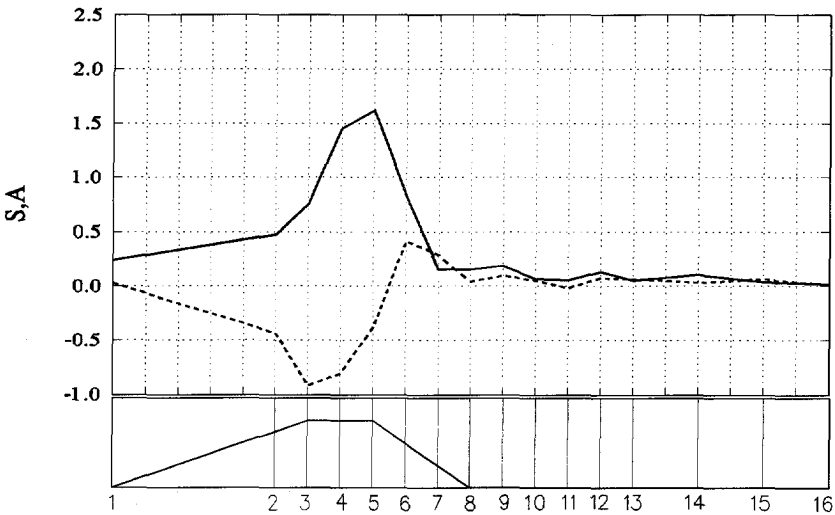


**Figure 3.17** *The spatial variations of skewness (solid line) and asymmetry (dashed line) for irregular waves.*

### 3.6 The evolution of the biphas

Since the biphas depends on the ratio of the imaginary to the real part of the bispectrum, which are related to skewness and asymmetry, respectively, it is not surprising that the biphas is related to the wave shape. For statistically independent free waves, in deep water, the biphas values are scatter over  $2\pi$ . A biphas of zero is associated with wave shape of sharp crest and flat trough (Stokes-type wave). A biphas-value of  $-\frac{1}{2}\pi$  is associated with a wave pitched forward (nearly saw-toothed shape).

Elgar and Guza (1986) have analyzed the evolution of the observed biphas between the energy-spectral peak and its harmonics in a shoaling wavefield on a beach. Their data show that the biphas evolves from values scattered around zero in 9 m depth to about  $\beta = -\frac{1}{2}\pi$  in very shallow water. They have also used a spectral Boussinesq model to examine numerically the effects of initial phase coupling and bottom slope on the nonlinear evolution. They found that the gross trends in the evolution of nonlinear quantities (such as skewness, asymmetry, and biphas) are insensitive to the initial phases as well as the bottom slope.

Recently Doering and Bowen (1995) examined the dependence of the biphas evolution on the relative depth  $kh$  by analyzing field data and confirmed that the evolution of the biphas for triad interaction does have a  $kh$  dependence. They also found indications for a dependence on the finite amplitude  $a/h$ . This combination of an  $(a/h)$  and  $(kh)^2$  suggests an Ursell number dependence.

To examine a possible parametrization for the biphas evolution, laboratory measurements for random wave propagation over a bar (Beji and Battjes, 1993) have been analyzed. The biphas evolution is investigated in nonbreaking as well as breaking waves with narrowband and broadband incident spectra. The data have been analyzed to evaluate the evolution of the biphas function and its dependence on a limited number of parameters such as those mentioned above.

Fig. 3.18 shows the biphase of the self-interactions of the primary ( $f_p f_p$ ), hereafter referred to as the primary interaction, plotted versus Ursell number, which is formally defined as the ratio of relative amplitude  $a/h$  to the square of the relative depth  $(kh)^2$ . It can be expressed in terms of integrated parameters of the wavefield as

$$Ur = \frac{g}{8\sqrt{2}\pi^2} \frac{H_s T_m^2}{h^2} \quad (3.18)$$

in which  $H_s$  is the significant wave height,  $T_m$  is the mean wave period, and  $h$  is the water depth.

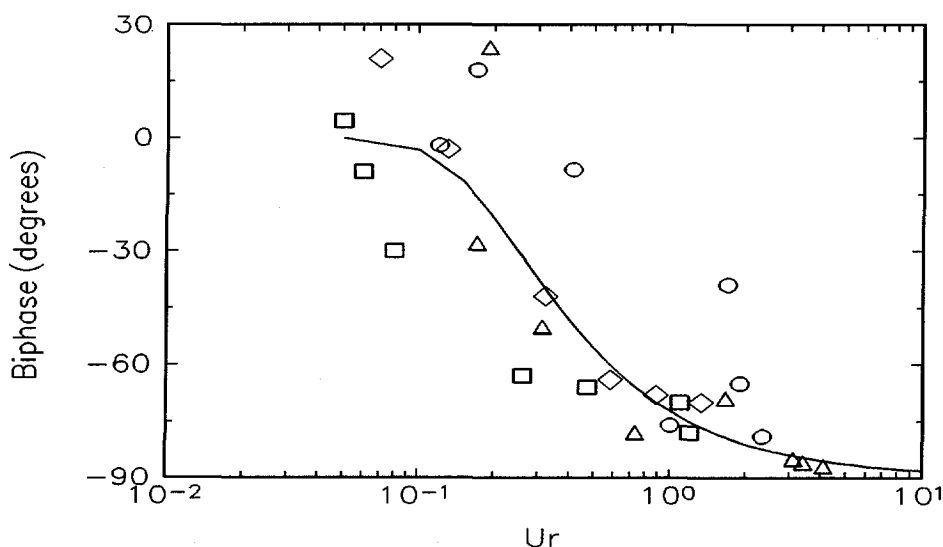


**Figure 3.18**

*Biphase of the self primary interaction ( $f_p f_p$ ) as a function of Ursell number for waves propagating over a bar.  $\square$  Nonbreaking waves with narrowband spectrum;  $\triangle$  breaking waves with narrowband spectrum;  $\diamond$  Nonbreaking waves with Jonswap spectrum;  $\circ$  breaking waves with Jonswap spectrum. Solid line: equation (3.19)*

Fig. 3.18 indicates that for small Ursell numbers (deep water), the biphase scatters round a mean value of about zero. With increasing Ursell number values, it converges toward a final value of  $-\frac{1}{2}\pi$ . These analyses suggest a crude parametrization of biphase in terms of Ursell number, expressing a gradual variation of zero biphase for  $Ur < 0.1$  (deep water) to a limit value of  $-\frac{1}{2}\pi$  in very shallow water ( $Ur \sim 10$ ). A hyperbolic tangent is fitted to the data. The relation between the biphase and Ursell number can be given by

$$\beta(f_p, f_p) = -\frac{\pi}{2} + \frac{\pi}{2} \tanh \left[ \frac{0.2}{Ur} \right] \quad (3.19)$$

Equation (3.19) will be used in a simplified representation of the effects of triad interactions in chapter 7. A similar relation for the biphase evolution has been given recently by Doering and Bowen (1995) for a parametrization of the orbital velocity asymmetries.

The dependence of the biphase on only local parameters (such as  $a/h$  and  $kh$ ) cannot be theoretically supported. The theoretical biphase evolution, based on Boussinesq equations simplified for horizontal bottom (Elgar and Guza, 1986), has a dependence on the relative depth  $kh$  and the propagation distance  $kx$ . The dependence on propagation distance is particularly evident in shallow water of constant depth: the biphase seems to evolve and yet the Ursell number is approximately constant. Inclusion of such dependency in the biphase parametrization is not desired in wind-wave application. Thus for application in spectral energy models the biphase will be parametrized in terms of the locally dependent Ursell parameter.

### 3.7 Summary and conclusions

The nonlinear transformation of wave spectra in shallow water is investigated using bispectral analyses. These analyses have been carried out to elucidate aspects of nonlinear dynamics of waves in shallow water. Laboratory observations of both shoaling waves over a beach profile and waves propagating over a shallow bar are analyzed to answer the following phenomenological questions:

1. What are the dominant triad interactions that lead to harmonic generation?
2. What is the influence of wave breaking on nonlinear couplings?
3. How do nonlinear couplings influence the phase evolution?
4. Can the biphasic evolution in shallow water be parametrized?
5. What are the dynamics of nonlinear couplings in waves propagating over a bar region?
6. Is the energy spectrum enough to describe the evolution of the wavefield beyond a bar region?

Observations of shoaling waves propagating over a laboratory beach profile showed that as the wavefield begins to shoal, phase-coupling occurs between the primary and the first harmonic. Weak nonlinearity in the shoaling region leads to significant increase in the skewness-values and yet the asymmetry-values are rather low. Further shoaling leads to phase-coupling between the primary and second harmonic and eventually with yet higher harmonics. In this region, strong nonlinearity results in a rapid increase in the asymmetry and farther enhancement of the skewness. Bicoherence levels observed just seaward of wave breaking are generally high, indicating strong nonlinear couplings. In the surf zone, wave breaking occurs leading to substantial reductions in the bicoherence, the skewness and asymmetry values.



Observations of waves passing over a shallow bar have been analyzed. The situation considered was such that significant harmonic generation took place on the upslope leading to the bar crest. The spatial variation of a number of quantitative indicators of nonlinear coupling over and beyond the bar has been investigated. These are the bispectrum function, the bicoherence function, the biphase, the skewness and the asymmetry. Results of inspection of their spatial variations can be summarized as follows.

- The variation of the values of the maximum bicoherence over the bar was very moderate (less than 50% increase between deep and shallowest water), despite the fact that significant harmonic generation took place in the approach to the bar crest.
- The region in the bispectral plane of significant bicoherence values is expanding in the shoaling region and remains extended in the deepening region, although with lower spectral levels than over the bar crest.
- The spatial variations of the skewness and asymmetry are very pronounced, with values ranging from near-zero on either side of the bar to a strong peak above it. This contrasts with the weak variation observed in the bicoherence. Also, the locations of the maximum skewness and asymmetry occur farther downwave than the maximum bicoherence. (In this regard, it should be pointed out that skewness and asymmetry are overall-measures of nonlinearity, whereas the bicoherence is a spectral variable.)
- The empirical values of skewness and asymmetry, obtained in the bar region, are well predicted with a numerical model based on the Boussinesq equations with improved dispersion characteristics.
- The numerically generated time series at the leeside of the bar showed that the skewness and asymmetry remain at near-zero values comparable to those on the exposed side of the bar, without any significant spatial variations.
- The observed evolution of biphase values is consistent with the visual observation that as waves shoal they evolve from a slightly peaked, nearly

sinusoidal shape in deep water (with biphas equals zero) to a shape characterized by a steep front face and a gently sloping rear face (biphas equals to  $-\pi/2$ ). As the waves deshoal over the downslope side of the bar, biphas of the harmonic interactions diverge from  $-\pi/2$  and tend to be randomly scattered.

- The biphas evolution seems to be dependent on local parameters such as the relative depth  $kh$  and relative wave amplitude  $a/h$ .

On the basis of the bispectral analyses carried out in this chapter, the following conclusions can be drawn.

- (1) The generation of the second spectral peak is primarily ascribed to the sum interactions between pairs of waves at the primary spectral peak.
- (2) The generation of the low-frequency waves is primarily ascribed to the difference interactions between pairs of waves at the primary spectral peak.
- (3) Wave breaking reduces the intensity of the bispectral levels and the skewness and asymmetry. Thus wave breaking weakens the strength of the nonlinear couplings.
- (4) In the initial shoaling region, weak nonlinearity leads to increase in the skewness-values only but not in those of the asymmetry, whereas strong nonlinearity in the region just before wave breaking leads to increase in the asymmetry-values.
- (5) The biphas evolution in shallow water can be crudely parametrized in terms of Ursell number. A simple algebraic relation can be used, expressing a gradual variation of zero biphas for  $Ur < 0.1$  (deep water) to a limit value of  $-\pi/2$  in very shallow water ( $Ur \sim 10$ ).
- (6) Nonlinear couplings induced by a bar region in a random wavefield vanish in the deepening region beyond the bar due to decreasing nonlinearity without memory of phase locks which existed over the bar. The wavefield on the downwave side is statistically homogeneous and can be fully described by the energy density spectrum, without the need for additional, site-dependent phase information.

---

Standard models for forecasting or hindcasting of random waves are based on phase-averaged energy formulations. In principle a nonlinear phase-resolving (Boussinesq) model can be used locally, e.g. in a bar region, the results of which can be phase-averaged afterwards to estimate energy spectra with which the computations can proceed using a phase-averaged (energy balance) model. The preceding result (6) imply that these models are suitable also on the downwave side of a shallow (bar) region with significant harmonic generation.



## Chapter 4

### 4. Deterministic modeling of wave evolution in shallow water

#### 4.1 Introduction

The nonlinear transformation of waves in shallow water is considered in this chapter from the deterministic point of view. Deterministic formulations require phase information at the deep-water boundary, and resolve the wave phase throughout the computational domain.

The arrangement of this chapter is as follows. Eulerian equations of motion for water waves are given in section 2. Various formulations of Boussinesq equations are briefly described in section 3, among which Boussinesq equations with improved dispersion characteristics. In section 4, some details of the derivation of the spectral evolution equations are given. The role of wave breaking is reviewed, formulated in a spectral form, and incorporated in the spectral evolution equations in section 5. The model is validated through comparisons with experimental data in section 6. Finally a summary and conclusions are given in section 7. (Parts of this chapter have been published in slightly different form in Eldeberky and Battjes (1996).)

#### 4.2 Eulerian equations of motion

Consider a surface gravity wavefield, with water-surface elevation  $\zeta(x,y,t)$ , propagating over a spatially varying bottom  $h(x,y)$ . A Cartesian coordinate system  $(x,y,z)$  is adopted, with  $z$  measured upwards from the still-water level. The fluid is assumed to be inviscid and incompressible, and the flow is assumed to be irrotational.

The governing equations for the fluid motion are the continuity equation and Euler's equations of motion. The continuity equation is

$$\nabla \cdot \mathbf{u} + \frac{\partial w}{\partial z} = 0 \quad (4.1)$$

and Euler's equations of motion are

$$\begin{aligned} \frac{\partial \mathbf{u}}{\partial t} + (\mathbf{u} \cdot \nabla) \mathbf{u} + w \frac{\partial \mathbf{u}}{\partial z} + \frac{1}{\rho} \nabla p &= 0, \\ \frac{\partial w}{\partial t} + (\mathbf{u} \cdot \nabla) w + w \frac{\partial w}{\partial z} + \frac{1}{\rho} \frac{\partial p}{\partial z} + g &= 0 \end{aligned} \quad (4.2)$$

where  $\mathbf{u}=(u,v)$  is the horizontal velocity vector;  $w$  is the vertical velocity;  $p$  is the pressure;  $g$  is the gravitational acceleration;  $\rho$  is the density; and  $\nabla=(\partial/\partial x, \partial/\partial y)$  is the horizontal gradient operator. The irrotationality condition is given by

$$\frac{\partial u}{\partial y} = \frac{\partial v}{\partial x} \quad \text{and} \quad \frac{\partial \mathbf{u}}{\partial z} = \nabla w \quad (4.3)$$

The fluid has to satisfy a dynamic boundary condition at the free surface and kinematic boundary conditions at the free surface and seabed. These can be expressed as:

$$p = 0 \quad \text{at} \quad z = \zeta(x, y, t) \quad (4.4)$$

$$\frac{\partial \zeta}{\partial t} + (\mathbf{u} \cdot \nabla) \zeta = w \quad \text{at} \quad z = \zeta(x, y, t) \quad (4.5)$$

$$(\mathbf{u} \cdot \nabla) h + w = 0 \quad \text{at} \quad z = -h(x, y) \quad (4.6)$$

There are three important length scales associated with the wave motion, the wave amplitude  $a$ , the wave length  $L$  (or  $k^{-1}$ ) and the water depth  $h$ . From these, two independent characteristic dimensionless parameters can be formed. One is the ratio of amplitude to depth, the so-called the nonlinearity parameter  $\epsilon$ , given by

$$\epsilon = a/h \quad (4.7)$$

The second is the relative depth, the so-called dispersion parameter  $\mu$ , defined by

$$\mu = k_0 h \quad (4.8)$$

where  $k_0$  is a characteristic wavenumber.

Combination of these two dependencies can be given by the Ursell number  $Ur$

$$Ur = \frac{\epsilon}{\mu^2} \quad (4.9)$$

In shallow water,  $\mu^2 \ll 1$ , the order of magnitude of Ursell number  $Ur$  determines the classification of the wave theory in question:

1.  $Ur \ll 1$  ( $\epsilon \ll \mu^2$ ) : linear shallow-water equations
2.  $Ur = O(1)$  ( $\epsilon = O(\mu^2)$ ) : Boussinesq equations
3.  $Ur \gg 1$  ( $\epsilon \gg \mu^2$ ) : nonlinear shallow-water equations

It is the regime with  $Ur = O(1)$  that is of interest for the present problem, in which nonlinearity significantly influences the wave propagation from deep to shallow water. Thus Boussinesq equations are the appropriate formulation to investigate harmonic generation in the course of wave evolution in shallow water.

### 4.3 Time-domain Boussinesq equations

#### 4.3.1 Introduction

Boussinesq equations represent the depth-integrated flow equations for the conservation of mass and momentum for an incompressible and inviscid fluid. For horizontal propagation of waves, the three-dimensional problem can be reduced to a two-dimensional one by integrating the equations over the water

depth. Details of the integration procedures can be found in Mei (1989).

The Boussinesq equations include nonlinearity as well as frequency dispersion. Basically the frequency dispersion is introduced in the flow equations by taking into account the effect of the vertical accelerations on the pressure distribution. The simplest way of including this effect in the vertically integrated momentum equations is to assume a horizontal velocity distribution which is uniform throughout the depth. This leads to a vertical velocity distribution which increases linearly from zero at the bed to a maximum at the free surface. However, there are other methods available to derive the Boussinesq equations, and a variety of different forms exist differing mainly in the choice of the velocity variable. Typical velocity variables are the surface velocity, the bottom velocity, the depth-averaged velocity, and the volume flux (depth-integrated velocity).

#### 4.3.2 Boussinesq-type equations

Peregrine (1967) derived the equations for varying water depth in terms of the depth-averaged velocity. For two-dimensional propagation they read

$$\frac{\partial \zeta}{\partial t} + \nabla \cdot [(h + \zeta) \bar{u}] = 0, \quad (4.10)$$

$$\frac{\partial \bar{u}}{\partial t} + (\bar{u} \cdot \nabla) \bar{u} + g \nabla \zeta - \frac{1}{2} h \frac{\partial}{\partial t} \nabla [\nabla \cdot (h \bar{u})] + \frac{1}{6} h^2 \frac{\partial}{\partial t} \nabla (\nabla \cdot \bar{u}) = 0$$

in which  $\bar{u}$  the instantaneous depth-averaged velocity

$$\bar{u} = \frac{1}{h + \zeta} \int_{-h}^{\zeta} u \, dz \quad (4.11)$$

The relative magnitude of each term in the formulations can be inferred using non-dimensional expressions. A commonly used scaling of variable is:



$$\frac{x}{L_0}, \frac{y}{L_0}, \frac{z}{h_0}, \frac{h}{h_0}, \frac{\xi}{a_0}, \frac{\sqrt{gh_0} t}{L_0}, \frac{h_0 \bar{u}}{a_0 \sqrt{gh_0}} \quad (4.12)$$

where  $L_0$ ,  $h_0$ , and  $a_0$ , is a characteristic wavelength, water depth and wave amplitude respectively. Expressing equations (4.10) in these non-dimensional variables, where the variables with prime denote the non-dimensional counterparts one obtains

$$\begin{aligned} \frac{\partial \xi}{\partial t} + \nabla \cdot [(\dot{h} + \epsilon \xi) \bar{u}] &= 0, \\ \frac{\partial \bar{u}}{\partial t} + \nabla \xi + \epsilon [(\bar{u} \cdot \nabla) \bar{u}] - \mu^2 \left[ \frac{1}{2} \dot{h} \frac{\partial}{\partial t} \nabla [\nabla \cdot (\dot{h} \bar{u})] - \frac{1}{6} \dot{h}^2 \frac{\partial}{\partial t} \nabla (\nabla \cdot \bar{u}) \right] \\ &= O(\epsilon^2, \epsilon \mu^2, \mu^4) \end{aligned} \quad (4.13)$$

The first equation in (4.13), i.e., the continuity equation, has a nonlinear term with  $\epsilon$ . The momentum equation can be divided into four parts; the first two are lowest order terms, the third is a nonlinear term with  $\epsilon$ , and the fourth is a dispersion term with  $\mu^2$ . The first and second terms correspond to the linear long wave approximation which gives a non-dispersive wavefield. The nonlinear term with  $\epsilon$  is responsible for nonlinear shallow-water effects. Taken together, the first three terms comprise the nonlinear shallow-water equations. The dispersion term with  $\mu^2$  makes the Boussinesq equations different from Airy's linear long wave theory and from the nonlinear shallow-water equations.

Madsen and Sørensen (1992) converted Peregrine's (1967) equations from the depth-averaged velocity into the volume flux (depth-integrated velocity). They also added an order  $\mu^2$  dispersion modification term which was chosen so as to match more closely the linear dispersion relation of Stokes theory. For the two-dimensional case, their equations are

$$\frac{\partial \zeta}{\partial t} + \nabla \cdot \mathbf{Q} = 0 ,$$

$$\begin{aligned} \frac{\partial \mathbf{Q}}{\partial t} + \left[ \frac{\mathbf{Q}}{h+\zeta} (\nabla \cdot \mathbf{Q}) + (\mathbf{Q} \cdot \nabla) \frac{\mathbf{Q}}{h+\zeta} \right] + g(h+\zeta) \nabla \zeta - \frac{1}{2} h^2 \nabla \left[ \nabla \cdot \frac{\partial \mathbf{Q}}{\partial t} \right] \\ + \frac{1}{6} h^3 \nabla \left[ \nabla \cdot \frac{1}{h} \frac{\partial \mathbf{Q}}{\partial t} \right] - B h^2 \nabla \left[ \nabla \cdot \left[ \frac{\partial \mathbf{Q}}{\partial t} + g h \nabla \zeta \right] \right] = 0 \end{aligned} \quad (4.14)$$

where

$$\mathbf{Q} = (h+\zeta) \bar{\mathbf{u}} = \int_{-h}^{\zeta} \mathbf{u} \, dz \quad (4.15)$$

The term containing  $B$  is a dispersion modification term of order  $\mu^2$ .  $B$  can be any number to maximize the accuracy of the linear dispersion relation. The value of  $B$  was determined by matching the resulting linear dispersion relation with a polynomial expansion of Stokes first-order theory combined with the use of a Padé approximant. By this approach the value The value of  $B=1/15$  is recommended as an optimal choice.

Beji and Battjes (1994) have performed numerical simulations using a 1-D extended Boussinesq model with improved dispersion characteristics, as in Madsen and Sørensen (1992). The model formulation, expressed in terms of depth-averaged velocity, is

$$\begin{aligned} \frac{\partial \zeta}{\partial t} + \frac{\partial}{\partial x} [(h+\zeta) \bar{u}] &= 0 \\ \frac{\partial \bar{u}}{\partial t} + \bar{u} \frac{\partial \bar{u}}{\partial x} + g(h+\zeta) \frac{\partial \zeta}{\partial x} &= \frac{1}{3} h^2 \frac{\partial^3 \bar{u}}{\partial t \partial x^2} + h \frac{\partial h}{\partial x} \frac{\partial^2 \bar{u}}{\partial t \partial x} \\ &+ \frac{1}{15} h^2 \frac{\partial^2}{\partial x^2} \left[ \frac{\partial \bar{u}}{\partial t} + g h \frac{\partial \zeta}{\partial x} \right] \end{aligned} \quad (4.16)$$

This set of equations has been integrated numerically using a difference scheme

and validated against measurements of wave propagation over a bar as described by Beji and Battjes (1994).

As this research concerns the influence of harmonic generation on the wave spectra, it is convenient to work with the spectral version of Boussinesq equations. The transformation from the time-domain to the frequency-domain is described in the next section.

## 4.4 Spectral Boussinesq equations

### 4.4.1 Evolution equations

Boussinesq-type equations are composed of two equations (continuity and momentum equations) with two unknown variables (surface elevation and velocity). Madsen and Sørensen (1993) used their extended equations for sloping bottom in depth-integrated velocity (Madsen and Sørensen, 1992), to derive a spectral evolution equation for complex wave amplitudes of harmonic components. This section describes some details of their derivation. For the one-dimensional case, their extended equations are

$$\begin{aligned} \frac{\partial \zeta}{\partial t} + \frac{\partial P}{\partial x} &= 0 \\ \frac{\partial P}{\partial t} + \frac{\partial}{\partial x} \left[ \frac{P^2}{h + \zeta} \right] + g(h + \zeta) \frac{\partial \zeta}{\partial x} &= \frac{1}{2} h^2 \frac{\partial^3 P}{\partial t \partial x^2} - \frac{1}{6} h^3 \frac{\partial^3}{\partial t \partial x^2} \left[ \frac{P}{h} \right] \\ &+ B h^2 \frac{\partial^2}{\partial x^2} \left[ \frac{\partial P}{\partial t} + g h \frac{\partial \zeta}{\partial x} \right] \end{aligned} \quad (4.17)$$

where  $P$  is the one-dimensional depth-integrated velocity. As mentioned before, higher order terms arising from  $\zeta$  are neglected when deriving the dispersion terms in the above equations. For a mild slope bathymetry,  $\partial h / \partial x$  becomes of small order and higher order terms such as  $\partial^2 h / \partial x^2$  or  $(\partial h / \partial x)^2$  can be neglected. Equations (4.17) can be combined into one equation after replacing  $\partial P / \partial x$  in the right-hand-members of the momentum equation by  $\partial \zeta / \partial t$  in accordance with the

continuity equation, and taking partial derivatives in time and space, respectively. Then,

$$\mathbf{L} = \mathbf{M} + \mathbf{N} \quad (4.18)$$

where

$$\mathbf{L} = \frac{\partial^2 \zeta}{\partial t^2} - gh \frac{\partial^2 \zeta}{\partial x^2} + Bgh^3 \frac{\partial^4 \zeta}{\partial x^4} - (B + \frac{1}{3})h^2 \frac{\partial^4 \zeta}{\partial t^2 \partial x^2} \quad (4.19)$$

$$\mathbf{M} = \left[ g \frac{\partial \zeta}{\partial x} + (2B+1)h \frac{\partial^3 \zeta}{\partial t^2 \partial x} - 5Bgh^2 \frac{\partial^3 \zeta}{\partial x^3} \right] \frac{\partial h}{\partial x} \quad (4.20)$$

$$\mathbf{N} = \frac{\partial}{\partial x^2} \left[ \frac{1}{2}g\zeta^2 + \frac{P^2}{h+\zeta} \right] \quad (4.21)$$

The operator  $\mathbf{L}$  contains lowest-order terms and dispersion terms of order  $\mu^2$ . The operator  $\mathbf{M}$  is of order  $\partial h/\partial x$ , representing effects of slowly varying bathymetry, while  $\mathbf{N}$  is of order  $\epsilon$ , representing nonlinear interactions.

### *Fourier representation*

Evolution equations for complex Fourier amplitudes have been previously derived from Boussinesq equations. Freilich and Guza (1984) transformed Peregrine's equations (1967) into spectral evolution equations for amplitude and phase of the harmonic components of the velocity potential. They improved the dispersion characteristics of the solution, but it is still based on the weak dispersion of the original Boussinesq equation.

To derive an evolution equation from (4.18), the free surface elevation  $\zeta$  and the volume flux  $P$  should be expanded in Fourier series. Assuming unidirectional propagation (no reflection), Madsen and Sørensen (1993) used a complex coefficient expansion for  $\zeta$  :

$$\zeta(x, t) = \sum_{p=-\infty}^{\infty} A_p(x) \exp[i(\omega_p t - \psi_p(x))] \quad (4.22)$$

in which  $p$  is the rank of the harmonic,  $A_{-p} = A_p^*$ ,  $\omega_{-p} = -\omega_p$ , and  $\psi_{-p} = -\psi_p$  where

$$\frac{d}{dx} \psi_p(x) = k_p(x) \quad (4.23)$$

$k_p$  can be obtained from  $\omega_p$  according to equation (4.26). The volume flux  $P$  can be expanded by combining (4.22) and the continuity equation in (4.17). Then

$$P(x, t) = \sum_{p=-\infty}^{\infty} \frac{\omega_p}{k_p} A_p(x) \exp[i(\omega_p t - \psi_p(x))] \quad (4.24)$$

It should be mentioned that there is no unique choice for a Fourier series expansion. For example, we can choose the range of summation from 1 to infinity instead of from negative infinity to infinity, in which case the coefficient  $A_p(x)$  becomes two times larger.

#### *The linear dispersion relation of extended Boussinesq equations*

In deriving Boussinesq equations, the dispersion parameter  $\mu^2$  as well as the nonlinear parameter  $\epsilon$  are assumed to be small. With this assumption, terms of order  $\epsilon$  and  $\mu^2$  can be neglected to give a linear long wave approximation which results in a non-dispersive wave field. At lowest order (i.e.,  $\mathbf{L}^{(0)}=0$ ) the linearized problem yields

$$\mathbf{L}^{(0)} = \sum_{p=-\infty}^{\infty} \left[ -\omega_p^2 + g h k_p^2 + B g h^3 k_p^4 - (B + \frac{1}{3}) \omega_p^2 h^2 k_p^2 \right] A_p = 0 \quad (4.25)$$

and

$$\frac{\omega_p^2 h}{g} = \frac{(k_p h)^2 + B (k_p h)^4}{1 + (B + \frac{1}{3}) (k_p h)^2} \quad (4.26)$$

The linear dispersion relation (4.26) obtained from the lowest order solution is compared with Stokes' linear dispersion relation in Fig. 4.1. It shows good agreement up to  $kh=2.5$  for  $B=1/15$ , while the original Boussinesq equation ( $B=0$ ) shows earlier discrepancies from  $kh=1.5$ .

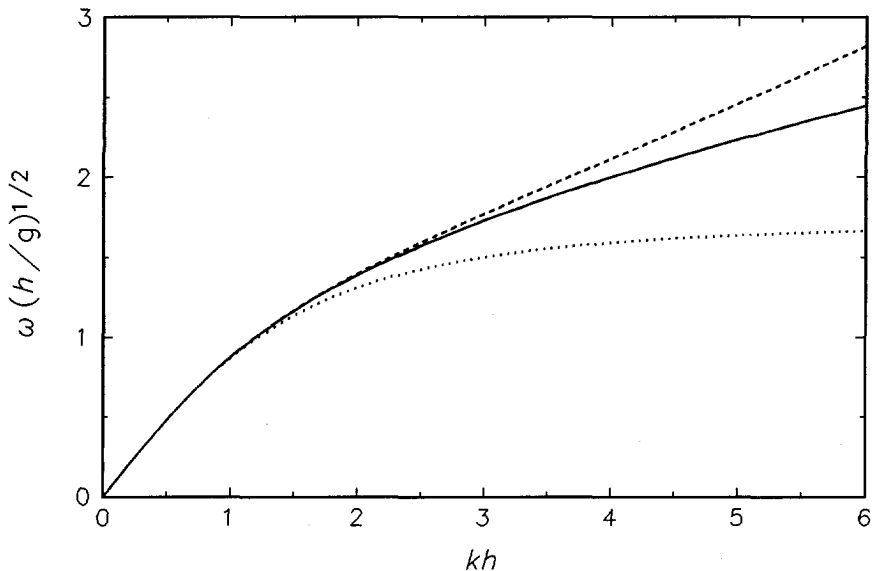


**Figure 4.1** Dispersion characteristics. Solid line denotes Stokes' exact linear dispersion relation; dotted line denotes Boussinesq with  $B=0$ ; and dashed line denotes Boussinesq with  $B=1/15$ .

#### *The evolution equations of Boussinesq model*

The evolution equation of complex Fourier amplitude can be derived by collecting the nonlinear interaction terms of order  $\epsilon$ , the varying bathymetry term with  $\partial h / \partial x$ , and the first order terms of the linear operator induced by the slow variation of water depth, wavenumber and wave amplitude. The operator  $L$  should include derivatives of the wavenumber  $k_p$ . First derivatives of  $A_p$ ,  $k_p$  and  $h$  are assumed to be small, and products of derivatives and higher derivatives of these quantities are neglected in the formulation. The first derivative of  $k_p$  is expressed in terms of the first derivative of  $h$  by differentiating the linear dispersion relations (4.26),

$$\frac{dk_p}{dx} = - \frac{gk_p^2 + 3Bgh^2k_p^4 - 2(B + \frac{1}{3})\omega_p^2hk_p^2}{2ghk_p + 4Bgh^3k_p^3 - 2(B + \frac{1}{3})\omega_p^2h^2k_p} \frac{\partial h}{\partial x} \quad (4.27)$$

and after algebraic manipulations the resulting evolution equations (Madsen and Sørensen, 1993) become

$$\frac{dA_p}{dx} = -\frac{\beta_2}{h} \frac{\partial h}{\partial x} A_p - i2g (F_p^+ + F_p^-) \quad (4.28)$$

The first term on the right represents linear shoaling, proportional to the bottom slope and the local amplitude; the second and the third term represent the triad sum and difference interactions, respectively, defined by

$$F_p^+ = \sum_{m=1}^{p-1} \frac{\alpha^+}{2\beta_1} A_m A_{p-m} \exp[-i(\psi_m + \psi_{p-m} - \psi_p)] \quad (4.29)$$

$$F_p^- = \sum_{m=1}^{\infty} \frac{\alpha^-}{\beta_1} A_m^* A_{p+m} \exp[-i(\psi_{m+p} - \psi_m - \psi_p)] \quad (4.30)$$

with  $\beta_1$ ,  $\alpha^+$ , and  $\alpha^-$  are defined by

$$\beta_1 = -2k_p [gh + 2Bgh^3k_p^2 - (B + \frac{1}{3})\omega_p^2 h^2] \quad (4.31)$$

$$\alpha^+ = (k_{p-m} + k_m)^2 \left[ \frac{1}{2} + \frac{1}{gh} \frac{\omega_m \omega_{p-m}}{k_m k_{p-m}} \right] \quad (4.32)$$

$$\alpha^- = (k_{p+m} - k_m)^2 \left[ \frac{1}{2} + \frac{1}{gh} \frac{\omega_m \omega_{p+m}}{k_m k_{p+m}} \right] \quad (4.33)$$

The linear shoaling coefficient  $\beta_2$  is defined as

$$\beta_2 = \frac{h}{\beta_1} \left[ \left[ \frac{\partial h}{\partial x} \right]^{-1} \frac{dk_p}{dx} \beta_3 - \beta_4 \right] \quad (4.34)$$

where  $dk_p/dx$  is determined from (4.27) and  $\beta_3$  and  $\beta_4$  are defined by

$$\beta_3 = -[gh + 6Bgh^3k_p^2 - (B + \frac{1}{3})\omega_p^2 h^2] \quad (4.35)$$

$$\beta_4 = k_p [g + 5Bgh^2k_p^2 - (2B+1)\omega_p^2 h] \quad (4.36)$$

Equation (4.28) describes the evolution of the complex Fourier amplitude of nonbreaking waves including the effects of linear shoaling and nonlinear interactions. This equation is verified in section 4.6.2 using experimental observations for nonbreaking random wave propagating over a submerged bar.

#### 4.4.2 Nonlinear correction to the linear phase speed

The linear phase speeds of the individual wave components can be obtained as follows

$$c_p^l = \frac{\omega_p}{k_p^l} \quad (4.37)$$

here  $k_p^l$  is the wavenumber obtained from the linear dispersion relation. Nonlinear couplings between various wave components result in phase modifications and consequently phase speeds differing from the linear predictions.

The nonlinear phase speed can be determined by introducing the nonlinear correction to the wavenumber  $\delta k_p$  such that

$$c_p^{nl} = \frac{\omega_p}{k_p^l + \delta k_p} \quad (4.38)$$

Here  $\delta k_p$  represents the spatial rate of change of the slowly varying phase. We express the slowly varying complex amplitude  $A_p$  in terms of its magnitude  $a_p$  and phase  $\theta_p$

$$A_p(x) = a_p(x) \exp[-i\theta_p(x)] \quad (4.39)$$

Here  $\theta_p$  is the slowly varying phase due to the nonlinear interactions. The nonlinear correction to the wavenumber  $\delta k_p$  can be expressed as



$$\delta k_p = \frac{d\theta_p(x)}{dx} \quad (4.40)$$

The evolution equation of the slowly varying phase can be obtained by differentiating equation (4.39) with respect to  $x$ . After straightforward algebra, we obtain the following phase evolution equation for each harmonic after omitting the  $x$ -dependency for abbreviation,

$$a_p \frac{d\theta_p}{dx} = \text{Im} \left[ \frac{dA_p}{dx} \right] \cos \theta_p - \text{Re} \left[ \frac{dA_p}{dx} \right] \sin \theta_p \quad (4.41)$$

In the application to be given below, equation (4.28) is integrated first to obtain the values of  $a_p$ ,  $\theta_p$ , and  $dA_p/dx$ . Then  $\delta k_p$  can be obtained directly from equation (4.41). The phase speed can then be obtained from equation (4.38). Calculations of the nonlinear estimate of the phase speed in random waves propagating over a bar are given in section 4.6.2. (Similar calculations have been published before in Eldeberky and Battjes (1994b) to examine nonlinear couplings in waves passing over a shallow bar.)

## 4.5 Spectral Boussinesq modeling of random breaking waves

Boussinesq equations incorporate generation of bound sub- and superharmonics, leading to significant changes in the spectral shape as well as the wave profile. These nonlinear cross-spectral transfers of energy and phase modifications lead to asymmetric and skewed wave profiles that are characteristic of nearly breaking and broken waves. However, the equations do not describe wave breaking.

The role of wave breaking and its influence on the spectral evolution has not yet rigorously been established. Knowledge of the spectral distribution of energy dissipation due to wave breaking is necessary for predication of wave evolution in the shoaling region and in the surf zone. This is the subject of this section.

### 4.5.1 Wave energy dissipation due to breaking

Wave breaking and the associated energy dissipation are extremely complex processes. Several models have been developed for describing wave decay in the surf zone for periodic or random waves, differing mainly in their formulation of the energy dissipation due to breaking. The models for random waves by Battjes and Janssen (1978) or Thornton and Guza (1983) assume a shape of the wave height distribution in the surf zone and transform a representative statistical wave height in the cross-shore direction. The dissipation of wave energy due to breaking is modeled using the bore analogy. The other class of models that was originally developed for periodic waves and has since been modified to simulate random waves uses a wave-by-wave approach (Mase and Iwagaki, 1982; Dally et al., 1985). In these models the probability density function of wave height at a seaward boundary is schematized to a discrete number of wave height classes, and it is assumed that each class behaves like a subgroup of periodic waves that propagates independently of the others. Both classes of models do not provide any information about the spectral distribution of the dissipated energy due to breaking.

The model of Battjes and Janssen (1978) for the total local rate of random-wave energy dissipation per unit area due to breaking ( $D_{\text{tot}}$ ), is used as a starting point toward a spectral formulation for wave breaking, both for energy-density models and complex-amplitude models. It is given by them (apart from a factor  $\rho g$  which is omitted here) as:

$$D_{\text{tot}} = \frac{\alpha}{4} f_c Q_b H_m^2 \quad (4.42)$$

in which  $\alpha$  is a free parameter of order 1,  $f_c$  is a characteristic frequency,  $Q_b$  is the fraction of broken waves given by

$$\frac{1 - Q_b}{\ln Q_b} = - \left[ \frac{H_{\text{rms}}}{H_m} \right]^2 \quad (4.43)$$

$H_{\text{rms}}$  is the root-mean-square wave height and  $H_m$  is the maximum wave height which for shallow-water waves is given by

$$H_m = \gamma h \quad (4.44)$$

where  $h$  is the water depth and  $\gamma$  is the breaking coefficient. Realistic results can normally be obtained for  $\alpha$  equal to 1 and with  $\gamma$  values in the range of 0.6 to 0.8 as proposed by Battjes and Stive (1985) in conjunction with the use of the peak frequency in (4.42).

As indicated above, this model gives the total energy dissipation rate due to breaking but not its spectral distribution. In what follows the influence of the breaking dissipation is formulated in a spectral form. Here wavefields with, initially, a single-peaked spectrum (in the linear approximation) are considered. Combinations of independent wave systems like sea and swell are not considered here.

It should be mentioned that the choice of the energy dissipation model is not essential in the spectral formulation of wave breaking. Other models that provide the total rate of energy dissipation by wave breaking (e.g., Thornton and Guza, 1983) can be incorporated in like manner in the spectral formulations given below.

In the experiments of Beji and Battjes (1993) for the transformation of random waves over a submerged bar, the evolution of the spectral shape, including the appearance of a high-frequency peak due to harmonic generation, was found to be virtually the same for nonbreaking and for breaking waves. In view of this, the following hypotheses have been used here as a basis to model the breaking-induced dissipation:

- (1) dissipation does not interact with other processes affecting the wave evolution, including triad interactions;
- (2) the total energy dissipation is distributed over the spectrum in such a manner that it does not influence the local rate of evolution of the spectral shape (but only of the total energy).

As it stands, the latter hypothesis is formulated for the entire spectrum. However, the observations by Beji and Battjes (1993) were restricted to

wavefields whose initial spectra were single-peaked, and they did not pertain to the low-frequency waves accompanying the shorter incident waves. It may be expected that the low-frequency waves are less affected by breaking than the higher-frequency components, but there is no firm theoretical foundation at present to formulate this in a quantitative sense. Two extremes are considered in the following. The simple hypothesis as formulated above is at first applied to the entire spectrum, including the low-frequency waves. As an alternative, the low-frequency part will be excluded from breaking-induced dissipation. Results of both will be presented and discussed in section 4.6.2.

In the context of a balance equation for the spectral energy density, the effect of wave breaking can be formulated as a spectral energy "source" term  $S_b$ , representing a (negative) contribution to the temporal rate of change of spectral density. According to the hypotheses stated above, it must be proportional to the local (in the spectral domain) spectral energy density, and its spectral integral should equal  $D_{\text{tot}}$ , the total local rate of energy dissipation. For one-dimensional (frequency) spectra  $E(f)$  this leads to the following quasi-linear expression:

$$S_b(f) = - \frac{D_{\text{tot}}}{E_{\text{tot}}} E(f) \quad (4.45)$$

Here  $E(f)$  is the energy density at frequency  $f$  and  $E_{\text{tot}}$  is the total wave energy (more precisely, the integral over the energy density spectrum). For two-dimensional frequency-direction spectra  $E(f, \theta)$  a relation similar to (4.45) can be formulated. This spectral energy formulation for wave breaking enables the incorporation of the effects of depth-induced wave breaking in spectral energy-density models.

For spectral phase-resolving models which are formulated in terms of space-dependent complex Fourier amplitudes of the surface elevation, such as equations (4.28), the effects of wave breaking can be accounted for in a similar manner. As a starting point, consider the energy balance equation for a monochromatic wave, expressing that the spatial gradient of the energy flux

should balance the rate of energy dissipation due to breaking  $D$ , i.e.,

$$\frac{d}{dx} (E c_g) = -D \quad (4.46)$$

where the energy  $E$  is proportional to the square of the wave amplitude  $|A|^2$ . After straightforward algebra, equation (4.46) can be expressed as follows

$$\frac{2}{A} \frac{dA}{dx} + \frac{1}{c_g} \frac{dc_g}{dx} = - \frac{D}{|A|^2 c_g} \quad (4.47)$$

Rearranging the terms in equation (4.47) yields

$$\frac{dA}{dx} = - \frac{1}{2} \left[ \frac{1}{c_g} \frac{dc_g}{dx} + \frac{D}{F} \right] A \quad (4.48)$$

Here  $F = |A|^2 c_g$  is the energy flux. The first term in the right-hand-side of equation (4.48) represents shoaling, the second the energy dissipation due to wave breaking.

Application of the dissipation term to the evolution equations of the space-dependent complex Fourier amplitude for irregular waves (4.28) is made by letting  $F$  represent the total energy flux,  $D$  the total rate of energy dissipation due to breaking, and  $A$  the complex amplitude of the individual wave component. This leads to the following quasi-linear dissipation term  $d_{bp}$  (contribution to spatial rate of change of complex amplitude  $A_p$ ):

$$d_{bp} = - \frac{1}{2} \frac{D_{\text{tot}}}{F_{\text{tot}}} A_p \quad (4.49)$$

Here  $F_{\text{tot}}$  is the total local rate of energy flux per unit width. In principle, both free waves and bound waves contribute to  $F_{\text{tot}}$ . However, in view of the crudeness of the hypothesis concerning the spectral dissipation formulation, a refined computation of  $F_{\text{tot}}$  is not warranted. We have used a simple linear

estimate, in which  $F_{\text{tot}}$  is given by

$$F_{\text{tot}} = \sum_p |A_p|^2 c_{g,p} , \quad (4.50)$$

with the group velocity  $c_{g,p}$  determined from the linear dispersion relation of the model. An alternative with more emphasis on the contribution of the bound waves is  $F_{\text{tot}} = E_{\text{tot}} c_{g0}$ , where  $c_{g0}$  is the group velocity at the peak frequency of the spectrum. It has also been tested, but it gave no significant differences. The results of the first alternative are shown below.

The dissipation term  $d_{bp}$  is proportional to  $A_p$  with a frequency-independent factor, so that the dissipation term reduces the spectral amplitudes in the same proportion; it does not affect the spectral shape. Strictly speaking, the breaking term  $d_{bp}$  could be a complex function. Its imaginary part would influence the phase of each harmonic, and therefore the free-surface profile in cases where breaking is significant. Liu (1990) used a complex form for his spectral breaking dissipation term, introducing both amplitude and phase modifications due to wave breaking. The consequences were that the predicted wave profiles were entirely wrong compared with the measurements, although the wave heights were correctly predicted. Here  $d_{bp}$  is chosen to be real; there is, at present, no basis for inclusion of certain phase shifts due to breaking.

To examine the performance of the spectral breaking model in shallow water it has been implemented in the evolution equation based on the extended Boussinesq equations. These are chosen because of their improved dispersion characteristics that make them applicable for a wide range of water depths. The resulting evolution equation and its numerical implementation are described below.

#### 4.5.2 Evolution equation for random breaking waves

Inclusion of the spectral dissipation term for wave breaking obtained in the previous section (equation 4.49) in equation (4.28), yields the following set of

evolution equations for breaking waves:

$$\frac{dA_p}{dx} = -\beta_2 \frac{h_x}{h} A_p - i2g (F_p^+ + F_p^-) - \frac{1}{2} \frac{D_{\text{tot}}}{F_{\text{tot}}} A_p \quad (4.51)$$

In (4.51) the total local rate of energy dissipation due to breaking  $D_{\text{tot}}$  is determined using (4.42-44). In the computations presented below the mean frequency of the local spectrum is used in (4.42) to allow for influence of higher harmonics. This is compensated by a higher value of  $\gamma$  (see below). (A reduction of  $\alpha$  in equation (4.42) while keeping  $\gamma$  constant would have given comparable results.)

The inclusion of the spectral breaking term in the Boussinesq equations should extend their range of applicability into the surf zone. Laboratory data for random breaking waves are used to validate the spectral Boussinesq equations with breaking dissipation. The model is used to simulate the surface elevation as well as the wave spectra. The boundary conditions and the numerical integration are described below.

## 4.6 Model to data comparison

### 4.6.1 Model implementation

The evolution equations (4.28) for nonbreaking waves and (4.51) for breaking waves comprise a set of first-order ordinary differential equations which require knowledge of the set of complex amplitudes  $A_p$  ( $p=1,2,3,\dots$ ) at an upwave location for their integration.

To simulate the wave profile, the measured time records at the upwave boundary are used to obtain the complex amplitudes using a standard fast Fourier transformation algorithm. Following numerical integration of the evolution equations using a fourth-order Runge-Kutta method, a set of complex amplitudes is obtained at each location. These are transformed into surface

elevations using backward (i.e., inverse) fast Fourier transformation. It should be noted that the evolution equations predict the complex Fourier amplitudes that contain only the nonlinear part of the phase function. In the simulations the linear contribution to the phase function is computed separately by spatial integration of  $k_p$  obtained from the linearized dispersion equation (4.26). This space dependent part of the phase is added to the nonlinear phase obtained from the evolution equation.

In applications of the deterministic evolution equations for complex Fourier amplitudes to random waves with only a given energy spectrum  $E(f)$  at the upwave location, this spectrum was discretized with bandwidth  $\Delta f$ ; initial amplitude values  $|A_p|$  were set equal to  $(\frac{1}{2}E_p\Delta f)^{1/2}$  (the frequencies are taken nonnegative). For each realization a set of initial phases was drawn at random, assuming them to be mutually independent, each uniformly distributed over  $2\pi$ . Following numerical integration of the evolution equations, raw values of spectral energy density at downwave locations were estimated as  $2|A_p|^2/\Delta f$ . These raw spectra appeared to vary between realizations, thus exhibiting influence of the particular set of initial phases (Won and Battjes, 1992). This was largely eliminated by averaging over 20 realizations, each with a different set of initial phases, and over three neighboring frequency bands, yielding a number of degrees of freedom in the spectral estimates of 120.

#### 4.6.2 Verification of the evolution equation for nonbreaking waves

For nonbreaking waves, the spectral evolution equation (4.28) has been verified against laboratory measurements of Beji and Battjes (1993) of transformation of nonbreaking waves over a shallow submerged bar (Fig. 4.2). Two tests are used in the verification. In the first test the incident wave spectrum is narrow-banded with peak frequency of 0.40 Hz and significant wave height of 2.37 cm. In the second test the incident wave spectrum is broad-banded with peak frequency of 0.40 Hz and significant wave height of 2.93 cm.

The wave spectra are simulated by averaging over 20 realizations, each with a



different set of initial random phases. The number of frequency components  $nf$  used in the computation is 78 with the bandwidth  $\Delta f$  equal to 0.039 Hz. The nonlinear phase speeds are computed using equations (4.38, 4.41), and compared to the linear predictions (equation 4.37) using the linearized dispersion relation (equation 4.26) obtained from the extended Boussinesq equations.

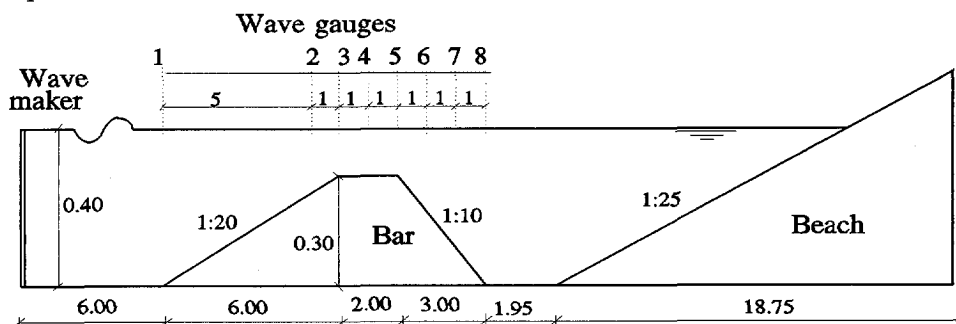


**Figure 4.2** Layout for the experimental setup (Beji and Battjes, 1993). All lengths are expressed in meters.

Figs. 4.3a,b and 4.4a,b show the energy spectra and the linear and the nonlinear phase speeds at different locations over the bar for narrow- and broad-band spectra, respectively. The overall results for the spectral evolution over the shallow bar show that the generation of higher harmonics is well predicted with the evolution equations of extended Boussinesq model. Over the shoaling region, strong energy transfers take place from the primary spectral peak to the higher harmonics.

The predicted nonlinear phase speeds, over the upslope of the bar, show that the higher harmonics propagate faster than the linear estimates due to the nonlinear couplings to the primary. Over the bar crest (station 4), the nonlinear phase speeds are nearly constant and equal to  $\sqrt{gh}$  (nondispersive shallow-water waves). Beyond the bar (station 8), the nonlinear predictions of phase speed agree with the linear estimates, implying full release of bound harmonics. These results are consistent with the findings of chapter 3, in which it is found that beyond the bar, the effects of nonlinear couplings vanish.

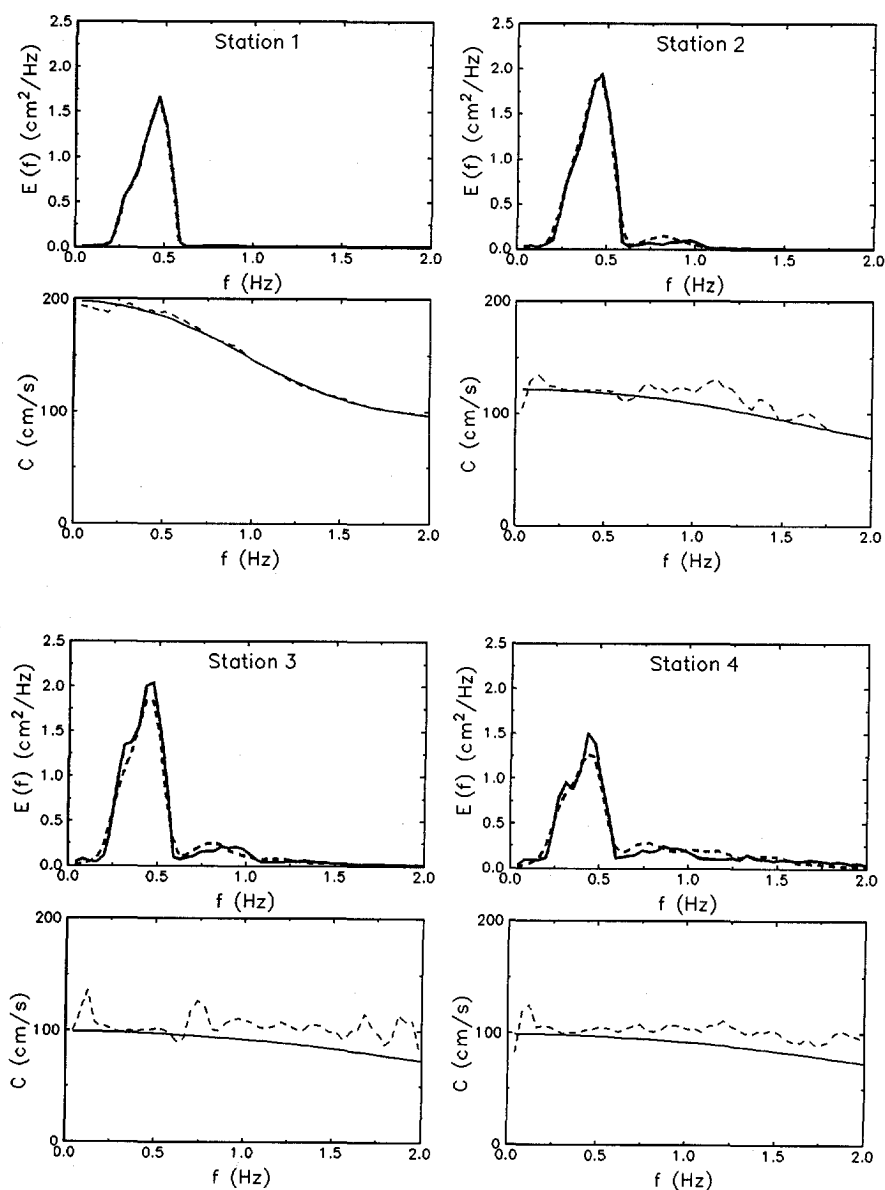


**Figure 4.3a** Energy spectra (upper panels) from experiments (solid lines) and from the Boussinesq evolution model (dashed lines) and computed phase speeds (lower panels): linear (solid lines); nonlinear (dashed lines) at stations 1, 2, 3, and 4 for waves propagating over a bar with narrow-banded spectrum.

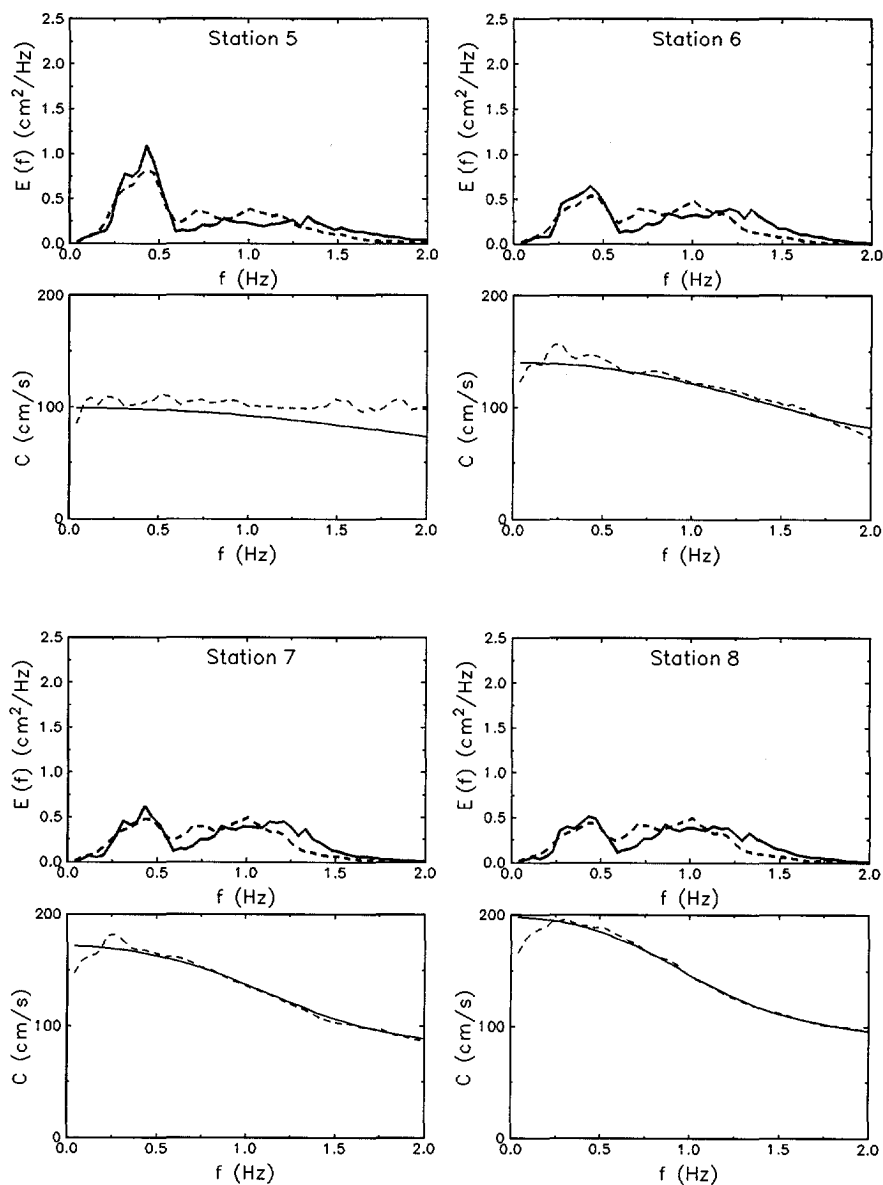
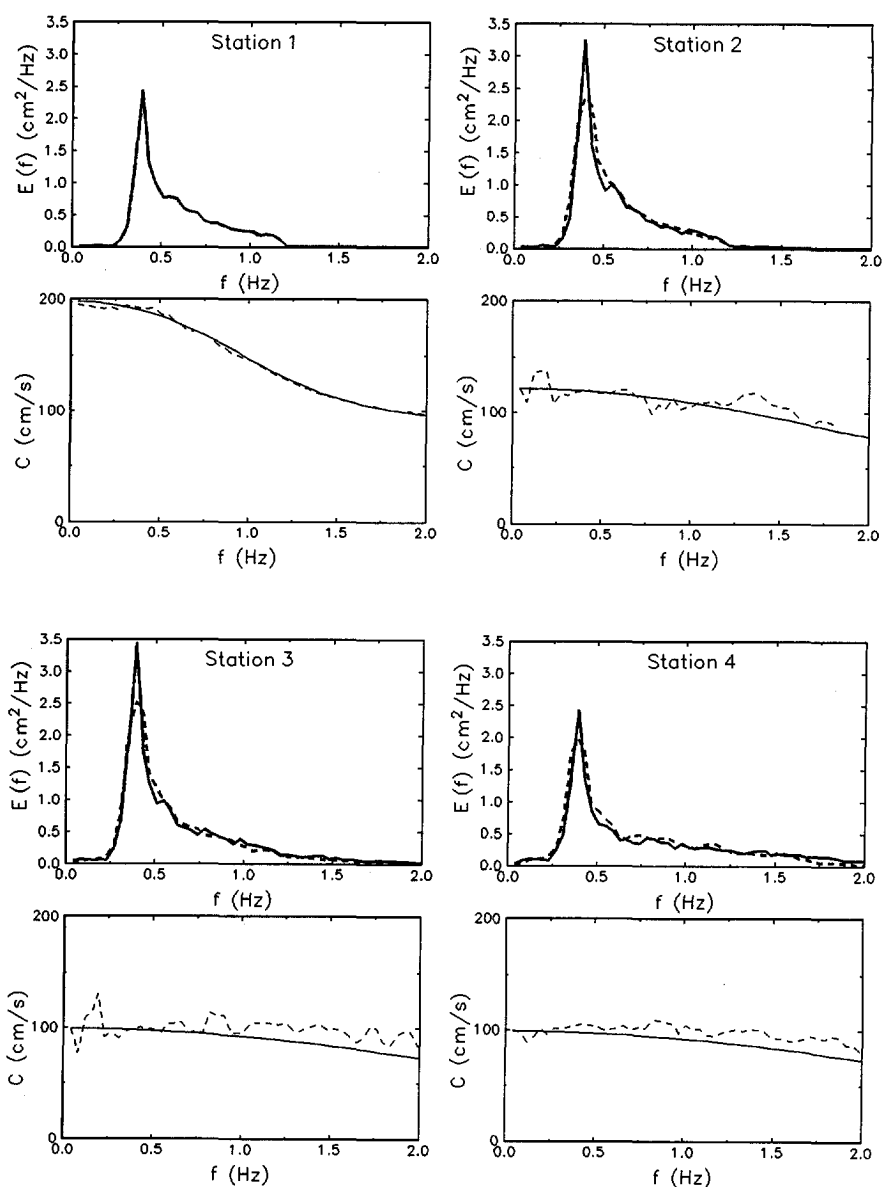
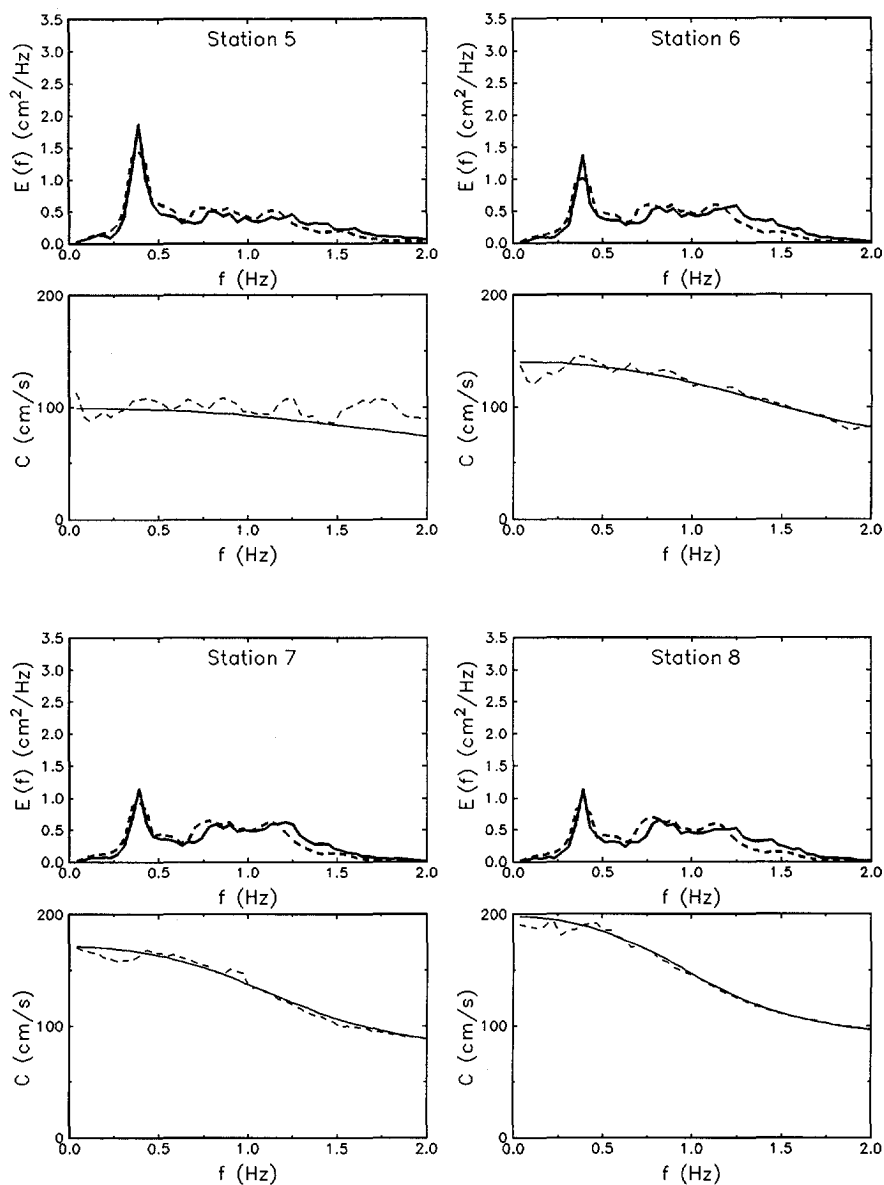


Figure 4.3b Continuation of figure 4.3a for stations 5, 6, 7, and 8.



**Figure 4.4a** *Energy spectra (upper panels) from experiments (solid lines) and from the Boussinesq evolution model (dashed lines) and computed phase speeds (lower panels): linear (solid lines); nonlinear (dashed lines) at stations 1, 2, 3, and 4 for waves propagating over a bar with broad-banded spectrum.*



**Figure 4.4b** Continuation of figure 4.4a for stations 5, 6, 7, and 8.

### 4.6.3 Verification of the evolution equation for breaking waves

#### *Input data*

The spectral evolution equation (4.51) has been verified against laboratory measurements for finite-amplitude waves propagating in shallow water with breaking dissipation. Four different experimental data sets have been used for wave transformation over barred and nonbarred profiles, as shown in Figs. 4.2, 4.7, 4.10 and 4.13. These experiments and the incident wave conditions are listed in Table 4.1, in which  $f_0$  is the peak frequency and  $H_{m0}$  is the significant wave height given by  $4(m_0)^{1/2}$  where  $m_0$  is the surface elevation variance ( $=E_{\text{tot}}$ ).

**Table 4.1** *Description of the Experiments and the Incident Wave Conditions.*

Test	Reference	Bed Profile	Breaking	$f_0$ , Hz	$H_{m0}$ , cm
A	Beji and Battjes (1993)	submerged bar	mild	0.47	5.4
B	Luth et al. (1993)	submerged bar	strong	0.55	21.7
C	Arcilla et al. (1994)	monotonic beach	strong	0.20	90.0
D	Arcilla et al. (1994)	barred beach	mild	0.125	58.0

Test A in Table 4.1 represents the case of narrow-spectrum of breaking waves of Beji and Battjes (1993), and tests C and D in Table 4.1 represent tests 1A and 1C of Arcilla et al. (1994). In each of these experiments, free-surface elevations were measured at several locations along the bottom profile.

These experiments are chosen because they feature various wave conditions and different bed configurations. These conditions are quantified using the following wave parameters: the nonlinearity parameter  $\epsilon = a/h$  (in which  $a$  is a wave amplitude equal to  $H_{m0}/8^{1/2}$ ), the dispersion parameter  $\mu = k_0 h$  (in which  $k_0$  is the wavenumber corresponding to the peak frequency  $f_0$ ), the Ursell number  $Ur = \epsilon/\mu^2$ , and the bottom slope parameter  $|h_x|/k_0 h$ . The values of these parameters are listed in Table 4.2. The subscripts  $d$  and  $s$  denote the parameter value in deep and shallow water, respectively, where the deep water values are computed at the upwave boundary and the shallow water values are taken over the bar crest for the barred profiles (i.e., tests A, B, and D) and at the

shallowest measurement location (station 8) for the monotonic beach (test C). The maximum value of the bottom slope parameter along each profile is given in Table 4.2, where in the cases with barred profile (i.e., tests A, B, and D) it is calculated at the beginning of the downslope of the bar (where the slope is maximal and  $k_0 h$  is minimal) and in the case of test C it is computed at the region with the steepest slope (i.e., between stations 5 and 6). In the simulations the upwave boundary conditions are specified from the measurements at station 1 for each test.

**Table 4.2** *Wave Parameters for Different Experiments in Deep and Shallow Water.*

Test	$\epsilon_d$	$\epsilon_s$	$\mu_d$	$\mu_s$	$Ur_d$	$Ur_s$	$ h_x /k_0 h$
A	0.05	0.17	0.63	0.30	0.13	1.88	0.33
B	0.10	0.26	1.18	0.52	0.07	0.96	0.19
C	0.08	0.23	0.91	0.36	0.10	1.77	0.09
D	0.05	0.24	0.53	0.21	0.18	4.96	0.52

*Variables are defined as follows:  $\epsilon$ , nonlinearity parameter;  $\mu$ , dispersion parameter;  $Ur$ , Ursell number;  $|h_x|/k_0 h$ , bottom slope parameter. The subscripts  $d$  and  $s$  refer to deep and shallow water, respectively.*

#### *Computational parameters and results*

To simulate the measured wave profiles, a large number of Fourier modes is needed with high resolution and high cutoff frequency to ensure adequate representation of the higher harmonics. The sampling rate in the measurements of tests A, C, and D is 10 Hz, implying a maximum cutoff frequency in the simulations of 5 Hz. In test B the data were available with 20 Hz sampling rate, implying a 10-Hz maximum cutoff frequency.

The wave spectra are simulated by averaging over 20 realizations, each with a different set of initial random phases. The number of frequency components  $nf$  and the bandwidth  $\Delta f$  used in the simulations are listed in Table 4.3, both for the simulations of the surface elevations and of the wave spectra. For all tests

the maximum frequency used in the computations of the surface elevations was equal to the cutoff frequency in the data. In equation (4.42),  $\alpha=1$  was used. The value of the breaking coefficient  $\gamma$  (equation 4.44) was set at 0.85. This value is on the high side to compensate for the use of the mean frequency in (4.42), instead of the more commonly used peak frequency.

**Table 4.3** *Computational Parameters Used in the Numerical Simulations*

Test	Surface Elevations			Wave Spectra		
	$nf$	$\Delta f$ , Hz	results	$nf$	$\Delta f$ , Hz	results
A	256	0.0195	Fig. 4.6	78	0.039	Fig. 4.5
B	512	0.0195	Fig. 4.9	85	0.025	Fig. 4.8
C	512	0.00975	Fig. 4.12	100	0.01	Fig. 4.11
D	512	0.00975	Fig. 4.15	100	0.01	Fig. 4.14

### *Discussion of the results*

Inspection of the comparisons of energy spectra and wave profiles shows, at a glance, that the model simulates the observed evolution of irregular waves with breaking dissipation fairly well for the case of a submerged artificial bar (tests A and B) as well as for the nearly monotonic sandy beach profile (test C) and the barred sandy beach (test D).

In the cases with a submerged artificial, trapezoidal bar (i.e., tests A and B) the initial nonlinear steepening on the seaward side is well represented and also the subsequent enhancement of higher harmonics and ensuing profile distortion (Figs. 4.6 and 4.9). As the waves travel upslope, they gradually lose their vertically symmetric profile and become pitched forward (nearly saw-toothed shape) due to the increasing nonlinearity and bottom slope influence. Over the bar crest, where the waves become nearly nondispersive, the resonant conditions are nearly satisfied and a very rapid energy exchange occurs between the primary and its harmonics (see chapter 3 for a detailed analysis of these phenomena). As the waves propagate into the deeper water, they decompose into several smaller-amplitude waves.



As wave breaking takes place, it reduces the degree of nonlinearity, hence weakens the intensity of the nonlinear interactions. The energy dissipation results in a reduction of the amplitudes of the harmonics which apparently is close to proportional in view of the realistic model predictions.

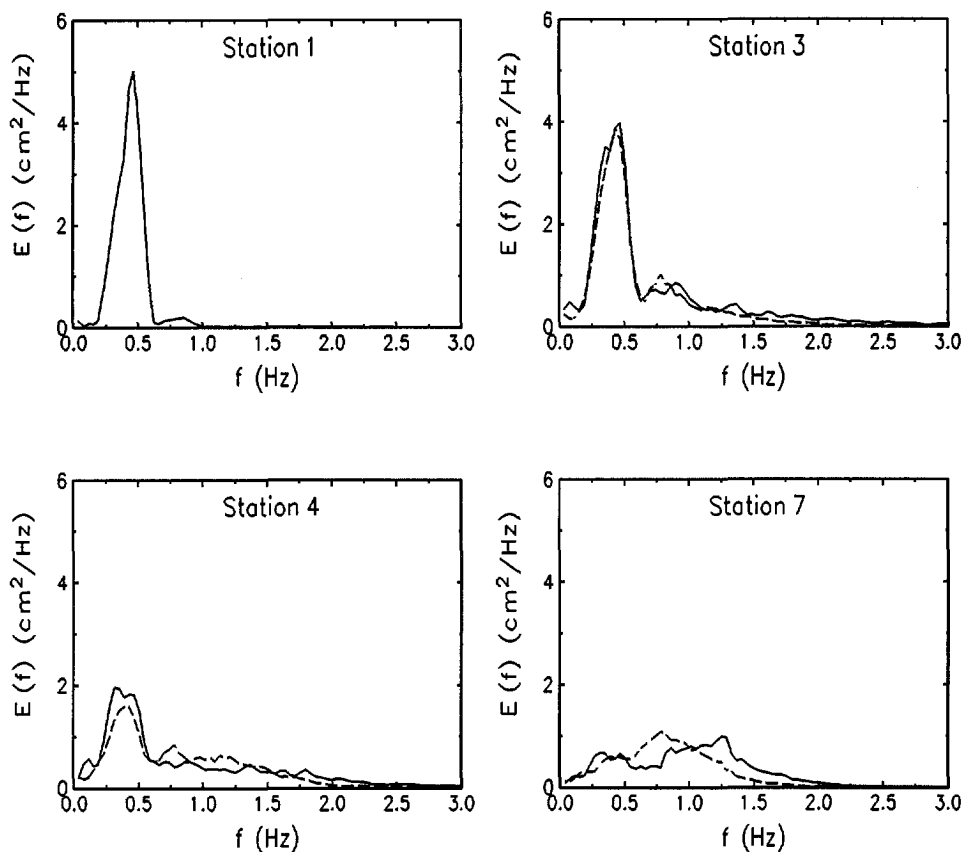


**Figure 4.5** Energy spectra at various locations for test A. Solid lines denote measurements; dashed lines denote computations.

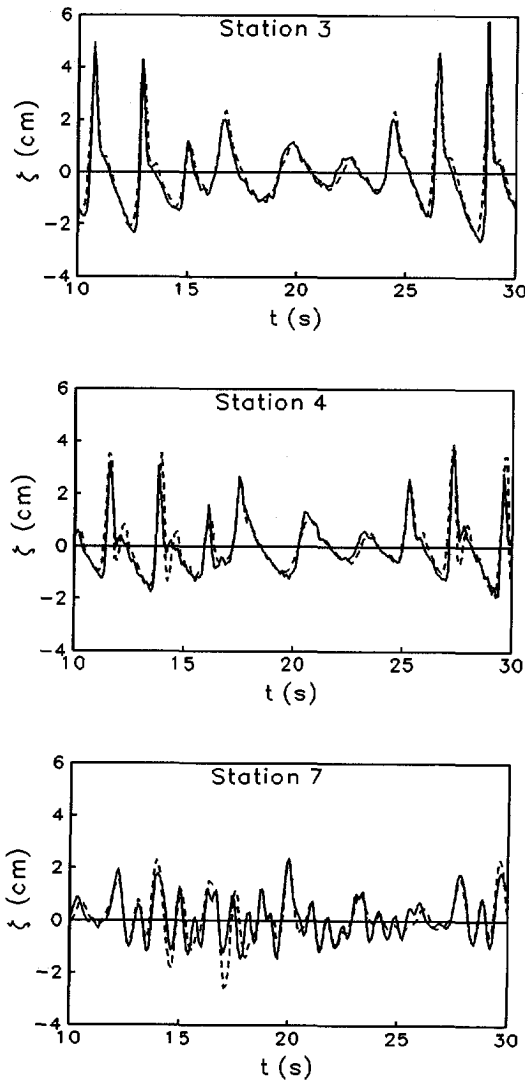


**Figure 4.6** Surface elevations at various locations for test A. Solid lines denote measurements; dashed lines denote computations.

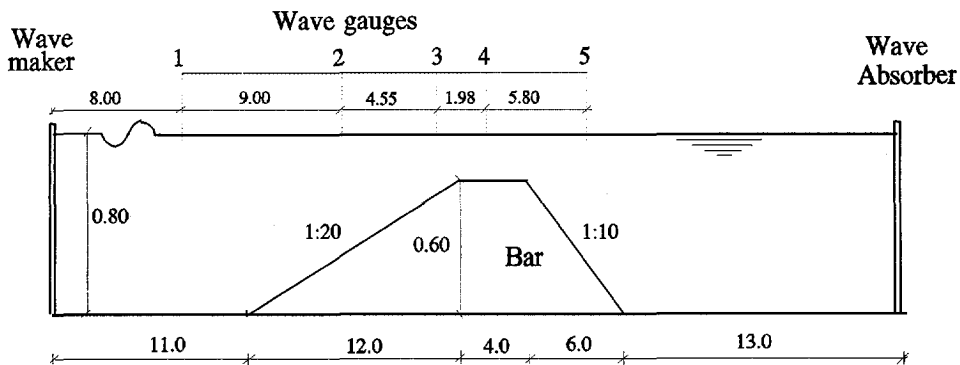


**Figure 4.7** Layout for the experimental setup for test B (Luth et al., 1993). All lengths are expressed in meters.

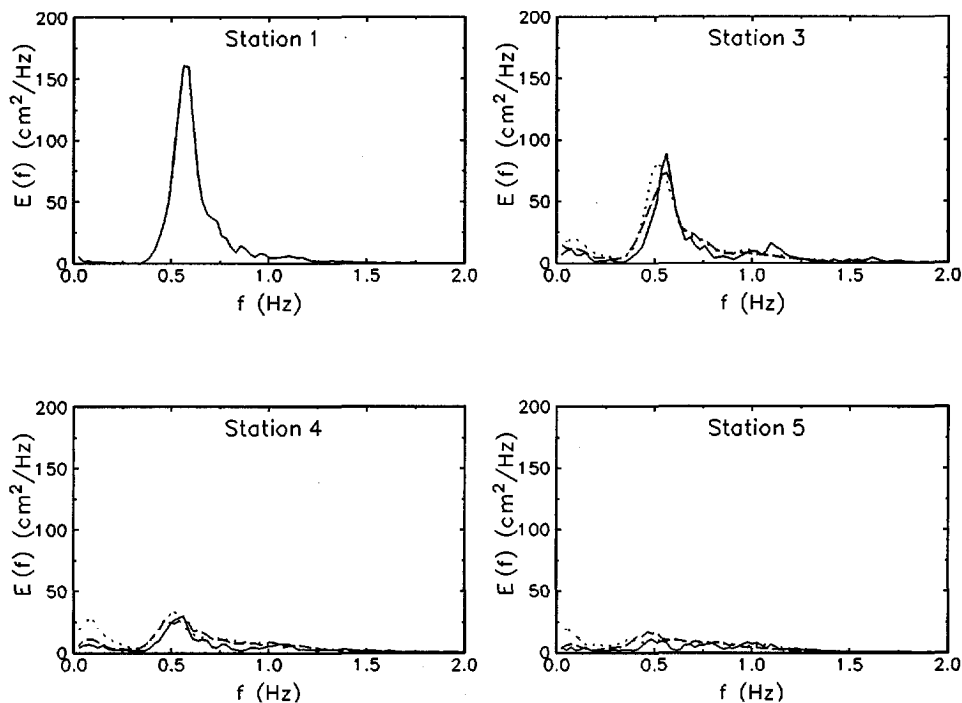


**Figure 4.8** Energy spectra at various locations for test B. Solid lines denote measurements; dashed lines denote computations with breaking dissipation for all frequencies; and dotted lines denote computations with breaking dissipation excluded for  $f < 0.275$  Hz.

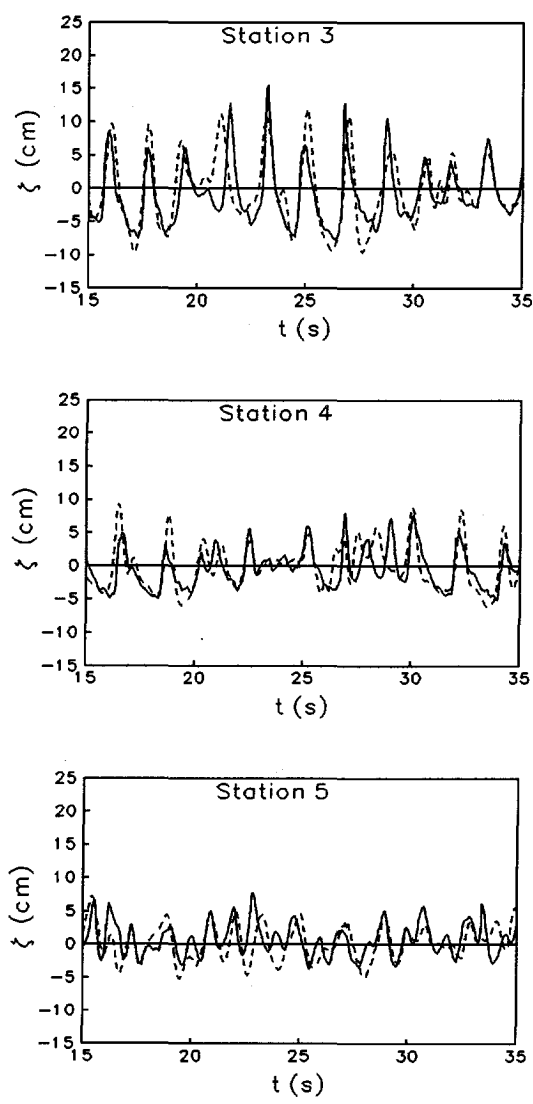


**Figure 4.9** *Surface elevations at various locations for test B. Solid lines denote measurements; dashed lined denote computations.*

Comparing the model performance for tests A and B, it can be seen that the energy spectra are predicted about equally well (Figs. 4.5 and 4.8), but that the time domain predictions for test B (Fig. 4.9) are not as good as those for test A (Fig. 4.6). It is worth noting in this respect that test B is more demanding than test A, both with respect to the dispersion characteristics and with respect to the representation of dissipation. Test B involves larger relative propagation distances than test A; the longitudinal dimension of the bar normalized with the initial wave length is almost 3 times larger than in test A. Also, the breaking in test B is significantly more intense than in test A. In test A the dissipated energy is about 20% of the incident wave energy, whereas it is about 75% in test B. Evidently, wave breaking is so strong in test B that breaking dissipation dominates harmonic generation. The data do not include lower, nonbreaking waves of the same length as in test B, so that we cannot pinpoint the source of the errors in test B with certainty.

The scenario in test C is different than in tests A and B because the monotonic profile in test C allows for wave breaking to continue for large propagation distance and for continuous generation of low-frequency energy, as inferred from the spectra (Fig. 4.11). The nonlinearity is dominant over the entire surf zone without the occurrence of wave decomposition, unlike the phenomena downwave from the bar, where the intensity of nonlinear couplings decreases due to the deepening water.

In test D the bottom topography (barred beach with steep slopes) highlights some interesting features about the model applicability. In the shoaling region the predicted surface elevations are in very good agreement with the measurements up to the bar crest (Fig. 4.15, station 6). This is an indication of the accurate predictions of the higher harmonics. The spectral evolution shows a distinct energetic second spectral peak which is ascribed to the nearly resonant triad interactions. Beyond the bar, discrepancies are noticeable in the model predictions, where the waves decompose without a distinct primary peak, which, however, is still observable in the measurements (Fig. 4.14, station 8). This is ascribed to the relatively steep bottom ( $|h_x|/k_0 h = 0.52$ ), which is in contrast to the assumption of slowly varying bottom ( $|h_x|/k_0 h \ll 1$ ). In fact, the

bottom slope condition implies that the smallest bottom variation should accommodate at least one wavelength. Beyond the bar crest the local wavelength of the incident peak frequency is about 22 m, whereas the length of the trough in the bottom profile is about 20 m (see Fig. 4.13). Note that a somewhat similar phenomenon (disappearance of primary peak in the computations) is noticeable in test A (Fig. 4.5, station 7), where also the bottom slope parameter was not very small compared with unity (0.33).

Generally, the realistic model predictions of the wave profile, even after breaking, support the use of a real function for the breaking dissipation term. There seems to be no need of additional assumptions about a complex dissipation function, that would introduce phase modifications due to energy dissipation by wave breaking.

It has been pointed out above that the dissipation model presented here is not intended for the low-frequency part of the spectrum. Nevertheless, in most of the computations referred to above, the formulation intended for the frequency range of the incident waves and their higher harmonics has provisionally been applied to the entire spectrum. Some computations have also been carried out of the energy spectra in which the dissipation was not applied to the low-frequency waves (frequencies less than about half the peak frequency of the incident waves). We show only results for tests B and C because these have strong breaking (see Table 4.1), both on a barred profile (test B) and on a monotonic beach (test C).

Fig. 4.8 shows the results for test B. Over the upslope (station 3), where breaking starts, the computation with dissipation switched off overpredicts the low-frequency energy somewhat. This discrepancy becomes significant where more breaking dissipation has occurred (station 4). Over the downslope (station 5) the low-frequency energy is reduced due to deshoaling in the measurements as well as in both computations. The computation with dissipation switched on in the low-frequency range shows good agreement with the experimental results in the whole range.

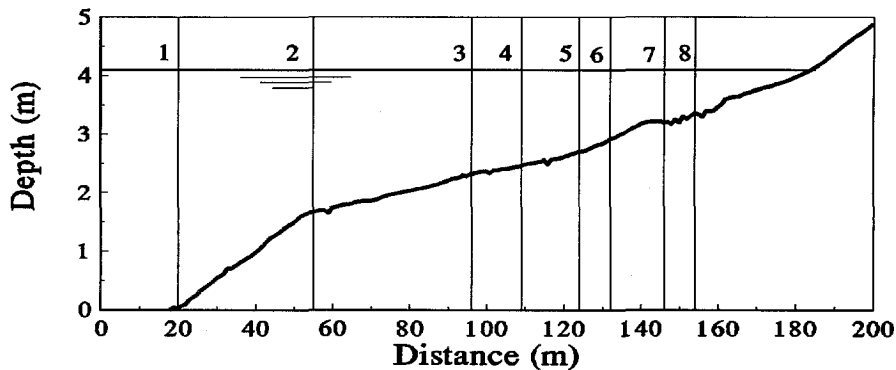


**Figure 4.10** *Bed profile and locations of wave gauges for test C (Arcilla et al., 1994).*

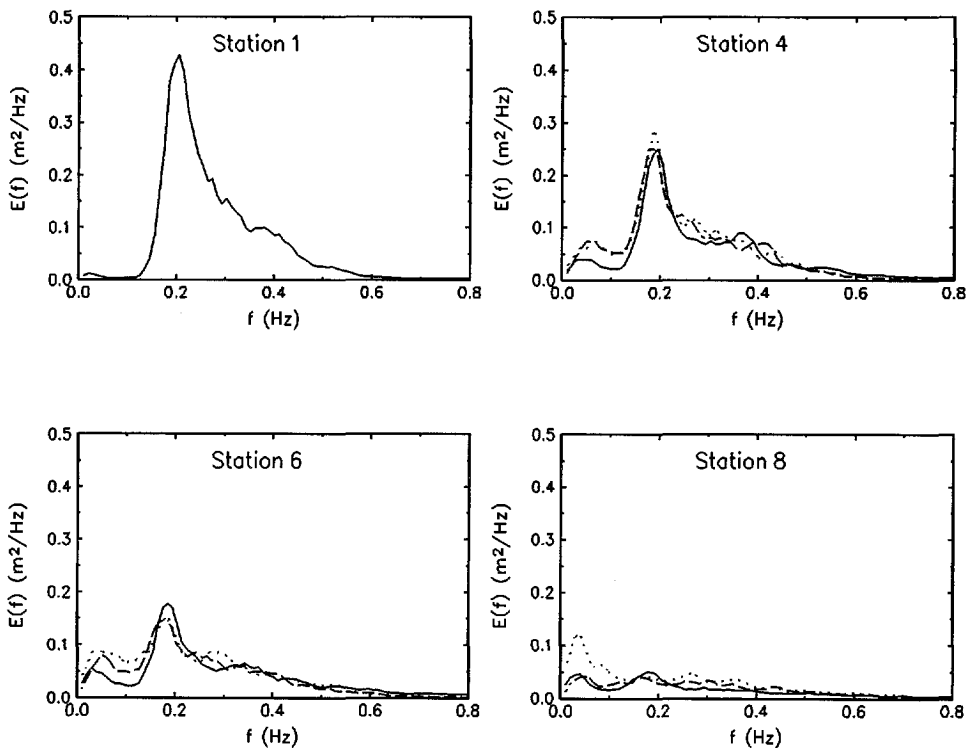


**Figure 4.11** *Energy spectra at various locations for test C. Solid lines denote measurements; dashed lines computations with breaking dissipation for all frequencies; and dotted lines computations with breaking dissipation excluded for  $f < 0.1$  Hz.*

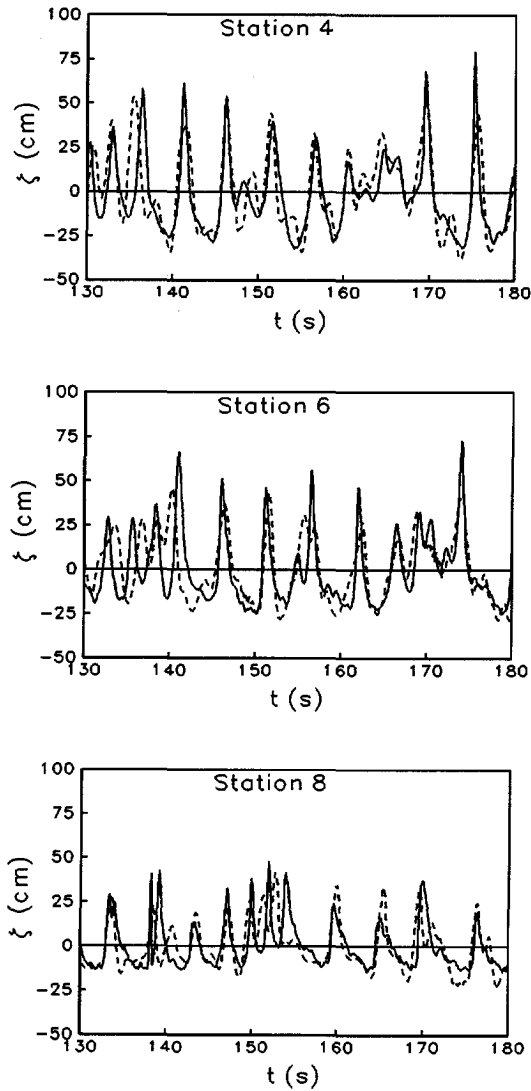


**Figure 4.12** *Surface elevations at various locations for test C. Solid lines denote measurements; dashed lines denote computations.*



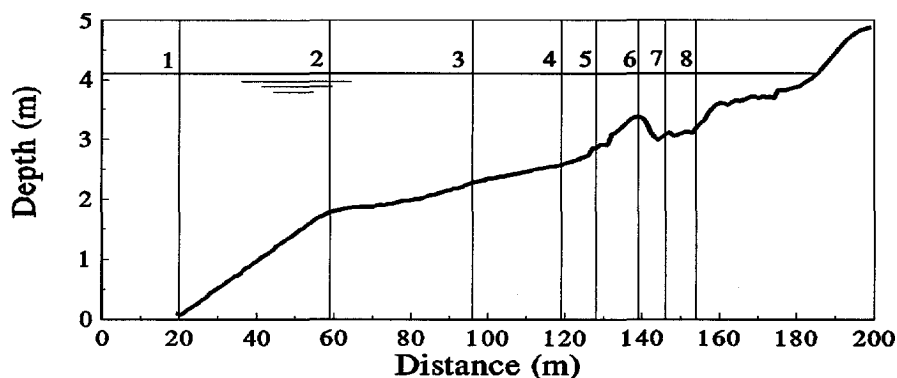


**Figure 4.13** *Bed profile and locations of wave gauges for test D (Arcilla et al., 1994).*

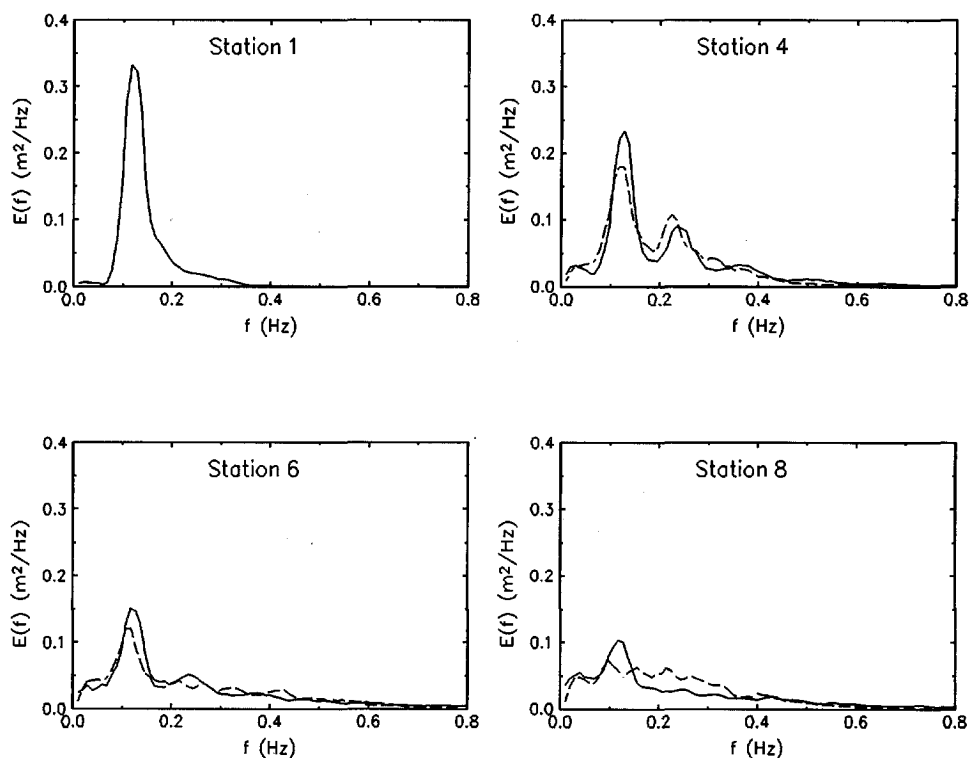


**Figure 4.14** *Spectral density functions of the surface elevations at various locations for test D. Solid lines denote measurements; dashed lines denote computations.*

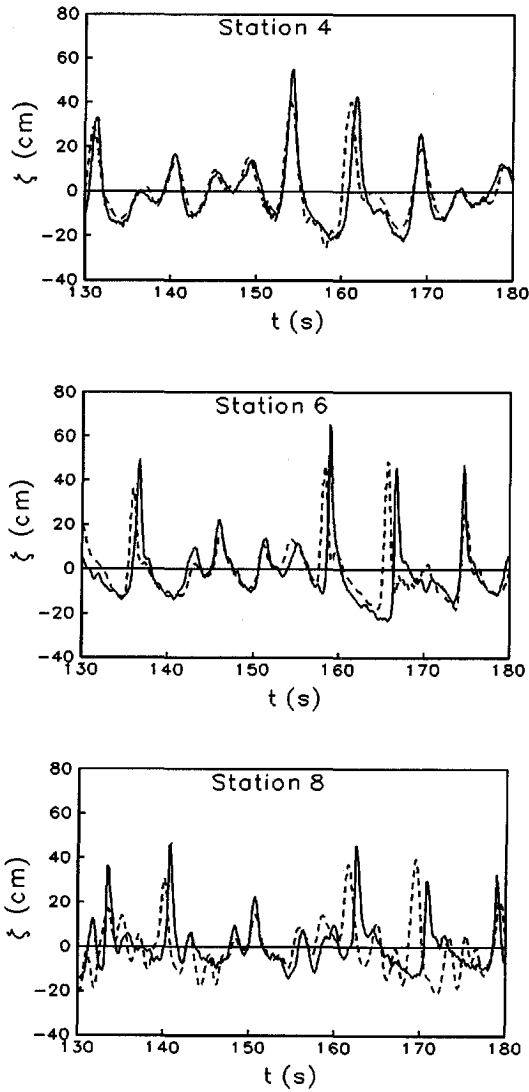


**Figure 4.15** Surface elevations at various locations for test D. Solid lines denote measurements; dashed lines denote computations.

Fig. 4.11 shows the results for test C. For unknown reasons the model overpredicts the low-frequency energy levels in the upwave region where breaking does not yet occur or is very weak (station 4). Farther downwave, this overprediction increases if the low-frequency dissipation is switched off. Unlike test B, the overestimation of the low-frequency energy increases up to station 8, which is ascribed to continued shoaling. In case dissipation is switched on, the model results tend to the experimental values in shallow water, but in view of the above, it can be argued that this may be due more to a fortuitous cancellation of model errors than the result of accurate modeling. Nevertheless, when combined with those of test B, the results do indicate that there is significant dissipation in the low-frequency range, but our limited results do not permit definite conclusions as to the mechanism causing this dissipation nor that our dissipation model is suitable to represent it.

It is noticeable in all four tests that at some locations in the shoaling region the spectral evolution equation tends to underestimate the crest elevation of the highest waves. This could be due to insufficient frequency range or resolution. To verify this, additional computations were carried out. The maximum frequency in the computations was already equal to that in the data, therefore it was not increased. The influence of resolution has been examined for test C by doubling it (frequency resolution 0.00488 Hz, instead of 0.00975 Hz). However, this did not seem to improve the numerical predictions. The same discrepancy has been noted by Madsen and Sørensen (1993).

#### **4.7 Summary and conclusions**

The nonlinear transformation of wave spectra in shallow water is considered from the deterministic modeling point of view. The governing equations for water waves have been reviewed. Various formulations of the Boussinesq-type equations for shallow-water waves have been briefly discussed .

Boussinesq equations incorporate nonlinear shallow-water effects, such as near resonant triad interactions and the generation of bound sub- and superharmonics.

The strength of the cross spectral energy transfer is governed by the mismatch between the bound and the free wavenumbers. This implies that the accuracy of the linear dispersion relation is of the utmost importance for the description of this phenomenon. For this reason, Boussinesq equations with improved dispersion characteristics have been employed in this study. The equations derived by Madsen and Sørensen (1992) seem the most suitable to be transformed into the frequency domain. Some details of this derivation (Madsen and Sørensen, 1993) have been described.

The nonlinear cross-spectral transfers of energy and phase modifications lead to the asymmetric and skewed profiles that are characteristics of nearly breaking and broken waves. The frequent occurrence of wave breaking in such regions required a link between the two processes from the modeling point of view. The role of wave breaking and its influence in the spectral shape is reviewed, with the aim of developing a model that combines the cross-spectral energy transfers due to triad interactions and breaking dissipation.

The main results of this chapter can be summarized with some conclusions as follows:

1. Spectral evolution equations based on Boussinesq model with improved dispersion characteristics are able to describe the generation of sub- and superharmonics. The phase mismatch is of utmost importance for the description of this phenomenon.
2. The model predicts nonlinear correction to the phase speeds of various wave components due to nonlinear interactions, leading to virtually nondispersive propagation in shallow water despite the presence (weak) frequency dispersion.
3. Energy dissipation due to wave breaking is formulated in a spectral form, both for energy-density models and complex amplitude models. The spectral breaking term is based on the total rate of energy dissipation by breaking. On the basis of observations of Beji and Battjes (1993), the spectral dissipation term is chosen such that it reduces the total (spectrally integrated) energy without affecting the spectral shape.
4. The spectral breaking model has been applied to a deterministic spectral evolution equation, based on extended Boussinesq equations. This formulation

is used to describe the evolution of random waves propagating into shallow water, including the simultaneous effects of harmonic generation and wave breaking.

5. The model is validated against laboratory measurements for random wave transformation over barred and nonbarred bed profiles. It has been found to yield realistic predictions of the spectral evolution in the shoaling region and inside the surf zone. This validation supports previous observational results in which wave breaking dissipation appeared to be proportional to the spectral energy level, without dependence on the frequency.

6. The model results are also compared to measured surface elevation. It is found to yield realistic prediction of the wave profile in the shoaling region and the outer surf zone. Some discrepancies are observed for the inner surf zone. The data do not support the need of a phase shift induced by breaking.

7. The nonlinearly generated low-frequency waves are significantly damped. The model proposed here for the higher-frequency range seems to predict the low-frequency energy reasonably well in comparison with experimental results, but that may be fortuitous. This problem deserves further study.



## Chapter 5

### 5. Random-wave modeling of wave evolution in shallow water

#### 5.1 Introduction

As shown in chapter 4, Boussinesq equations can be used to establish evolution equations for the amplitudes and phases of waves propagating over slowly varying topography, simulating harmonic generation. For computational efficiency, phase-averaged energy based models are preferred. For application in such models, Abreu et al. (1992) have presented an energy source term representing the average effect of triad interactions. Their derivation is restricted to nondispersive shallow-water waves with resonant colinear triad interactions. This is a grave restriction in application to dispersive waves in shallow water depths. Thus a model for the effect of triad interactions in dispersive waves is highly desired.

Two approaches for modeling triad interactions in dispersive waves are described in chapters 6 and 7. The governing equations used in these approaches are essentially based on established formulations for nonlinear random wave interaction theory, in particular the Zakharov kinetic equation for resonant triad interactions. In this chapter a resume of the derivation of this equation is given to prepare the ground for the following chapters. The material presented in this chapter is mainly taken from Zakharov et al. (1992). Further details may be found in Eldeberky (1995).

The arrangement of this chapter is as follows. The Hamiltonian equations of motion for surface gravity water waves are presented in section 2. In section 3, evolution equations of the canonical variable are given. A statistical description in terms of the spectral density function is presented in section 4. In section 5,

the hierarchy of moment equations is constructed and truncated. The kinetic equation for three-wave interactions is given in section 6. A summary and conclusions are finally given in section 7.

## 5.2 Hamiltonian equations of motion

The problem of gravity-water waves in a depth-limited ocean is considered. The fluid is assumed incompressible and inviscid in a homogeneous gravitational field. Potential flow is assumed and surface tension effects are neglected. The bottom is a rigid and impermeable surface at  $z = -h(\mathbf{r})$ , where  $\mathbf{r}$  is the two-dimensional horizontal coordinate. The free surface elevation is  $\zeta(\mathbf{r}, t)$ , and  $\Phi(\mathbf{r}, z, t)$  is the velocity potential. The velocity potential at the surface is  $\Psi(\mathbf{r}, t) = \Phi(\mathbf{r}, z = \zeta(\mathbf{r}, t), t)$

The fluid flow is described by Laplace's equation

$$\nabla^2 \Phi + \frac{\partial^2 \Phi}{\partial z^2} = 0 \quad -h(\mathbf{r}) \leq z \leq \zeta(\mathbf{r}, t) \quad (5.1)$$

with the bottom boundary condition

$$\frac{\partial \Phi}{\partial z} + \nabla h \cdot \nabla \Phi = 0 \quad z = -h(\mathbf{r}) \quad (5.2)$$

The sea surface  $z = \zeta(\mathbf{r}, t)$  and the velocity potential  $\Psi(\mathbf{r}, t)$  are the canonical variables. The kinematic and the dynamic free surface boundary conditions are respectively (Zakharov, 1968)

$$\frac{\partial \zeta}{\partial t} = \frac{\delta H}{\delta \Psi} \quad (5.3)$$

$$\frac{\partial \Psi}{\partial t} = - \frac{\delta H}{\delta \zeta} \quad (5.4)$$



where  $\delta/\delta\zeta$  and  $\delta/\delta\Psi$  designate variational derivatives and  $H$  is the total energy per unit mass of the fluid, the so-called Hamiltonian, defined as the summation of the kinetic energy and the potential energy:

$$H = \frac{1}{2} \int dr \int_{-h}^{\zeta} \left[ (\nabla\Phi)^2 + \left( \frac{\partial\Phi}{\partial z} \right)^2 \right] dz + \frac{g}{2} \int \zeta^2 dr \quad (5.5)$$

For the problem of shallow-water weakly nonlinear waves, shoaling over a mildly sloping bottom, equation (5.5), in terms of the free surface variable, reduces to

$$H = \frac{1}{2} \int dr \left[ (h+\zeta)(\nabla\Psi)^2 + g\zeta^2 \right] \quad (5.6)$$

The formulation (5.6) includes the effects of weak nonlinearity via the term  $\zeta(\nabla\Psi)^2$  and the effect of slowly varying depth ( $h=h(r)$ ).

For a formulation in a spectral domain, equation (5.6) is to be expressed in terms of the Fourier transforms of  $\zeta$  and  $\Psi$ . The Fourier transforms of  $\zeta$  and  $\Psi$  are given by:

$$\zeta(r,t) = \frac{1}{2\pi} \int dk \hat{\zeta}(k) \exp(ik \cdot r) \quad (5.7)$$

$$\Psi(r,t) = \frac{1}{2\pi} \int dk \hat{\Psi}(k) \exp(ik \cdot r) \quad (5.8)$$

where  $k$  is the wavenumber vector. Upon substitution of (5.7) and (5.8) for  $\zeta$  and  $\Psi$  in equation (5.6), the spectral formulation reads

$$\begin{aligned}
 H = & \frac{1}{2} \int dk [k^2 h \hat{\Psi}(k) \hat{\Psi}(-k) + g \hat{\zeta}(k) \hat{\zeta}(-k)] \\
 & - \frac{1}{4\pi} \iiint dk dk_1 dk_2 k \cdot k_1 \hat{\Psi}(k) \hat{\Psi}(k_1) \hat{\zeta}(k_2) \delta(k+k_1+k_2)
 \end{aligned} \tag{5.9}$$

Here

$$\delta(k) = \frac{1}{(2\pi)^2} \int dr \exp(ik \cdot r) \tag{5.10}$$

is the Dirac delta function. The first integral in (5.9), which is quadratic in the Fourier modes of both  $\Psi$  and  $\zeta$ , represents the linear part. The second integral, which is cubic in a combination of the Fourier modes for  $\Psi$  and  $\zeta$ , represents the nonlinear contribution due to the three-wave interactions.

Instead of a formulation in terms of  $\hat{\zeta}$  and  $\hat{\Psi}$ , Zakharov (1968) suggested a formulation in a complex variable  $G(k, t)$  given by

$$G(k, t) = \frac{1}{\sqrt{2}} \left[ \lambda \hat{\zeta}(k, t) + i \frac{\hat{\Psi}(k, t)}{\lambda} \right] \tag{5.11}$$

Here  $\lambda$  is a dimensional factor such that the real and the imaginary parts of  $G(k, t)$  (i.e.,  $\lambda\zeta$  and  $\Psi/\lambda$  respectively) have the same dimension. The form of  $\lambda$  depends on the governing dispersion relation. For surface gravity water waves in intermediate depth, with the exact linear dispersion relation,

$$\omega_k^2 = g k \tanh(kh) \tag{5.12}$$

where  $k$  is the wavenumber magnitude, the general form of  $\lambda$  is given by (Zakharov and Kharitonov, 1970):

$$\lambda = \left[ \frac{g}{\omega(k)} \right]^{\frac{1}{2}} \tag{5.13}$$

Using the canonical transformation to the complex variable  $G(k, t)$  (with the shorthand notation  $G_k$ ),  $\hat{\zeta}$  and  $\hat{\Psi}$  can be expressed as follows:

$$\hat{\zeta} = \frac{1}{\sqrt{2} \lambda} (G_k + G_{-k}^*) \quad (5.14)$$

$$\hat{\Psi} = -i \frac{\lambda}{\sqrt{2}} (G_k - G_{-k}^*) \quad (5.15)$$

Here  $G_k^*$  is the complex conjugate of  $G_k$ . The canonical equations (5.3 and 5.4) can be expressed in terms of the variables  $G_k^*$  and  $G_k$  as follows

$$\frac{\partial G_k}{\partial t} = -i \frac{\delta H}{\delta G_k^*}, \quad \frac{\partial G_k^*}{\partial t} = -i \frac{\delta H}{\delta G_k} \quad (5.16)$$

Using equations (5.14), (5.15) and (5.16), the total energy (5.9) can be expressed in the form of a series in powers of  $G_k$  and  $G_k^*$ . Retaining only the quadratic and cubic terms, the total energy becomes

$$H = \int dk \omega_k G_k G_k^* + \iiint dk dk_1 dk_2 [V_{k12} (G_k^* G_1 G_2 + G_k G_1^* G_2^*) \delta_{k-1-2} + \frac{1}{3} \hat{V}_{k12} (G_k G_1 G_2 + G_k^* G_1^* G_2^*) \delta_{k+1+2}] \quad (5.17)$$

with the shorthand notation  $\delta_{k+1+..} = \delta(k + k_1 + ..)$ . The first integral, which is quadratic in the complex variable, represents the linear part of the formulation. The second integral, which is cubic in the complex variable, represents the nonlinear part ascribed to the three-wave interactions. Equation (5.17) is similar to that obtained by Zakharov (1968). (Zakharov's equation has an extra integral describing the four-wave interactions.)

The general form of the interaction matrix  $V_{k12}$  for water waves in intermediate depth is given by (Stiassnie and Shemer, 1984):

$$V_{kl2} = \frac{g^{1/2}}{8\pi\sqrt{2}} \left\{ [k \cdot k_1 - (\omega_k \omega_1 / g)^2] (\omega_2 / \omega_k \omega_1)^{1/2} \right. \\ + [k \cdot k_2 - (\omega_k \omega_2 / g)^2] (\omega_1 / \omega_k \omega_2)^{1/2} \\ \left. + [k_1 \cdot k_2 + (\omega_1 \omega_2 / g)^2] (\omega_k / \omega_1 \omega_2)^{1/2} \right\} \quad (5.18)$$

The nonlinear part of equation (5.17) (i.e., the second integral) contains four terms of triple products of the complex amplitude. Zakharov et al. (1992) point out that the third and fourth terms represent mutual annihilation of three waves and their creation from vacuum respectively; their contributions in surface gravity water waves can be neglected.

### 5.3 The evolution equations

The approximation for the total energy (5.17) is repeated here for convenience after keeping only the relevant terms for the process of three-wave interactions

$$H = \int dk \, \omega_k G_k G_k^* + \iiint dk dk_1 dk_2 \, V_{kl2} (G_k^* G_1 G_2 + G_k G_1^* G_2^*) \delta_{k-k_1-2} \quad (5.19)$$

The dynamic equation for the complex variable  $G_k$  can be derived from the equation (5.19) using the canonical equations (5.16). The evolution equation of the complex variable is

$$\frac{dG_k}{dt} = -i\omega_k G_k - i \iint dk_1 dk_2 \, (V_{kl2} G_1 G_2 \delta_{k-k_1-2} + 2V_{lk2} G_1 G_2^* \delta_{k+2-1}) \quad (5.20)$$

The first term on the right-hand-side represents the linear evolution term. The second term represents the interaction integral with two contributions: the first

is the sum interaction; the second term is the difference interaction.

The dynamic equations (5.20) for  $k=1,2,\dots$  constitute a set of coupled nonlinear differential equations which can be integrated to determine the time evolution of the amplitudes  $|G_k|$  and their phases  $\phi_k$ , i.e.,  $G_k = |G_k| \exp[-i\phi_k]$ . Here  $\phi_k = \omega_k t + \theta_k$ , where  $\omega_k t$  is the rapid wave phase, which is ascribed to the linear evolution, and  $\theta_k$  is the slow wave phase ascribed to the three-wave interactions.

#### 5.4 Statistical description of random waves

The formulation given by (5.20) is deterministic since it yields both amplitudes and phases. In general, a statistical formulation is preferred when the system is inherently chaotic or unpredictable, when there is insufficient knowledge of the initial conditions to pose a deterministic problem, or, perhaps most often, when the information desired is a measure of "typical" or "average" properties of the system. This is the case for wind-generated waves. The following derivation of a statistical formulation for nonlinear triad wave interactions is mainly taken from Zakharov et al. (1992).

In a statistical description of random waves it would be natural to average over the ensemble of random phases. Such averages will be denoted with  $\langle . \rangle$ . After such averaging, only moments that are independent of the wave phase will be nonzero. For example

$$\begin{aligned} \langle G_k \rangle &= \langle |G_k| \exp[-i\phi_k] \rangle = 0 \\ \langle G_k G_{k'} \rangle &= \langle |G_k| |G_{k'}| \exp[-i(\phi_k + \phi_{k'})] \rangle = 0 \\ \langle G_k G_{k'}^* \rangle &= \langle |G_k| |G_{k'}| \exp[-i(\phi_k - \phi_{k'})] \rangle \neq 0 \end{aligned} \quad (5.21)$$

The complex canonical variable  $G(k, t)$  can be seen as the Fourier transform of the random variable  $\nu(r, t)$  given by

$$G(k, t) = \frac{1}{(2\pi)^2} \int dr \nu(r, t) \exp(-i k \cdot r) \quad (5.22)$$

The second statistical moment is by definition

$$\langle G_1 G_2^* \rangle = \frac{1}{(2\pi)^4} \iint dr_1 dr_2 \langle \nu(r_1) \nu(r_2) \rangle \exp[-i(k_1 \cdot r_1 - k_2 \cdot r_2)] \quad (5.23)$$

in which  $\langle \nu(r_1) \nu(r_2) \rangle$  is the second-order correlation function denoted by  $C(r_1, r_2)$  or equivalently  $C(r_1, \hat{r})$ , where  $\hat{r} = r_1 - r_2$  is the spatial separation vector. If the statistical properties of  $\nu(r, t)$  are independent of  $r$ , i.e., a homogeneous wavefield, the correlation function becomes only dependent on the spatial separation vector  $\hat{r}$

$$\langle \nu(r_1) \nu(r_2) \rangle = C(\hat{r}) \quad (5.24)$$

The continuous energy spectrum of the sea surface elevation is defined as the Fourier transform of the second-order correlation function. Substituting equation (5.24) in (5.23), we find

$$\langle G_1 G_2^* \rangle = n(k_1) \delta(k_1 - k_2) \quad (5.25)$$

where

$$n(k_1) \equiv \frac{1}{(2\pi)^2} \int d\hat{r} C(\hat{r}) \exp(-i k_1 \cdot \hat{r}) \quad (5.26)$$

is the spectral density function of the complex variable  $G_k$ , and

$$\delta(k_1 - k_2) \equiv \frac{1}{(2\pi)^2} \int dr \exp[i(k_1 - k_2) \cdot r] \quad (5.27)$$

is the Dirac delta function.

In the next section, we elucidate a transition from a deterministic description of the problem of nonlinear triad interactions in random waves in terms of amplitude and phase to a statistical one in terms of average quantities such as  $\langle G_0 \rangle$ ,  $\langle G_0 G_1 \rangle$ ,  $\langle G_0 G_1 G_2 \rangle$ .

### 5.5 The hierarchy of moment equations

#### *The moment equations*

The evolution equation for the so-called second-order moment  $\langle G_k G_k^* \rangle$  can be derived by multiplying (5.20) by  $G_k^*$ , the complex conjugate equation of (5.20) by  $G_k$ , adding the latter to the former, and averaging.

Multiplying equation (5.20) by  $G_k^*$  yields

$$G_k^* \frac{dG_k}{dt} = -i\omega_k G_k G_k^* - i \iint dk_1 dk_2 [V_{k12} G_k^* G_1 G_2 \delta_{k-1-2} + 2V_{1k2} G_k^* G_1 G_2^* \delta_{k+2-1}] \quad (5.28)$$

Similarly, multiplying the complex conjugate equation of (5.20) by  $G_k$  yields

$$G_k \frac{dG_k^*}{dt} = i\omega_k G_k^* G_k + i \iint dk_1 dk_2 [V_{k12} G_k G_1^* G_2^* \delta_{-k+1+2} + 2V_{1k2} G_k G_1^* G_2 \delta_{-k-2+1}] \quad (5.29)$$

Now the evolution equation for the second-order moment is:

$$\frac{d}{dt} \langle G_k G_k^* \rangle = \langle G_k \frac{dG_k^*}{dt} \rangle + \langle G_k^* \frac{dG_k}{dt} \rangle \quad (5.30)$$

Substitution of equation (5.28) and (5.29) into (5.30), yields

$$\begin{aligned} \frac{d}{dt} \langle G_k G_k^* \rangle = & -i \iint dk_1 dk_2 (V_{k12} [\langle G_k^* G_1 G_2 \rangle - \langle G_k G_1^* G_2^* \rangle] \delta_{k-1-2} \\ & + 2V_{1k2} [\langle G_k^* G_1 G_2^* \rangle - \langle G_k G_1^* G_2 \rangle] \delta_{k+2-1}) \end{aligned} \quad (5.31)$$

Simplification of the terms between brackets gives

$$\begin{aligned} \frac{d}{dt} \langle G_k G_k^* \rangle = & -2 \text{Im} \iint dk_1 dk_2 [V_{k12} \langle G_k^* G_1 G_2 \rangle \delta_{k-1-2} \\ & - 2V_{1k2} \langle G_k G_1^* G_2 \rangle \delta_{k+2-1}] \end{aligned} \quad (5.32)$$

Equation (5.32) for the second-order moment is consistently derived from the evolution equation of the complex amplitude (equation 5.20), but it cannot describe the evolution of the second-order moment without additional information about the third-order moment (triple product of complex amplitudes).

For simplicity we use shorthand notation for the moments  $M_{kk} = \langle G_k G_k^* \rangle$  and  $M_{k12} = \langle G_k^* G_1 G_2 \rangle$ . Equation (5.32) can be written as

$$\frac{d}{dt} M_{kk} = -2 \text{Im} \iint dk_1 dk_2 (V_{k12} M_{k12} \delta_{k-1-2} - 2V_{1k2} M_{1k2} \delta_{k+2-1}) \quad (5.33)$$

The evolution equation for the third-order moment  $M_{k12}$  can be obtained as follows

$$\frac{d}{dt} \langle G_k^* G_1 G_2 \rangle = \langle G_k^* G_1 \frac{dG_2}{dt} \rangle + \langle G_k^* G_2 \frac{dG_1}{dt} \rangle + \langle G_1 G_2 \frac{dG_k^*}{dt} \rangle \quad (5.34)$$

Substituting equation (5.20) in (5.34) and performing some algebraic manipulations (Eldeberky, 1995), the evolution equation of the third-order moment  $M_{k12}$  becomes



$$\frac{d}{dt} M_{k12} = i(\omega_k - \omega_1 - \omega_2) M_{k12} - i \iint dk_3 dk_4 [2V_{324} M_{k413} \delta_{2+4-3} + 2V_{314} M_{k423} \delta_{1+4-3} - V_{k34} M_{3412} \delta_{k-3-4}] \quad (5.35)$$

with the shorthand notation  $M_{k123} = \langle G_k^* G_1^* G_2 G_3 \rangle$  for the fourth-order moment, in which the indices are dummy arguments. This equation is similar to that obtained by Zakharov et al. (1992). Clearly the third-order moment evolves in terms of fourth-order moments. So a hierarchy of moment equations is obtained where every moment evolves in terms of the next higher one, i.e., the second-order moment evolves in terms of the third one, the third-order moment in terms of the fourth one, and so on. To solve this infinite system of moment equations we need to truncate the hierarchy at a certain level.

#### *Truncation of the moment equations*

The fourth-order moments can be expressed in terms of products of second-order moments and an irreducible quantity  $b$ , a so-called fourth-order cumulant:

$$M_{1234} = M_{12} M_{34} + M_{13} M_{24} + M_{14} M_{23} + b_{1234} \quad (5.36)$$

where  $M_{ij} = \langle G_i G_j \rangle$ . Reference is made to Monin and Yaglom (1979) for the definition of cumulants both for random variables and random fields. For decreasing steepness the ensemble of non-interacting waves tends to a Gaussian state. The nonlinearities will tend to create correlations (higher cumulants). These are important because they measure the extent to which the probability distribution of the sea surface differs from normal (Gaussian). If nonlinearity is weak, then the fourth-order cumulants  $b_{1234}$  can be neglected. This is called the "quasi-Gaussian hypothesis", in which the statistics of the sea surface elevation are assumed to be near-Gaussian. The use of the "zero fourth-order cumulants" assumption means that the fourth-order moment can be expressed in terms of pairs of products of second-order moments, and consequently enables the closure of the hierarchy of the evolution equations.

## 5.6 Kinetic wave equation

The evolution equation of the second moment (5.33) can be rewritten in terms of the spectral density function  $n_k$  (Zakharov et al., 1992) as

$$\frac{d}{dt} n_k = -2 \text{Im} \iint dk_1 dk_2 (V_{k12} J_{k12} \delta_{k-1-2} - 2 V_{1k2} J_{1k2} \delta_{k+2-1}) \quad (5.37)$$

Here  $J_{k12}$  is the third-order correlation function defined by

$$J_{k12} \delta_{k-1-2} = M_{k12} \quad (5.38)$$

In order to calculate the evolution of  $n_k$ , one should know  $J_{k12}$ . Using definition (5.38) in the evolution equation of the third-order moment (5.35),

$$\begin{aligned} \frac{d}{dt} J_{k12} = i(\omega_k - \omega_1 - \omega_2) J_{k12} - i \iint dk_3 dk_4 [2 V_{324} J_{k413} \delta_{2+4-3} \\ + 2 V_{314} J_{k423} \delta_{1+4-3} - V_{k34} J_{3412} \delta_{k-3-4}] \end{aligned} \quad (5.39)$$

Here  $J_{k123}$  is the fourth-order correlation function defined by

$$J_{k123} \delta_{k+1-2-3} = M_{k123} \quad (5.40)$$

The chain of evolution equations for the wave correlators (5.37 and 5.39) can be truncated using the quasi-Gaussian hypothesis, in which the fourth-order wave correlator  $J_{k123}$  can be expressed via the second-order correlators  $n_k$ . Reference is made to Zakharov et al. (1992) for the underlying theory. The evolution equation of the third-order correlator becomes

$$\frac{d}{dt} J_{k12} = i(\omega_k - \omega_1 - \omega_2) J_{k12} - 2i V_{k12} [n_k n_1 + n_k n_2 - n_1 n_2] \quad (5.41)$$

To integrate this equation, one should neglect the time dependence of  $n_k$ , i.e.,

set the second term on the right-hand-side equal to constant. Integrating from  $t=0$  to  $\tau$ , we get

$$J_{k12} = -2iV_{k12}[n_k n_1 + n_k n_2 - n_1 n_2] \left[ \frac{\exp[-i(\omega_k - \omega_1 - \omega_2)\tau] - 1}{-i(\omega_k - \omega_1 - \omega_2)} \right] \quad (5.42)$$

Substitution of (5.42) into (5.37) gives two kinds of contributions. First an integral (over the wavenumber spectrum) of a fast oscillating function; Zakharov et al. (1992) neglected its contribution based on the phase-mixing effect. Second a steady contribution that gives for  $J$  an expression that is slowly varying in time and depends on  $n$  according to

$$J_{k12} = -2iV_{k12}[n_k n_1 + n_k n_2 - n_1 n_2] \frac{1}{\Omega + i(\omega_k - \omega_1 - \omega_2)} \quad (5.43)$$

$\Omega$  is an auxiliary frequency parameter added to circumvent the pole at  $\omega_k - \omega_1 - \omega_2 = 0$ . Substitution of (5.43) into (5.37) gives the following integral for three-wave interactions

$$\frac{dn_k}{dt} = 4 \iint dk_1 dk_2 [V_{k12}^2 N_{k12} \mu_{k-1-2} \delta_{k-1-2} - 2V_{1k2}^2 N_{1k2} \mu_{k-1+2} \delta_{k-1+2}] \quad (5.44)$$

where

$$N_{k12} = -(n_k n_1 + n_k n_2 - n_1 n_2) \quad (5.45)$$

and

$$\mu_{k-1-2} = \text{Re} [\Omega + i(\omega_k - \omega_1 - \omega_2)]^{-1} \quad (5.46)$$

Using the shorthand notation  $\Delta\omega = \omega_k - \omega_1 - \omega_2$  and  $\mu$  for  $\mu_{k-1-2}$ , we have

$$\mu = \frac{\Omega}{\Omega^2 + \Delta\omega^2} \quad (5.47)$$

The factor  $\mu$  functions as a frequency filter. It is useful to gain insight in its behavior. A normalized representation of  $\mu$  is given in Fig. 5.1 in which  $\Omega\mu$  is plotted versus  $\Delta\omega/\Omega$ . The plot indicates that  $\mu$  is a spiky-type distribution. Its integral has the value  $\pi$ .

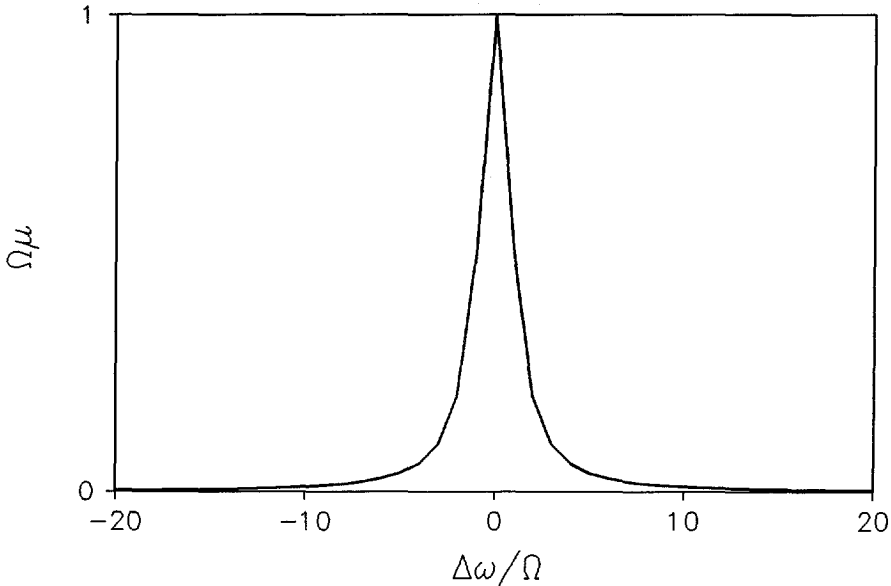


**Figure 5.1** Normalized representation of  $\mu$

A non-normalized representation of  $\mu$  is given in Fig. 5.2, in which  $\mu$  is plotted versus  $\Delta\omega$  for various values of  $\Omega$ . The plot indicates that the filter becomes narrower and more spiky by decreasing the value of  $\Omega$ , but the integral always equals  $\pi$  independent of  $\Omega$ .

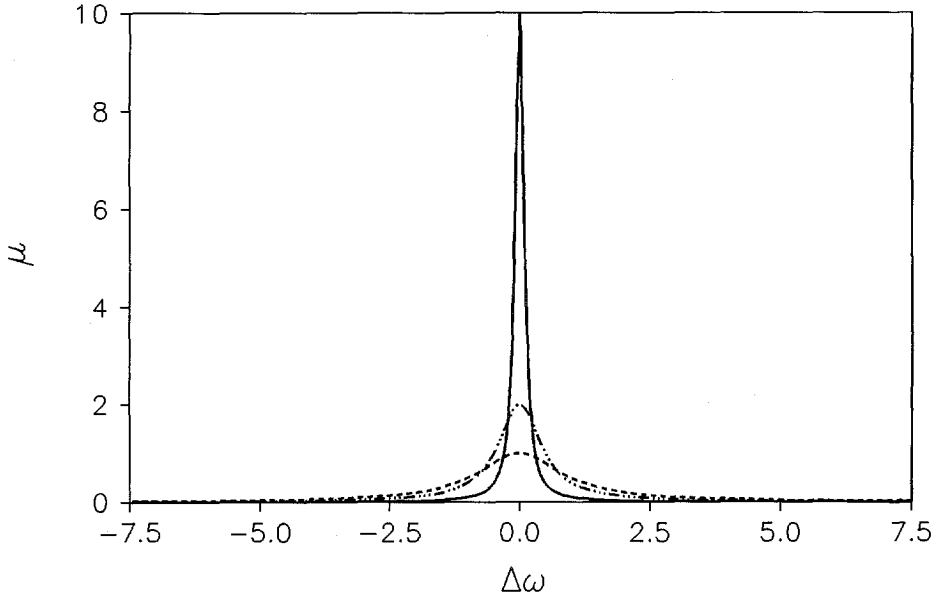


**Figure 5.2** Non-normalized representation of  $\mu$ . Dashed line:  $\Omega=1.0$ ; Dot-dashed line:  $\Omega=0.5$ ; Solid line:  $\Omega=0.1$ .

In the limit of  $\Omega \rightarrow 0$ , we have  $\mu_{k-1-2} = \pi \delta(\omega_k - \omega_1 - \omega_2)$ . Zakharov et al. (1992) use this limit, which upon substitution in (5.44) results in the kinetic equation for three-wave interactions

$$\begin{aligned} \frac{dn_k}{dt} = 4\pi \iint dk_1 dk_2 \{ & V_{k12}^2 N_{k12} \delta(k - k_1 - k_2) \delta(\omega_k - \omega_1 - \omega_2) \\ & + 2 V_{1k2}^2 N_{1k2} \delta(k_1 - k - k_2) \delta(\omega_1 - \omega_k - \omega_2) \} \end{aligned} \quad (5.48)$$

The evolution equation (5.48) gives nonzero contributions only for waves satisfying the resonance conditions  $k - k_1 - k_2 = 0$  and  $\omega_k - \omega_1 - \omega_2 = 0$ . For the problem of off-resonant energetic triad interaction, Holloway (1982) suggested to use

(5.46) for  $\mu_{k12}$  with a small but finite value of  $\Omega$  instead of its limit for  $\Omega \rightarrow 0$ , i.e.,  $\pi\delta(\omega_k - \omega_1 - \omega_2)$ . He used  $\Omega$  as a prognostic variable related to the rate of growth of individual harmonics. A similar approach to include the off-resonant energetic triad interactions is investigated in chapter 6.

### 5.7 Summary and conclusions

A resume has been presented of results from literature for a statistical formulation of spectral energy transfer due to triad interactions, mainly taken from Zakharov et al. (1992).

Random-wave modeling of wave evolution in shallow water is considered using the Hamiltonian formulation. The governing equations of motion and the Hamiltonian formalism for surface gravity water waves are viewed at an introductory level with emphasis on the nonlinear three-wave interactions. Evolution equations for the moments of the complex canonical variable are derived from the governing equations of motion; they represent a chain of interconnected equations. The solution of this chain requires a closure using the quasi-Gaussian assumption under which the wavefield is assumed to be near Gaussian. This is used to express the fourth-order moment in terms of products of the second-order moments. The kinetic equation for three-wave interactions is derived in terms of the spectral density function. Zakharov et al. (1992) used this equation to formulate the kinetic wave equation for resonant three-wave interactions. This is a grave restriction in application to dispersive waves in intermediate water depths. The inclusion of off-resonant energetic triad interactions in dispersive waves is considered in the next chapter.







## Chapter 6

### 6. Energy formulation for triad wave interactions

#### 6.1 Introduction

The problem of off-resonant triad wave interactions is considered in this chapter. The kinetic integral for three-wave interactions derived in chapter 5 is used with an analytical formula as suggested by Holloway (1982) to allow for the off-resonant energetic triad interactions. The purpose of this chapter is to investigate the feasibility of such approach for application in spectral energy wave models to represent the cross-spectral energy transfers between various spectral components.

The arrangement of this chapter is as follows. In section 2, the kinetic equation for off-resonant triad wave interactions is presented for the energy spectrum. The kinetic equation is expressed in non-dimensional form, numerically investigated, and the results are analyzed in section 3. In section 4, the kinetic integral is used as an energy source/sink term in a spectral evolution model that is used for verification against experimental data. In section 5, a discussion is given about the consequences of the approximation made in the kinetic equation. Finally a summary and conclusions are given in section 6.

#### 6.2 Kinetic equation for off-resonant triad interactions

##### 6.2.1 Formulation for the energy spectrum of the canonical variable

The problem of off-resonant triad interactions of surface gravity waves is treated mathematically using the Zakharov kinetic equation, which is described

in details in chapter 5. The evolution equation of the spectral "energy" density  $n_k$  due to triad interaction between components  $k$ ,  $k_1$  and  $k_2$ , is repeated here for convenience

$$\frac{dn_k}{dt} = 4 \iint dk_1 dk_2 [V_{k12}^2 N_{k12} \mu_{k-1-2} \delta_{k-1-2} - 2 V_{1k2}^2 N_{1k2} \mu_{k-1+2} \delta_{k-1+2}] \quad (6.1)$$

where

$$N_{k12} = n_1 n_2 - n_k (n_1 + n_2) \quad (6.2)$$

and

$$\mu_{k-1-2} = \frac{\Omega}{(\omega_k - \omega_1 - \omega_2)^2 + \Omega^2} \quad (6.3)$$

$\Omega$  is an auxiliary frequency parameter which is small compared to the spectral peak frequency ( $\Omega \ll \omega_p$ ). Resonance corresponds to  $\Omega \rightarrow 0$  in which case  $\mu_{k-1-2}$  reduces to  $\pi \delta(\omega_k - \omega_1 - \omega_2)$  (Zakharov et al., 1992), leading to the Zakharov kinetic equation for resonant three-wave interactions (described in chapter 5). The restriction to resonant interactions means that wave components contributing to the nonlinear transfer rate  $dn_k/dt$  must satisfy the following resonance conditions

$$\begin{aligned} \omega(k) - \omega(k_1) - \omega(k_2) &= 0 \\ k - k_1 - k_2 &= 0 \end{aligned} \quad (6.4)$$

Exact resonance cannot be satisfied for surface gravity waves in water of arbitrary depth (Phillips, 1960; Hasselmann, 1962) with the following frequency dispersion

$$\omega^2 = gk \tanh(kh) \quad (6.5)$$

Thus for practical applications in intermediate depth, a formulation which allows for a degree of phase mismatch between the interacting waves is required to include the effect of the off-resonant energetic triad interactions. Mathematically this can be done by using a finite value for  $\Omega$  (instead of  $\Omega \rightarrow 0$ ) in equation (6.3).

The factor  $\mu$  with small parameter  $\Omega$  is a narrow frequency filter of finite but small bandwidth; it has the effect of broadening the resonance condition. In Holloway (1982),  $\Omega$  is a prognostic variable related to the rate of growth of individual harmonics. Polnikov (1995) suggested to treat  $\Omega$  as a constant to be determined empirically. This approach will be taken up in the following.

Multiple time scales are used to separate different scales of motion. There is a fast time scale of the wave phase evolution ( $t_0 = t_p \sim \omega_p^{-1}$ ) and a slow time scale of the spectral energy evolution ( $t_1 \gg t_p \sim \omega_p^{-1}$ ). The latter is the time scale in which the cross-spectral energy transfers take place due to triad interactions. Assuming that the spectral energy is of second-order in nonlinearity:  $E(k) \sim \epsilon^2$ , one can put  $t_1 = t_p \epsilon^{-2}$ . Then an appropriate value for  $\Omega$  should be of the order  $\Omega \cong t_1^{-1} = \epsilon^2 \omega_p$ .

Substituting equation (6.3) into equation (6.1) and integrating in  $k$  space yield the time evolution of the spectral "energy" density  $n_k$  due to triad interaction between components  $k$ ,  $k_1$  and  $k_2$

$$\frac{dn_k}{dt} = 4 \int dk_1 \left\{ V_{k12}^2 N_{k12} \frac{\Omega}{(\omega_k - \omega_1 - \omega_2)^2 + \Omega^2} - 2 V_{1k2}^2 N_{1k2} \frac{\Omega}{(\omega_k - \omega_1 + \omega_2)^2 + \Omega^2} \right\}. \quad (6.6)$$

This is the final equation describing the slow time evolution of the wave spectrum due to off-resonant triad interactions. In the first term of the integrand,  $k_2 = k - k_1$ , representing the sum interaction ( $k = k_1 + k_2$ ); in the second term,  $k_2 = k_1 - k$ , representing the difference interaction ( $k = k_1 - k_2$ ). Note that the resonance condition (6.4) does not necessarily have to be fulfilled in (6.6).

$N_{ijl}$  is expressed in terms of pairs of products of the spectral density function  $n_k$ , given by equation (6.2), and  $V_{kl2}$  is the interaction coefficient given by equation (5.18). The present formulation is directionally coupled in which the integral over the vector wavenumber space allows for both colinear and noncolinear interactions.

### 6.2.2 Formulation for the energy spectrum of the sea surface elevation

The kinetic wave equation (6.6) is expressed in terms of the spectral density function  $n(k)$  of the canonical variable  $G(k)$ . In application to spectral wave models based on the energy (or action) balance equation, source/sink terms are normally expressed in terms of energy (or action) density function  $E(\omega, \theta)$  of the sea surface elevation. Here the relation between  $n(k)$  and the spectral energy density  $E(k)$  is given, followed by transition from the wavenumber spectrum  $E(k)$  to the frequency-directional spectrum  $E(\omega, \theta)$ .

#### *Transition from $n(k)$ to $E(k)$*

The relation between the spectral density function  $n(k)$  of the complex variable  $G_k$  and the wavenumber energy spectrum  $E(k)$  of the sea surface elevation can be found from equation (5.14), yielding

$$n(k) = \frac{(2\pi)^2 g}{\omega(k)} E(k) \quad (6.7)$$

In fact equation (6.7) indicates that apart from a constant factor  $4\pi^2 g$ ,  $n(k)$  can be regarded as the wave action density.

#### *Transition from $E(k)$ to $E(\omega, \theta)$*

The relation between the wavenumber spectrum  $E(k)$  and the frequency-directional spectrum  $E(\omega, \theta)$ , Komen et al. (1994), is

$$E(\omega, \theta) d\omega d\theta \equiv E(k) dk \quad (6.8)$$

( $d\omega$  is the angular frequency bandwidth,  $d\theta$  is the directional bandwidth,  $dk$  is the area in wavenumber space) or equivalently.

$$E(\omega, \theta) d\omega d\theta \equiv E(k) k dk d\theta \quad (6.9)$$

Substitution of  $k=\omega/c$  and  $dk=d\omega/c_g$  in the right-hand-side, in which  $c$  and  $c_g$  are the phase speed and group velocity respectively, yields

$$E(k) = \frac{c c_g}{\omega} E(\omega, \theta) \quad (6.10)$$

Substitution of (6.10) in (6.8) gives

$$dk = \frac{\omega}{c c_g} d\omega d\theta \quad (6.11)$$

*Transition from  $n(k)$  to  $E(\omega, \theta)$*

The relation between  $n(k)$  and  $E(\omega, \theta)$  can be finally obtained by substituting (6.10) in (6.7)

$$n(k) = (2\pi)^2 \frac{g c c_g}{\omega^2} E(\omega, \theta) \quad (6.12)$$

*Evolution equation of  $E(\omega, \theta)$*

The evolution equation of the frequency-directional energy spectrum  $E(\omega, \theta)$  can be found by substitution of (6.12) into (6.6) and rearranging

$$\frac{dE(\omega_k, \theta_k)}{dt} = 16\pi^2 g \int_0^{2\pi} \int_0^\infty d\omega_1 d\theta_1 \frac{c_2 c_{g2}}{\omega_1 \omega_2^2} (T_{k12}^+ - 2T_{1k2}^-) \quad (6.13)$$

Here

$$T_{k12}^+ = V_{k12}^2 \left[ \frac{\omega_k^2}{c_k c_{g,k}} E_1 E_2 - \frac{\omega_2^2}{c_2 c_{g2}} E_k E_1 - \frac{\omega_1^2}{c_1 c_{g1}} E_k E_2 \right] \left[ \frac{\Omega}{(\omega_k - \omega_1 - \omega_2)^2 + \Omega^2} \right] \quad (6.14)$$

$$T_{1k2}^- = V_{1k2}^2 \left[ \frac{\omega_1^2}{c_1 c_{g1}} E_k E_2 - \frac{\omega_2^2}{c_2 c_{g2}} E_k E_1 - \frac{\omega_k^2}{c_k c_{g,k}} E_1 E_2 \right] \left[ \frac{\Omega}{(\omega_k - \omega_1 + \omega_2)^2 + \Omega^2} \right] \quad (6.15)$$

Note that the dimension of  $E(\omega, \theta)$  is  $\text{m}^2/\text{Hz}/\text{rad}$ . The interaction coefficient  $V_{k12}$  is given by

$$V_{k12} = \frac{g^{1/2}}{8\pi\sqrt{2}} \left\{ [k \cdot k_1 - (\omega_k \omega_1 / g)^2] (\omega_2 / \omega_k \omega_1)^{1/2} \right. \\ + [k \cdot k_2 - (\omega_k \omega_2 / g)^2] (\omega_1 / \omega_k \omega_2)^{1/2} \\ \left. + [k_1 \cdot k_2 + (\omega_1 \omega_2 / g)^2] (\omega_k / \omega_1 \omega_2)^{1/2} \right\} \quad (6.16)$$

Equations (6.13-15) describe the time evolution of wave energy spectrum  $E(\omega, \theta)$  due to the off-resonant triad interactions. The first term of the integrand  $T_{k12}^+$  represents the sum interaction ( $k = k_1 + k_2$ ), the second  $T_{1k2}^-$  the difference interaction ( $k = k_1 - k_2$ ). The present formulation is directionally coupled and thus allows for both colinear and noncolinear interactions.

### 6.2.3 Nondimensional representation

For numerical investigation it is more convenient to express the interaction integral in nondimensional form. We introduce the following nondimensional variables

$$\frac{\omega}{\omega_p}, \quad \frac{k g}{\omega_p^2}, \quad \frac{h \omega_p^2}{g}, \quad \frac{c \omega_p}{g}, \quad \frac{c_g \omega_p}{g}, \quad \frac{E(\omega, \theta)}{E_p}, \quad \frac{\Omega}{\omega_p} \quad (6.17)$$

where  $E_p$  is the peak value of the energy density  $E(\omega, \theta)$ . For simplicity we introduce the modified spectrum defined by

$$\hat{E}(\omega, \theta) = \frac{c}{\omega^2} \frac{c_g}{g} E(\omega, \theta) \quad (6.18)$$

After using the non-dimensional variables given in (6.17), we use the normalized modified spectrum  $\tilde{E}(\omega, \theta)$

$$\tilde{E}(\omega, \theta) = \frac{\omega_p^4}{E_p g^2} \hat{E}(\omega, \theta) \quad (6.19)$$

All variables in the right-hand-side of (6.13-15) need to be made non-dimensional. The interaction coefficient (6.16) in nondimensional form is

$$\tilde{V}_{k12} = 8\pi\sqrt{2} g^{3/2} \omega_p^{-7/2} V_{k12} \quad (6.20)$$

After some algebraic manipulations, the evolution equation of the energy density  $E(\omega, \theta)$  can be expressed in terms of non-dimensional kinetic integral as follows

$$\frac{dE(\omega, \theta)}{dt} = C_d \tilde{I} \quad (6.21)$$

where

$$C_d = \frac{1}{8} g^{-2} \omega_p^6 E_p^2 \quad (6.22)$$

is a dimensional constant and

$$\begin{aligned} \tilde{I} = \frac{\tilde{\omega}_k^2}{\tilde{c}_k \tilde{c}_{g,k}} \int_0^{2\pi} \int_0^\infty d\tilde{\omega}_1 d\theta_1 [\tilde{V}_{k12}^2 [\tilde{E}_1 \tilde{E}_2 - \tilde{E}_k (\tilde{E}_1 + \tilde{E}_2)]] & \left[ \frac{\tilde{\Omega}}{(\tilde{\omega}_k - \tilde{\omega}_1 - \tilde{\omega}_2) + \tilde{\Omega}^2} \right] \\ - 2\tilde{V}_{1k2}^2 [\tilde{E}_k \tilde{E}_2 - \tilde{E}_1 (\tilde{E}_k + \tilde{E}_2)] & \left[ \frac{\tilde{\Omega}}{(\tilde{\omega}_k - \tilde{\omega}_1 + \tilde{\omega}_2) + \tilde{\Omega}^2} \right] \frac{\tilde{\omega}_1}{\tilde{c}_1 \tilde{c}_{g1}} \end{aligned} \quad (6.23)$$

is the non-dimensional interaction integral. In (6.23) all variables are nondimensional and  $\tilde{E}$  is the non-dimensional modified wave energy density given by (6.18-19). The value of  $\tilde{\Omega}$  should be between 0.01 and 0.1. For generality, all output results of the numerical investigations will be presented in units of the dimensional constant  $C_d$ .

### 6.3 Numerical investigation of energy transfer rate

#### 6.3.1 Aim of investigation

The interaction integral (6.23) is computed to investigate the nonlinear rate (NLR) of energy transfer in a Jonswap-type spectrum. The dependence of NLR on the filter bandwidth  $\Omega$  and relative depth  $kh$  is examined. The Jonswap spectrum is used to describe the frequency distribution of the wave energy. The spectrum  $E(\omega, \theta)$  is then given by

$$E(\omega, \theta) = E_p \alpha \left[ \frac{\omega}{\omega_p} \right]^{-5} \exp \left[ -\frac{5}{4} \left[ \frac{\omega}{\omega_p} \right]^4 \right] \Gamma^\sigma \cos^n(\theta) \quad (6.24)$$

where

$$\sigma = \exp \left[ -\frac{1}{2} \left[ \frac{\omega - \omega_p}{\nu \omega_p} \right]^2 \right] \quad (6.25)$$

in which  $\omega_p$  is the peak frequency (at which the spectrum has its maximum),  $\Gamma$  is the peak enhancement parameter,  $\nu$  is the width of the peak enhancement (set to 0.1),  $n$  is the angular spreading parameter,  $\alpha$  is a multiplication constant such that the maximum value of the spectrum equals  $E_p$ . The choice of  $E_p$  is arbitrary.



The general purpose of the investigations is to study the characteristics of the kinetic integral. The following points are considered:

1. The dependence of the nonlinear rate (NLR) of energy transfer on the filter bandwidth  $\Omega$  and relative depth  $kh$  for two spectral shapes. These are a wide-banded Pierson-Moskovitz spectrum with  $\Gamma=1$ , and a narrow-banded Jonswap spectrum with  $\Gamma=3.3$ .
2. The dependence of the nonlinear rate (NLR) of energy transfer on the directional spreading. The angular spreading parameter is varied from  $n=8$  to 20 in combination with a narrow-banded Jonswap spectrum with  $\Gamma=7$ .
3. The nonlinear rate (NLR) of energy transfers in the case of a directionally bi-modal spectrum of the kind

$$E(\omega, \theta) = E_1(\omega, \theta) + c_2 E_2(\omega, \theta) \quad (6.26)$$

where the spectral energy distribution for  $E_1(\omega, \theta)$  and  $E_2(\omega, \theta)$  is determined using (6.24), and  $c_2$  is the nondimensional coefficient that determines the relative contributions of the second mode with respect to the first one.

### 6.3.2 Discretization of the interaction integral

For numerical implementation, the interaction integral (6.23) has to be discretized. The interaction integral can be divided into two parts, the sum interaction integral  $I^+$  and the difference interaction integral  $I^-$ . In a discrete form  $I^+$  is

$$I^+(\omega_i, \theta_j) = \frac{\omega_i^2}{c_i c_{gi}} \sum_{m=1}^{nf} \sum_{n=1}^{na} \Delta\omega_m \Delta\theta_n \tilde{V}^2(\omega_i, \theta_j, \omega_m, \theta_n) \frac{\Omega}{(\omega_i - \omega_m - \dot{\omega})^2 + \Omega^2} \frac{\omega_m}{c_m c_{gm}} \quad (6.27)$$

$$[\tilde{E}(\omega_m, \theta_n) \tilde{E}(\dot{\omega}, \dot{\theta}) - \tilde{E}(\omega_i, \theta_j) \tilde{E}(\dot{\omega}, \dot{\theta}) - \tilde{E}(\omega_i, \theta_j) \tilde{E}(\omega_m, \theta_n)]$$

Here  $i$  and  $m$  are running counters in frequency domain, and  $j$  and  $n$  are running counters in the directional domain. All variables are expressed in non-

dimensional form. In the sum interaction term (6.27), any two discrete spectral components  $(\omega_i, \theta_j)$  and  $(\omega_m, \theta_n)$  with wavenumbers  $k$  and  $k_1$  respectively can interact with a third component  $(\omega, \theta)$  with wavenumber  $k_2$  such that  $k_2 = k - k_1$ .

The difference interaction integral  $I^-$  in a discrete form is

$$I^-(\omega_i, \theta_j) = \frac{\omega_i^2}{c_i c_{gi}} \sum_{m=1}^{nf} \sum_{n=1}^{na} \Delta\omega_m \Delta\theta_n \tilde{V}^2(\omega_m, \theta_n, \omega_i, \theta_j) \frac{\Omega}{(\omega_i - \omega_m + \omega)^2 + \Omega^2} \frac{\omega_m}{c_m c_{gm}} \quad (6.28)$$

$$[\tilde{E}(\omega_i, \theta_j) \tilde{E}(\omega, \theta) - \tilde{E}(\omega_m, \theta_n) \tilde{E}(\omega, \theta) - \tilde{E}(\omega_i, \theta_j) \tilde{E}(\omega_m, \theta_n)]$$

In the difference interaction term (6.28), any two discrete spectral components  $(\omega_i, \theta_j)$  and  $(\omega_m, \theta_n)$  with wavenumbers  $k$  and  $k_1$  respectively can interact with a third component  $(\omega, \theta)$  with wavenumber  $k_2$  such that  $k_2 = k_1 - k$ .

### 6.3.3 Numerical grid

For a sufficiently fine calculation grid  $(\omega, \theta)$ , the values obtained for the kinetic integral do not significantly depend on the choice of grid. This choice is important from the point of view of good resolution of spectral form  $E(\omega, \theta)$  and covering a proper interval of frequencies and directions for the output rate  $dE/dt$ . After some test calculations, the following numerical grid  $(\omega, \theta)$  was chosen (in nondimensional units)

$$\omega_i = 0.25(1.06)^i, \quad \text{for } i = 1, \dots, nf \quad (6.29)$$

and

$$\theta_j = -\pi + \left(\frac{\pi}{na}\right)j, \quad \text{for } j = 1, \dots, na \quad (6.30)$$

Here  $nf$  and  $na$  are the number of frequency and directional components respectively. It should be mentioned that comparison of calculations for different grids showed a significant dependence of the nonlinear rate (NLR) on the frequency and angular resolution. After some test calculations, we set

$nf=48$  and  $na=24$ . For this choice, the accuracy of quantitative characteristics of NLR in our calculations is of the order 10%. This grid permits to investigate the integral properties in the frequency interval  $0.265 \leq \omega/\omega_p \leq 4$ .

### 6.3.4 Results of calculations and analysis

#### *Dependence of NLR on parameter $\Omega$ and relative depth $kh$*

The calculations of the kinetic integral (6.23) have been carried out for two spectral shapes: Pierson-Moskovitz (PM) and Jonswap spectra with directional spreading of a  $\cos^2$ -distribution. For each spectral shape, the kinetic integral is considered for a range of relative depths  $k_ph=3, 1.2, 0.6$ , and  $0.3$ . Two values for the nondimensional parameter  $\Omega/\omega_p$  are considered, these are  $0.01$  and  $0.1$ .

Figs. 6.1 and 6.2 show NLR for PM and Jonswap spectra, respectively, for  $k_ph=0.3$  and  $\Omega/\omega_p=0.01$ . The results are given in one-dimensional form (top), i.e., integrated over directions, and in two-dimensional form (bottom). The results show an energy flux from the region near the primary peak toward the higher harmonics. The behavior of the NLR indicates the following two features. First the maximum of the positive lobe occurs at  $f/f_p=1.9$  (less than the location of the first harmonic  $2f_p$ ). This is due to the fact that a triad of waves is considered such that two wave components  $(\omega_1, \mathbf{k}_1)$  and  $(\omega_2, \mathbf{k}_2)$  can force a motion at the vector sum or difference wavenumber  $\mathbf{k}=\mathbf{k}_1 \pm \mathbf{k}_2$  and frequency  $\omega(\mathbf{k})$ . This consideration implies that the first harmonic appears in the wavenumber spectrum at  $2k_p$ , which corresponds to a peak in the frequency spectrum at  $\omega < 2\omega_p$  (in intermediate water). The second feature is that the area under the positive lobe is smaller than the area under the negative lobe, implying attenuation in the total energy.

Figs. 6.3 and 6.4 show NLR for PM and Jonswap spectra, respectively, for  $k_ph=1.2$  and  $\Omega/\omega_p=0.01$ . Similar to the previous results, the NLR has a negative lobe around the primary peak and energy gain over a wide range of

frequencies higher than two times the primary peak. In general the intensity of NLR is much weaker than in case  $k_p h = 0.3$ .

For quantitative analysis we used the following characteristics:

- maximum value of positive lobe of two-dimensional NLR:  $MT^+$ ;
- maximum absolute value of negative lobe of two-dimensional NLR:  $MT^-$ ;
- ratio of total NLR (two-dimensional NLR integrated over frequency and direction) to the absolute value of the total negative part of NLR:  $D$

Tables 6.1 and 6.2 summarize the results for PM and Jonswap spectra, respectively, for various relative depths and  $\Omega$ -values. Note that the parameter  $D$  is a measure of energy conservation within the system. Positive values of  $D$  indicate energy gain and negative values indicate energy attenuation. Tables 6.1 and 6.2 indicate that NLR is proportional to the value of  $\Omega$ .

The parameter  $D$  measures the percentage of energy gain/loss from the total energy flux across the spectrum. In deep water  $D$  reaches large values but there the energy transfers are weak, so that the nonconservation of energy is weak also. As the water depth decreases in shallow water, the NLR increases strongly. In shallow water, although the values of  $D$  decrease, the energy attenuation becomes significant because of the strong increase in the NLR values. In fact for  $\Omega/\omega_p = 0.01$ ,  $D$  indicates an energy gain in shallow water ( $k_p h = 0.6, 0.3$ ). The intensity of nonlinear interactions in the Jonswap spectrum is lower than that in the PM spectrum because the total energy content is larger in PM compared with Jonswap (the spectra are normalized with  $E_p$ ).

#### *Dependence of NLR on angular spreading*

The dependence of the nonlinear rate (NLR) of energy transfer on the angular spreading is examined in the case of a Jonswap spectrum with  $\Gamma = 7$ . NLR of transfer is calculated for a  $\cos^8$ -distribution (Fig. 6.5) and a  $\cos^{20}$ -distribution (Fig. 6.6). The results show clearly that the directional width of the primary peak influences the directional width of the generated second peak. Nonlinearity

in the initially narrow directional spectrum leads to a directionally narrow second peak and vice versa.

#### *NLR in bi-modal directional spectrum*

Fig. 6.7 shows the NLR for a spectrum with double peaks of equal magnitude and peak frequency and located 90 degrees apart. High directional resolution ( $\Delta\theta=5$  degrees,  $na=72$ ) is used in the computation to insure accurate representation of the spectral peaks. The results show generation of two spectral peaks, at the first harmonics, that are directionally aligned with the initial spectral peaks. These are ascribed to the colinear interactions between waves within each directional peak. The results do not show a directional peak at the sum wavenumber vector of the initial spectral peaks, i.e.,  $\theta=0$  degrees, implying absence of noncolinear interactions.

The preceding analysis permits to state the following peculiarities of NLR of energy transfers due to off-resonant triad interactions:

1. NLR strongly depends on the relative depth  $k_p h$ . With decreasing  $k_p h$ , the intensity of NLR increases.
2. NLR has a non-conservativity feature. Generally it results in an energy attenuation in intermediate and shallow water depths.
3. The intensity of NLR increases proportionally with increasing  $\Omega$ .
4. The directional width of the primary spectral peak influences the NLR of energy transfers. The directional width of the generated second peak is proportional to the directional width of the primary peak.
5. The NLR of energy transfers in directionally bi-modal spectrum indicates the absence of noncolinear interactions.

**Table 6.1** *Statistics of nonlinear rate (NLR) of energy transfer for Pierson-Moskovitz spectrum with direction spreading of  $\cos^2$ -distribution*

$k_p h$	3		1.2		0.6		0.3	
$\Omega/\omega_p$	0.01	0.1	0.01	0.1	0.01	0.1	0.01	0.1
$MT^+$	0.3	2.8	1.3	12.6	90	780	4,106	23,546
$MT^-$	-1.6	-15.3	-4	-38	-124	-930	-5,433	-30,676
$D$	-0.51	-0.51	-0.41	-0.44	+0.08	-0.16	+0.11	-0.08

**Table 6.2** *Statistics of nonlinear rate (NLR) of energy transfer for Jonswap spectrum with direction spreading of  $\cos^2$ -distribution*

$k_p h$	3		1.2		0.6		0.3	
$\Omega/\omega_p$	0.01	0.1	0.01	0.1	0.01	0.1	0.01	0.1
$MT^+$	0.1	1.1	1.1	10.7	48	401	2,031	11,071
$MT^-$	-0.6	-6.1	-1.9	-18.4	-64	-548	-2,566	-17,646
$D$	-0.48	-0.48	-0.26	-0.32	+0.16	-0.13	+0.12	-0.07

Variables are defined as,  $\Omega$ ; filter bandwidth,  $MT^+$ ; positive maximum value of NLR,  $MT^-$ ; maximum (absolute) value of NLR, and  $D$  is the ratio of total (spectrally integrated) NLR to the absolute total negative part.

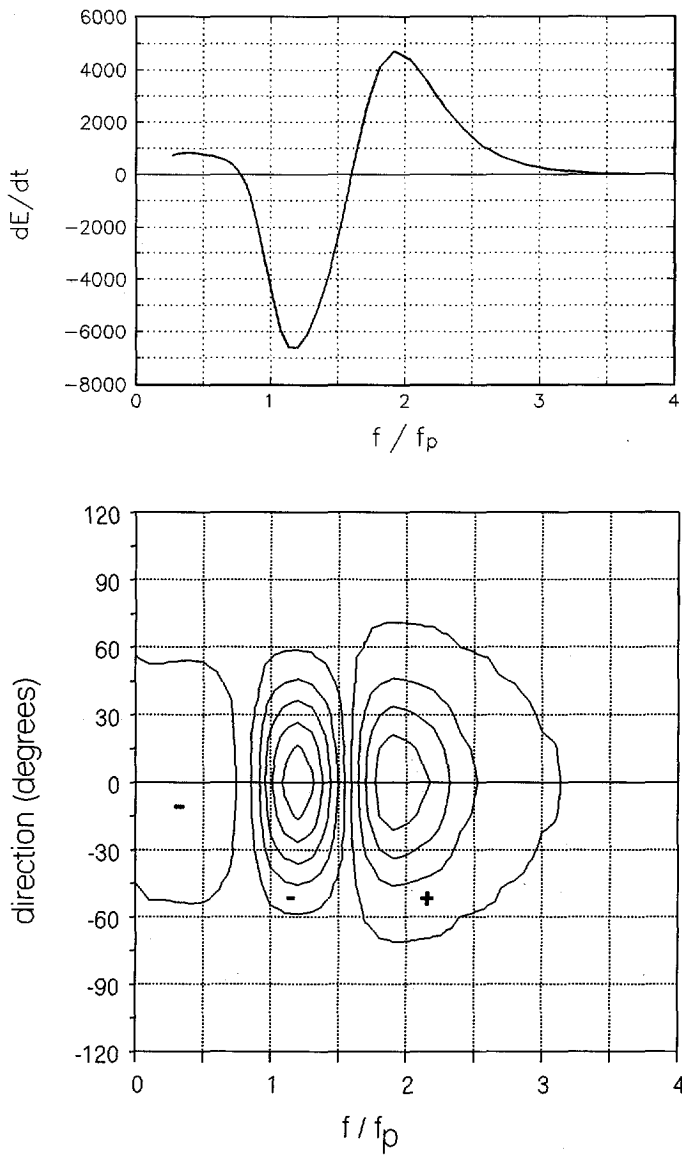


**Figure 6.1** Nondimensional rate of energy transfer for PM spectrum,  $\Omega/\omega_p=0.01$ ,  $k_ph=0.3$ , directional spreading;  $\cos^2$ -distribution. Top: one-dimensional, bottom: two-dimensional ( $MT^+=4106$ ,  $MT^-=-5433$ )

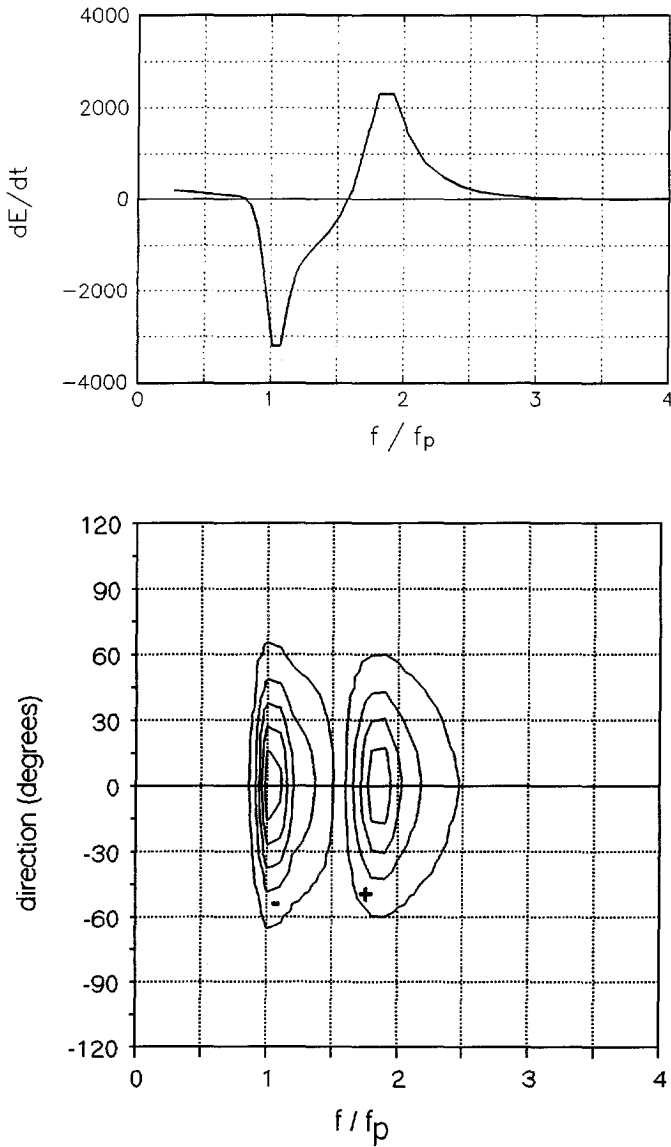


**Figure 6.2** *Nondimensional rate of energy transfer for Jonswap spectrum,  $\Omega/\omega_p=0.01$ ,  $k_ph=0.3$ , directional spreading:  $\cos^2$ -distribution. Top: one-dimensional, bottom: two-dimensional ( $MT^+=2031$ ,  $MT^-=-2566$ )*



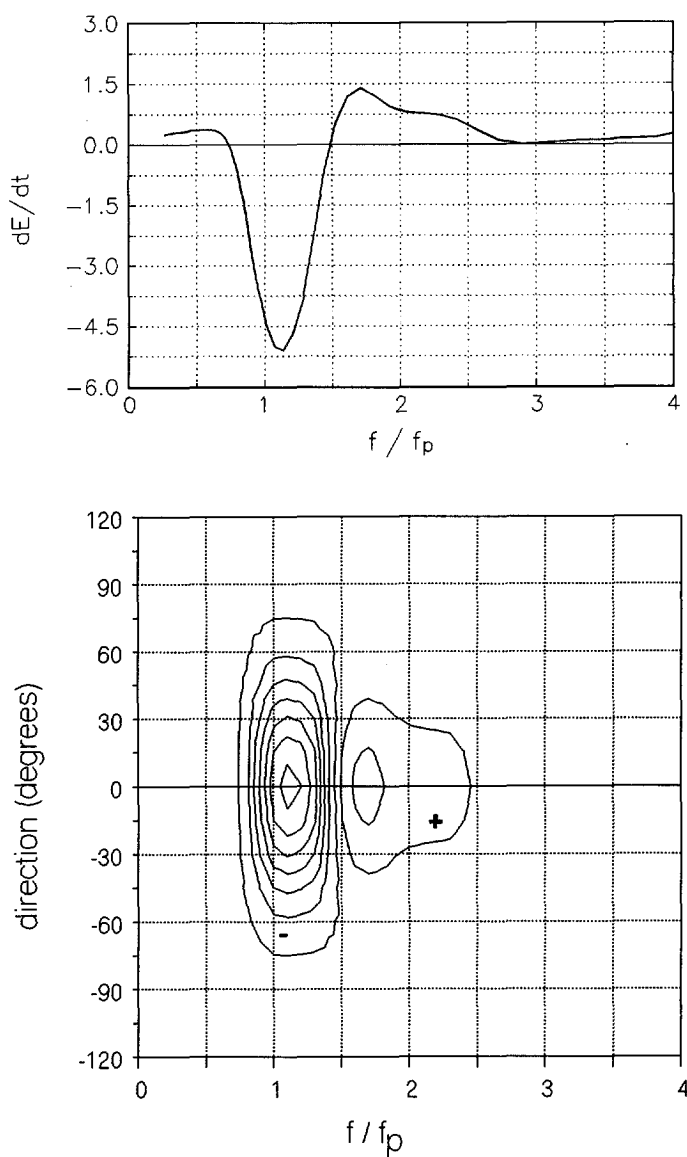


**Figure 6.3** Nondimensional rate of energy transfer for PM spectrum,  $\Omega/\omega_p=0.01$ ,  $k_ph=1.2$ , directional spreading;  $\cos^2$ -distribution. Top: one-dimensional, bottom: two-dimensional ( $MT^+=1.3$ ,  $MT=-4.0$ )

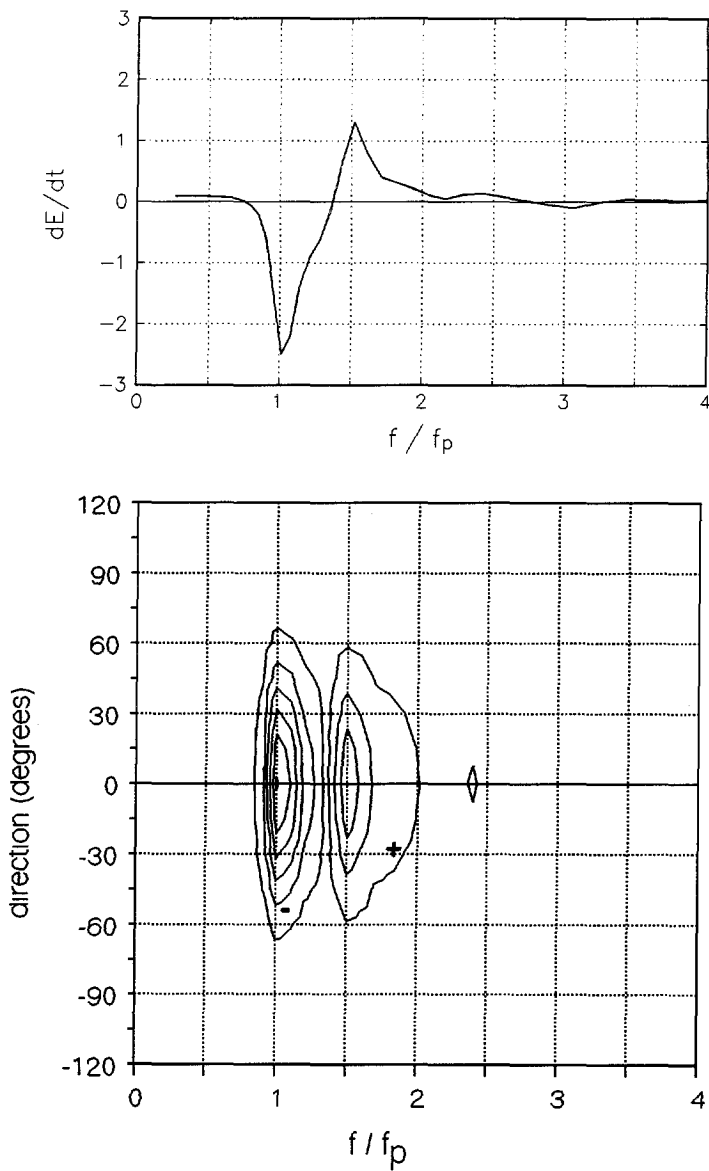


**Figure 6.4** Nondimensional rate of energy transfer for Jonswap spectrum,  $\Omega/\omega_p=0.01$ , relative depth;  $k_ph=1.2$ , directional spreading;  $\cos^2$ -distribution. Top: one-dimensional, bottom: two-dimensional ( $MT^+=1.1$ ,  $MT^-=-1.9$ )

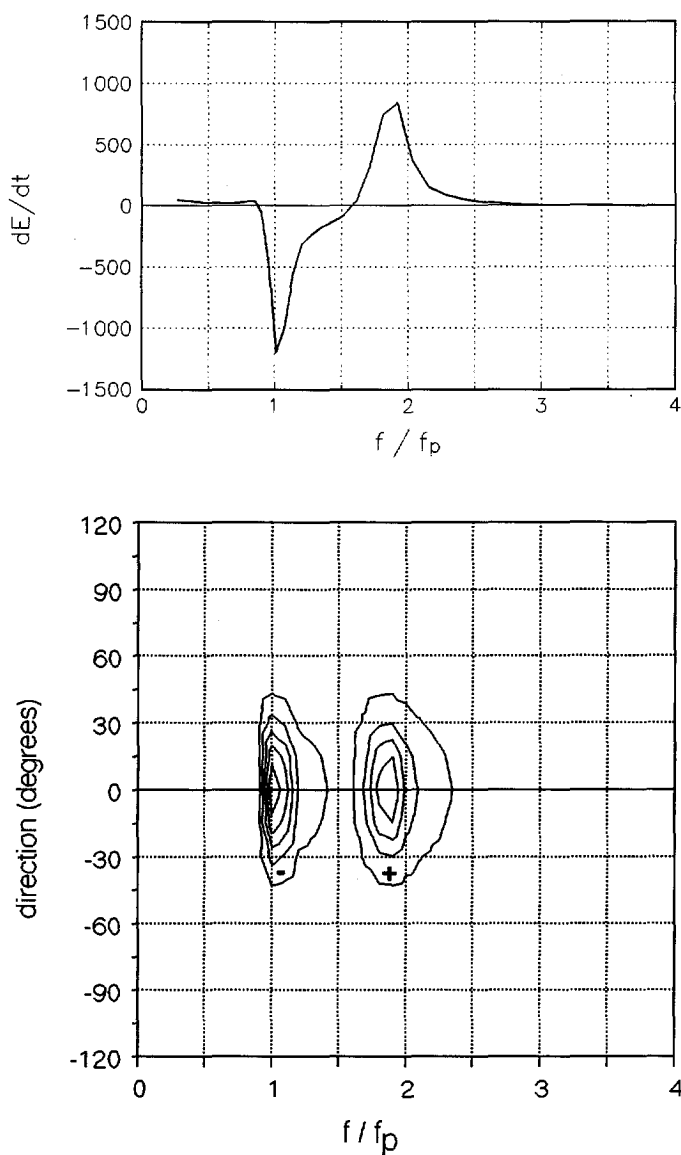


**Figure 6.5** Nondimensional rate of energy transfer for Jonswap spectrum,  $\Omega/\omega_p=0.01$ ,  $k_ph=0.3$ , directional spreading;  $\cos^8$ -distribution. Top: one-dimensional, bottom: two-dimensional ( $MT^+=1375$ ,  $MT^-=-1652$ )

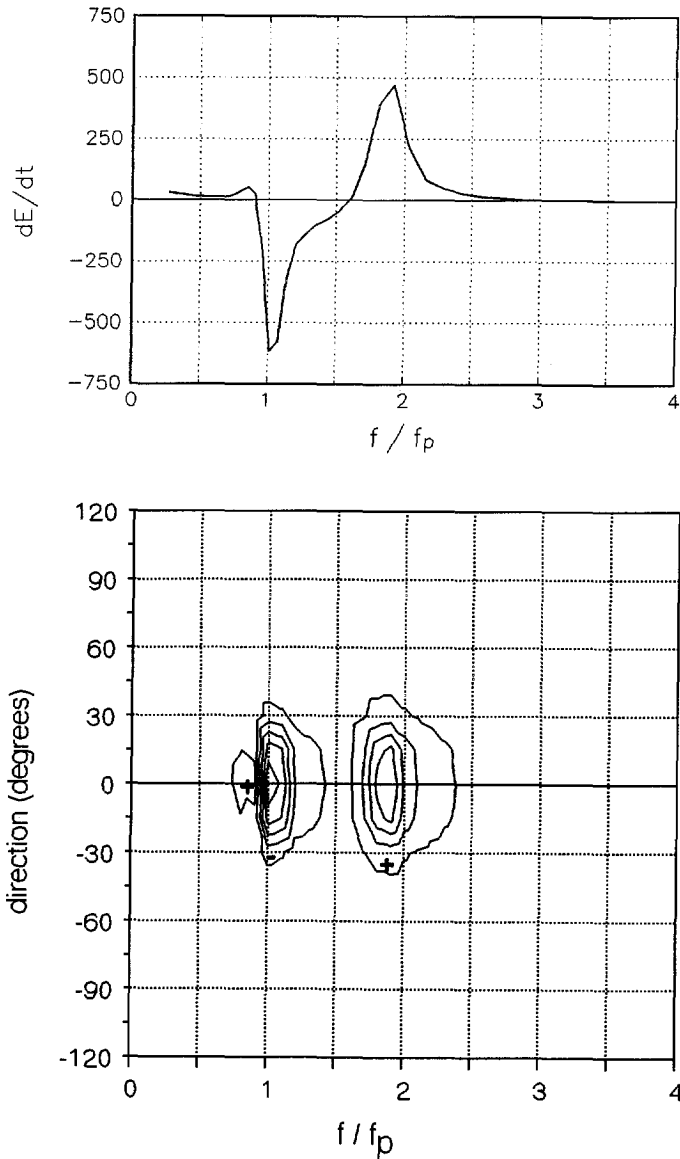


**Figure 6.6** Nondimensional rate of energy transfer for Jonswap spectrum,  $\Omega/\omega_p = 0.01$ ,  $k_p h = 0.3$ , directional spreading:  $\cos^{20}$ -distribution. Top: one-dimensional, bottom: two-dimensional ( $MT^+ = 1205$ ,  $MT^- = -1385$ )

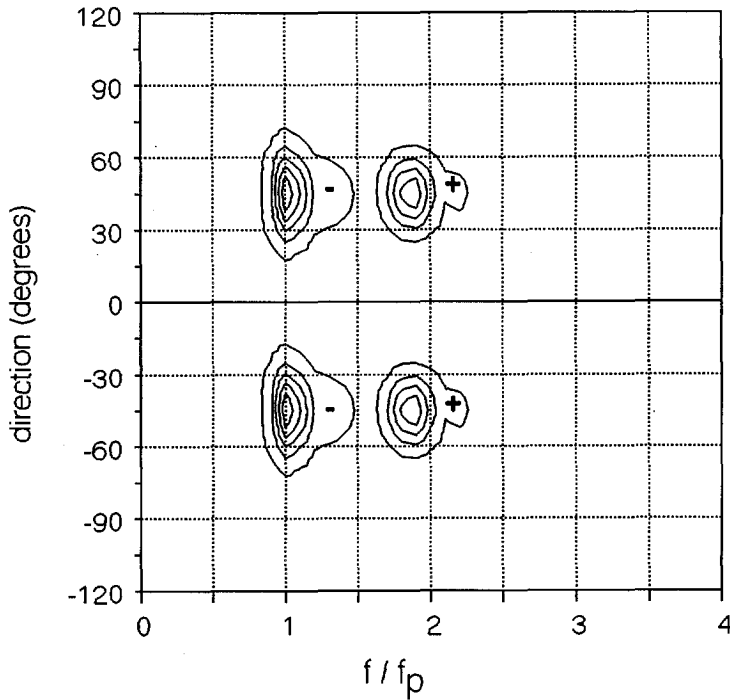


**Figure 6.7** Two-dimensional rate of energy transfer in bimodal directional spectrum. The spectral shape of the two peaks is identical with a Jonswap frequency distribution  $\Gamma=7$  and directional spreading of  $\cos^{20}$ -distribution.  $\Omega/\omega_p=0.01$ ,  $k_ph=0.3$  ( $MT^+=1205$ ,  $MT^-=-1395$ )

## 6.4 Spectral evolution

### 6.4.1 Model formulation and implementation

Assessment of the characteristics of the kinetic integral for three-wave interactions requires verification with observations. Various observations that show harmonic generation have been used throughout this study and will be used here to verify the present triad formulation.

For numerical simulation of the experiments, we need to develop a spatial evolution model for the energy spectrum with a source/sink term representing the effect of triad wave interactions. Since the experiments used here are characterized by long-crested waves, a one-dimensional evolution model is required for the simulations.

We start from the energy balance equation (WAM Development and Implementation Group, 1988) in a fixed coordinate system,

$$\frac{\partial E(\iota, \mathbf{r}, t)}{\partial t} + \nabla_{\mathbf{r}} \cdot [\mathbf{c}_g E(\iota, \mathbf{r}, t)] + \nabla_{\iota} \cdot [\mathbf{c}_{\iota} E(\iota, \mathbf{r}, t)] = S \quad (6.31)$$

where  $E(\iota, \mathbf{r}, t)$  is the essential five-dimensional energy density spectrum,  $\mathbf{r}$  is the two-dimensional horizontal space,  $\iota$  are the independent spectral variables (e.g.  $\iota = k$  or  $\iota = (\omega, \theta)$ ),  $\mathbf{c}_g$  is the two-dimensional propagation velocity in  $\mathbf{r}$  space,  $\mathbf{c}_{\iota}$  is the two-dimensional propagation velocity in  $\iota$  space, and  $\nabla$  is the two-dimensional differential operator. The left-hand-side of (6.31) represents the propagation part of the energy balance equation, while the right-hand-side (the net source/sink terms) represents the generation and dissipation.

For one-dimensional propagation in  $x$ -direction and steady state solution ( $t$ -independent), we obtain the following simplified energy balance equation

$$\frac{d}{dx} [c_{g,k} E(\omega_k)] = S_k \quad (6.32)$$

Here  $E(\omega_k)$  is the frequency energy density,  $c_{g,k}$  is the one-dimensional group velocity and  $S_k$  is the net source/sink term.

To implement the effect of triad wave interactions in equation (6.32), the kinetic integral should be simplified to a one-dimensional form and cast in a source/sink term. For a unidirectional wavefield (no directional spreading) with frequency energy spectrum  $E(\omega)$ , the kinetic integral (6.13-15) can be cast in an energy source/sink term as follows:

$$S_{tr}(\omega_k) = 16 \pi^2 g \int_0^\infty d\omega_1 \frac{c_2 c_{g2}}{\omega_1 \omega_2^2} (T_{k12}^+ - 2 T_{1k2}^-) \quad (6.33)$$

$$T_{k12}^+ = V^2(\omega_k, \omega_1) \left[ \frac{\omega_k^2}{c_k c_{g,k}} E_1 E_2 - \frac{\omega_2^2}{c_2 c_{g2}} E_k E_1 - \frac{\omega_1^2}{c_1 c_{g1}} E_k E_2 \right] \frac{\Omega}{(\omega_k - \omega_1 - \omega_2)^2 + \Omega^2}$$

$$T_{1k2}^- = V^2(\omega_1, \omega_k) \left[ \frac{\omega_1^2}{c_1 c_{g1}} E_k E_2 - \frac{\omega_2^2}{c_2 c_{g2}} E_k E_1 - \frac{\omega_k^2}{c_k c_{g,k}} E_1 E_2 \right] \frac{\Omega}{(\omega_k - \omega_1 + \omega_2)^2 + \Omega^2}$$

Note that here we have transformed the directional formulation (given by 6.13-15) to a unidirectional formulation. On the other hand one can derive a kinetic integral for unidirectional waves from the beginning by expanding the canonical variable in unidirectional Fourier components.

The energy source/sink term given in (6.33), for the effect of triad wave interactions, represents a (positive/negative) contribution to the temporal rate of change of spectral density. The first term under the integral  $T_{k12}^+$  represents the sum interaction  $\mathbf{k} = \mathbf{k}_1 + \mathbf{k}_2$ , the second  $T_{1k2}^-$  the difference interaction  $\mathbf{k} = \mathbf{k}_1 - \mathbf{k}_2$ . The interaction coefficient  $V$  given by (6.16) can be simplified to a one-dimensional form as follows

$$V_{k12} = \frac{g^{1/2}}{8 \pi \sqrt{2}} \left\{ [k k_1 - (\omega_k \omega_1 / g)^2] (\omega_2 / \omega_k \omega_1)^{1/2} \right. \\ + [k k_2 - (\omega_k \omega_2 / g)^2] (\omega_1 / \omega_k \omega_2)^{1/2} \\ \left. + [k_1 k_2 + (\omega_1 \omega_2 / g)^2] (\omega_k / \omega_1 \omega_2)^{1/2} \right\} \quad (6.34)$$

The one-dimensional nonlinear rate (NLR) of energy transfer has been evaluated numerically. In the computations, the normalized filter bandwidth  $\Omega/\omega_p$  was set to 0.01. Fig. 6.8 shows the NLR computed for a Jonswap frequency spectrum for  $k_p h = 0.3$  and  $k_p h = 1.2$ . Not surprisingly the unidirectional NLR shows a similar behavior to the directional NLR, in which energy is transferred from the primary peak to the harmonics. The intensity of NLR increases strongly for decreasing relative depth.

The energy balance equation (6.32) together with (6.33) comprises a set of first-order ordinary differential equations that describe the evolution of the energy spectrum  $E(\omega)$ . Giving the initial energy spectrum at the upwave boundary, equation (6.32) has been numerically integrated using a fourth-order Runge-Kutta method.

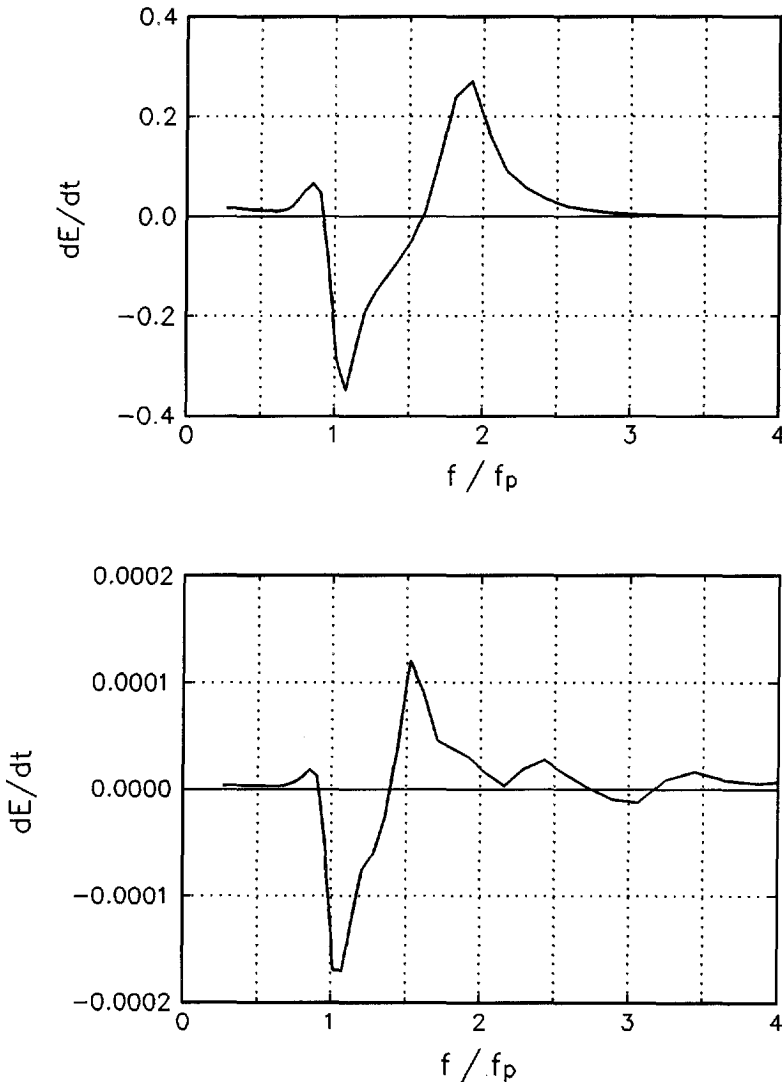


**Figure 6.8** Nondimensional rate of energy transfer using unidirectional formulation and Jonswap spectrum,  $\Omega/\omega_p = 0.01$ . Top:  $k_p h = 0.3$ , bottom:  $k_p h = 1.2$ .



### 6.4.2 Simulation of spectral evolution

The numerical investigation of the nonlinear rate (NLR) of energy transfer presented in the previous section has shown a strong dependence on the filter bandwidth  $\Omega$ . In this section the influence of the parameter  $\Omega$  on the computed spectral evolution will be examined using observations for harmonic generation in random waves propagating over a shallow bar (Beji and Battjes, 1993) as well as over a beach profile (Arcilla et al., 1994). These data sets are described in detail in chapter 3.

To simulate nonlinear shoaling and breaking of random waves, the energy balance equation (6.32) is supplemented with source/sink terms for triad wave interactions and wave breaking. For triad wave interactions the source term is given by (6.33), and for depth induced wave breaking it is given by equation (4.45).

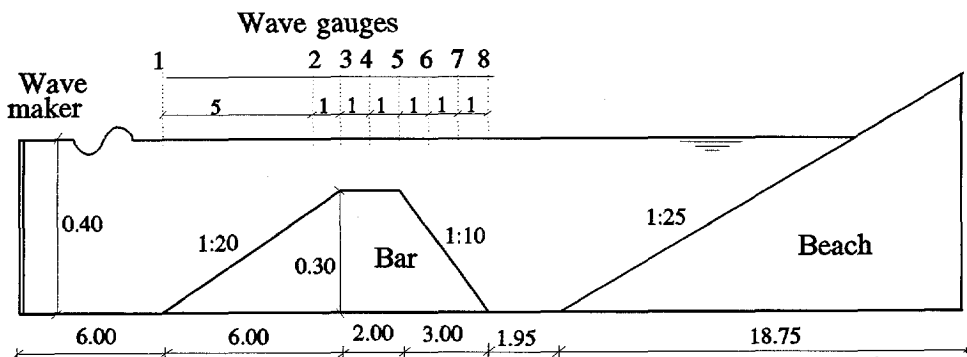


**Figure 6.9** Layout for the experimental setup of Battjes and Beji (1992). All lengths are expressed in meters.

To examine the sensitivity of the spectral evolution to the choice of  $\Omega$ , two values are used in the computations:  $\Omega/\omega_p = 0.01$  and 0.1. The computed spectra are compared to the measured ones in nonbreaking waves propagating over a

bar (Fig. 6.9) and breaking waves over a beach profile (Fig. 6.10). The results are given in Figs. 6.11 and 6.12 respectively.

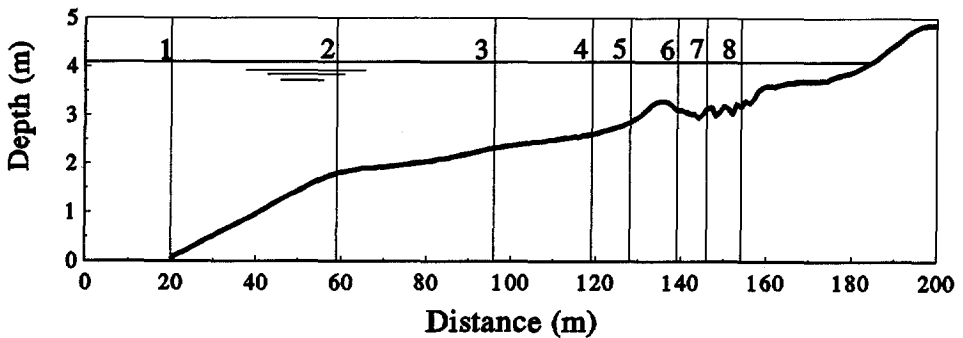


**Figure 6.10** *Bed profile and locations of wave gauges (Arcilla et al., 1994)*

The comparisons indicate the following characteristics of the effects of the triad source term.

1. The intensity of energy transfers from the primary spectral peak to the higher frequencies is mainly controlled by the choice of  $\Omega$ -value. Increasing  $\Omega$ -value results in stronger energy transfers, extended to higher frequencies.
2. The energy transfers to higher harmonics are underestimated when  $\Omega/\omega_p=0.01$ , and overestimated when  $\Omega/\omega_p=0.1$ . The latter results in an unwanted behavior for the energy spectrum at the high frequency range (spectral tail).
3. The second spectral peak (in frequency-domain) is shifted to a lower frequency compared with observation. It appears at a frequency less than two times the primary peak. This is ascribed to the fact that triads are considered such that  $k=k_1+k_2$ , which results in  $\omega_k < \omega_1 + \omega_2$  in intermediate water depths.
4. The total energy (spectrally integrated) is underestimated (Fig. 6.12, stations 7 and 8) due to the fact that the present triad interaction approximation does not conserve energy.

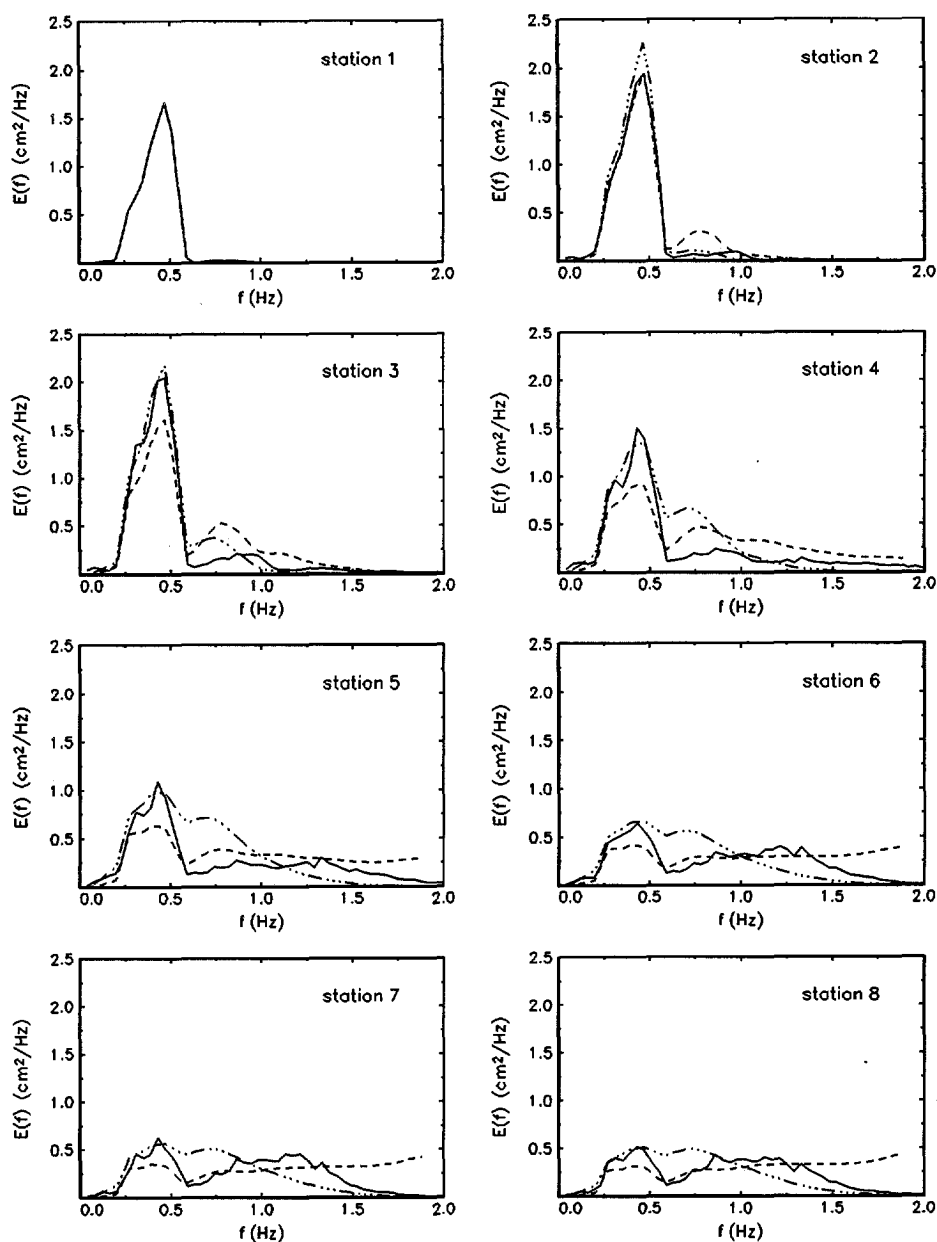


**Figure 6.11** Energy spectra from experiments (solid lines) and from the evolution model: with  $\Omega/\omega_p=0.01$  (dashed lines) and  $\Omega/\omega_p=0.1$  (dot-dashed lines) for waves propagating over a shallow bar.

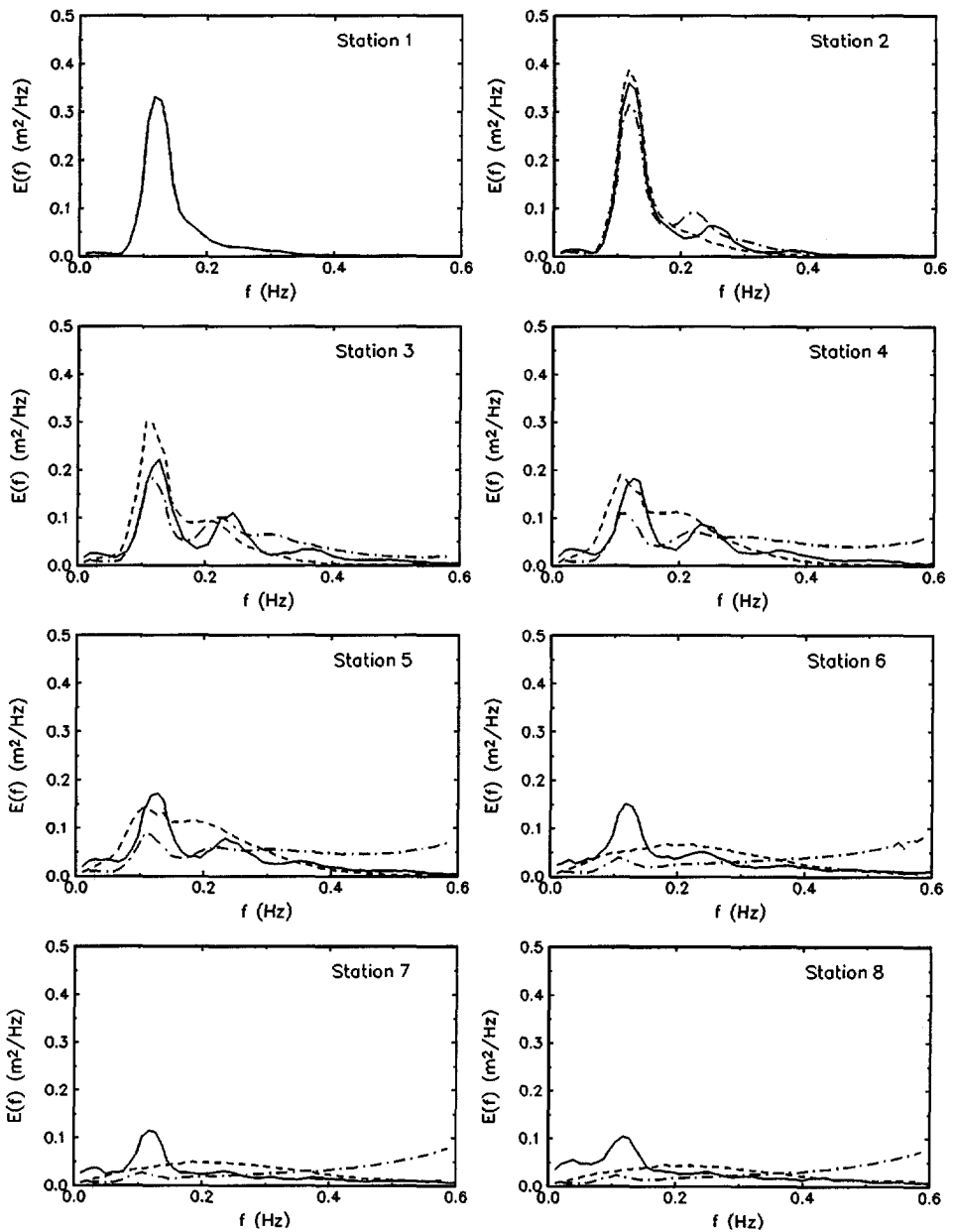


**Figure 6.12** Energy spectra from experiments (solid lines) and from the evolution model: with  $\Omega/\omega_p=0.01$  (dashed lines) and  $\Omega/\omega_p=0.1$  (dot-dashed lines) for waves propagating over a beach profile.

### 6.4.3 Remedy to the nonconservative approximation

The investigation of the nonlinear rate (NLR) of energy transfers of the triad formulation presented in section 6.3 has shown that the present formulation is not conservative. The numerical simulation of the spectral evolution over a beach profile (presented in section 6.4.2) has shown that the non-conservative feature of the formulation can be significant and results in an artificial energy decay/gain. In fact this energy attenuation is a characteristics of the present formulation resulting from the specification of the filter bandwidth  $\Omega$ .

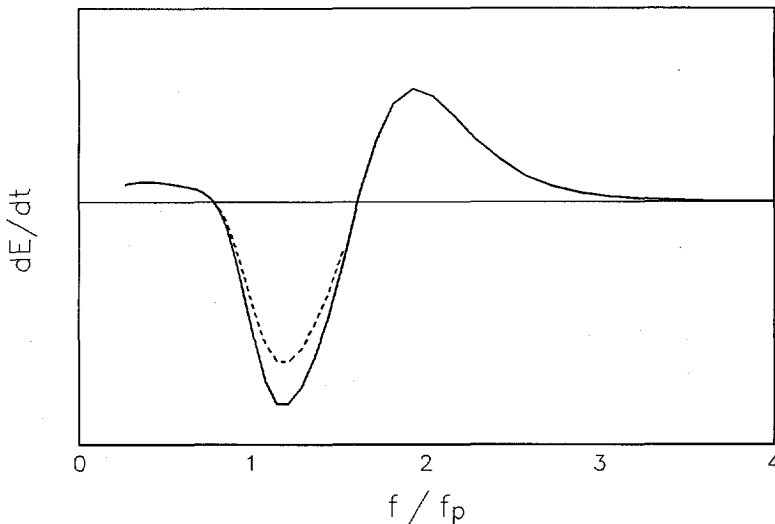


**Figure 6.13** *Sketch of NLR of energy transfer; solid line: present approximation with energy attenuation; dashed line: modified negative lobe to ensure energy conservation.*

To eliminate these effects, the present formulation is temporarily remedied to insure energy conservation during the nonlinear interactions. The energy attenuation in the present formulation can be explained using Fig. 6.13 for the NLR of energy transfers. In such case the area under the negative lobe, that represents the energy transfers from the primary peak, does not equal (larger than) the area under the positive lobe that represents the energy gained by the harmonics.

To ensure energy conservation the following *ad hoc* method is used. First the NLR of energy transfer is estimated as a first guess using the present formulation. Next the integral (of NLR) over the spectrum which represents the total energy gain/loss  $\check{D}$  is computed. The NLR of energy transfer is then rescaled by adding (or subtracting) the quantity  $\check{D}$ . If  $\check{D}$  is negative, implying energy loss, then the area of negative lobe is reduced with  $\check{D}$  in proportion to the values of the NLR (see Fig. 6.13). On the other hand if  $\check{D}$  is positive, implying energy gain, then the area of positive lobe is reduced with  $\check{D}$  in proportion to the values of the NLR. Computations with the non-conservative approximation are hereafter referred to as NCTI, while computations with the conservative approximation are referred to as CTI. The *ad hoc* method proposed here to ensure energy conservation does not change the general features of the interaction mechanism between the primary and the harmonics.

Additional numerical simulation of waves propagating over a beach profile has been performed using the CTI model for comparison with that performed previously with the NCTI model. The computed spectra with the CTI model using  $\Omega/\omega_p = 0.01$  as well as 0.1 are compared with the observation in Fig. 6.14. The effect of the method proposed to ensure energy conservation is clearly seen at stations 5, 6, 7, and 8 in which a substantial amount of energy exists in the present computation (CTI) compared with the previous computation (NCTI).

It is noticeable that the primary spectral peak has disappeared in the computed spectra in contrast with the observations. This indicates that the energy transfer from the primary peak to the harmonics is overestimated in the present numerical simulation. In addition, the computed spectra seem to have energy transfer over a wider range of harmonics compared with that in the observation. The latter can be explained as follows. In the present triad formulation, any three waves participating in the sum interaction must satisfy the relation  $k - k_1 - k_2 = 0$ . For the special case of self interaction of the primary, in which  $k_1 = k_2 = k_p$ , the first harmonics appear at  $k = 2k_1$ . This implies that the second spectral peak appears at frequency  $f(2k_1)$  given by (in intermediate water depths)

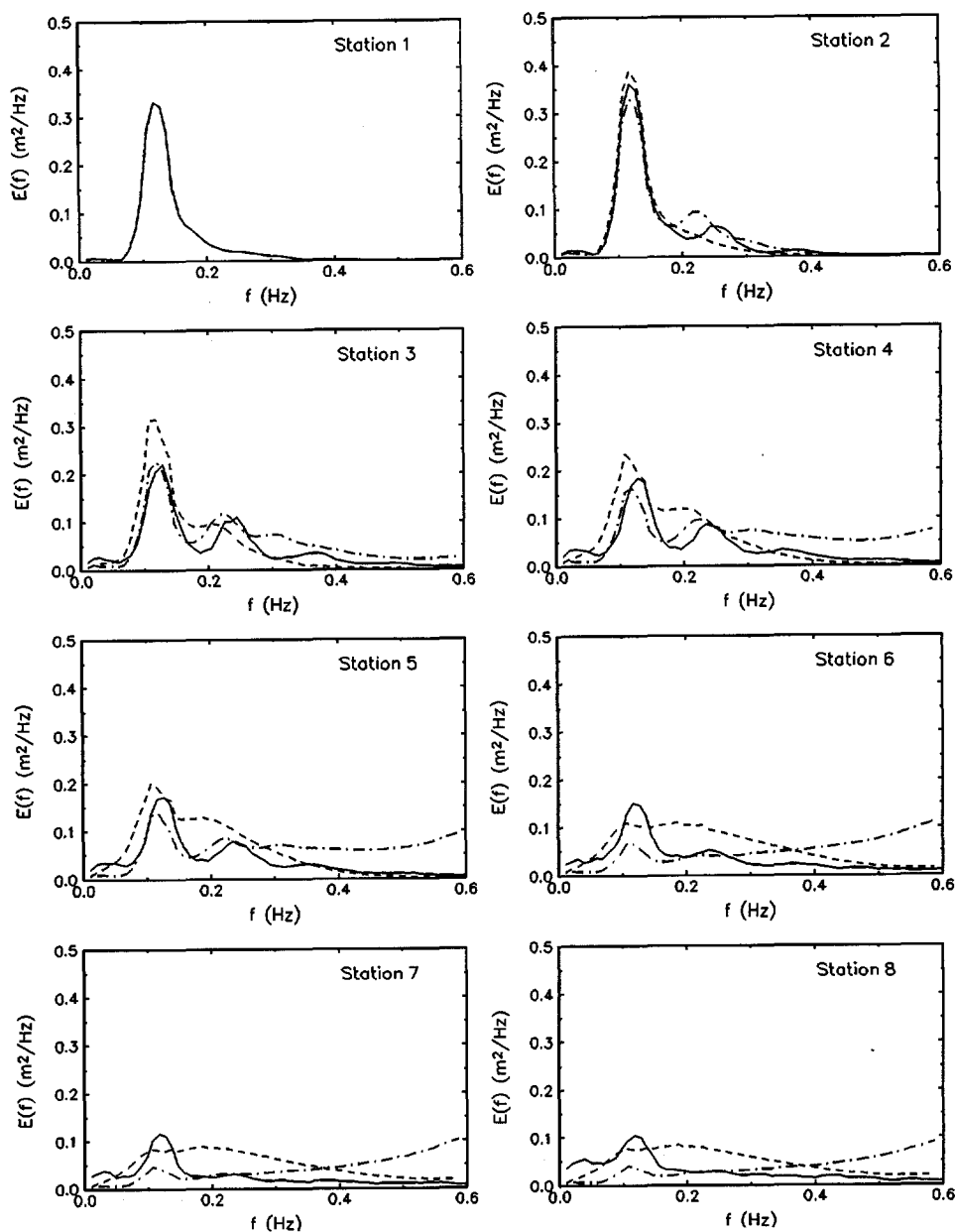


Figure 6.14

Energy spectra from experiments (solid lines) and from the evolution model with conservative approximation: with  $\Omega/\omega_p = 0.01$  (dashed lines) and  $\Omega/\omega_p = 0.1$  (dot-dashed lines) for waves propagating over a beach profile.

$$f(2k_1) = \frac{1}{2\pi} [2gk_1 \tanh(2k_1 h)]^{1/2} < 2f(k_1) \quad (6.35)$$

In shallow water  $f(2k_1)$  is given by

$$f(2k_1) = \frac{1}{2\pi} [2k_1 (gh)^{1/2}] = 2f(k_1) \quad (6.36)$$

The consequence is that in intermediate water depths, the energy transfer is to frequency less than  $2f_p$ . In shallow water as waves become nondispersive the energy transfer is to  $2f_p$ . The overall energy transfers in both intermediate and shallow water depths result in a broader second spectral peak compared with the observed one.

#### 6.4.4 Sensitivity to the filter bandwidth

The previous results for the computed spectral evolution have shown dependence of the NLR of energy transfer on the choice of the filter bandwidth  $\Omega$ . Additional numerical simulations for wave propagation over a shallow bar and beach profile have been carried out with different values of  $\Omega$ . To evaluate the variation in the spectral evolution for various values of  $\Omega$ , the variations in the mean frequency of the spectrum are computed. The mean frequency of the energy spectrum is defined as

$$f_m = \frac{\int f E(f) df}{\int E(f) df} \quad (6.37)$$

Fig. 6.15 shows the observed variations in the mean frequency in waves passing over a shallow bar and those computed by the CTI model with different values of  $\Omega/\omega_p$ . The observed variation in the mean frequency shows a rapid increase (from 0.43 Hz to 0.85 Hz) over the upslope side and the horizontal part of the bar, which is ascribed to generation of higher harmonics. Beyond the bar crest, the mean frequency remains at a high level without significant change. The



computed variations in the mean frequency using the CTI model show a strong dependence on the value of the parameter  $\Omega$ . The larger the value of  $\Omega/\omega_p$ , the stronger the energy transfers and hence the shift in the mean frequency to higher harmonics. From the results one can see that the best choice for the parameter  $\Omega/\omega_p$ , for best simulation of the observed shift in the mean frequency, in this case is between 0.01 and 0.03.

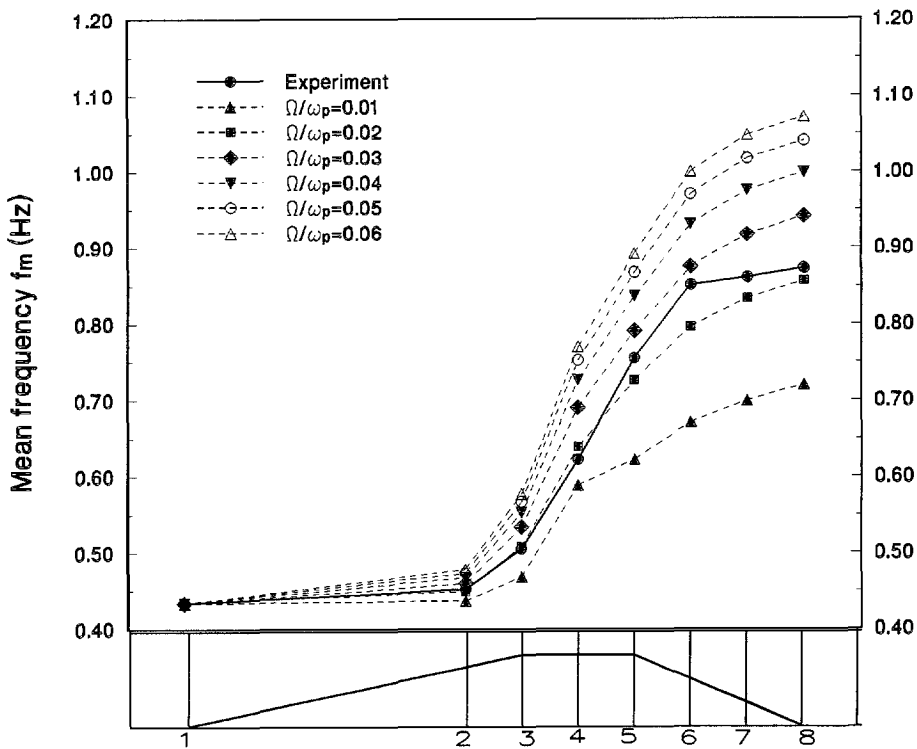


**Figure 6.15** *Spatial variation of mean frequency  $f_m$  in waves propagating over a shallow bar. Solid line: experiment; Dashed lines: evolution model with conservative approximation using different values for  $\Omega/\omega_p$ .*

Fig. 6.16 shows the observed variations in the mean frequency in waves propagating over a beach profile and those computed by the CTI model with different values of  $\Omega$ . The observed variation in the mean frequency shows a

rapid increase in intermediate water from 0.14 Hz to 0.21 Hz due to harmonic generation. In very shallow water, the mean frequency nearly attains a constant level. The computed variations in the mean frequency using the CTI model show a strong dependence on the value of  $\Omega$ . In intermediate water depths (between stations 1 and 3) computations with  $\Omega/\omega_p = 0.04$  and 0.05 seem to best match the observed shift in the mean frequency. In shallow water, all computations with different values of  $\Omega$  result in a trend which differs strongly from the observed one, significantly overestimating the mean frequency.

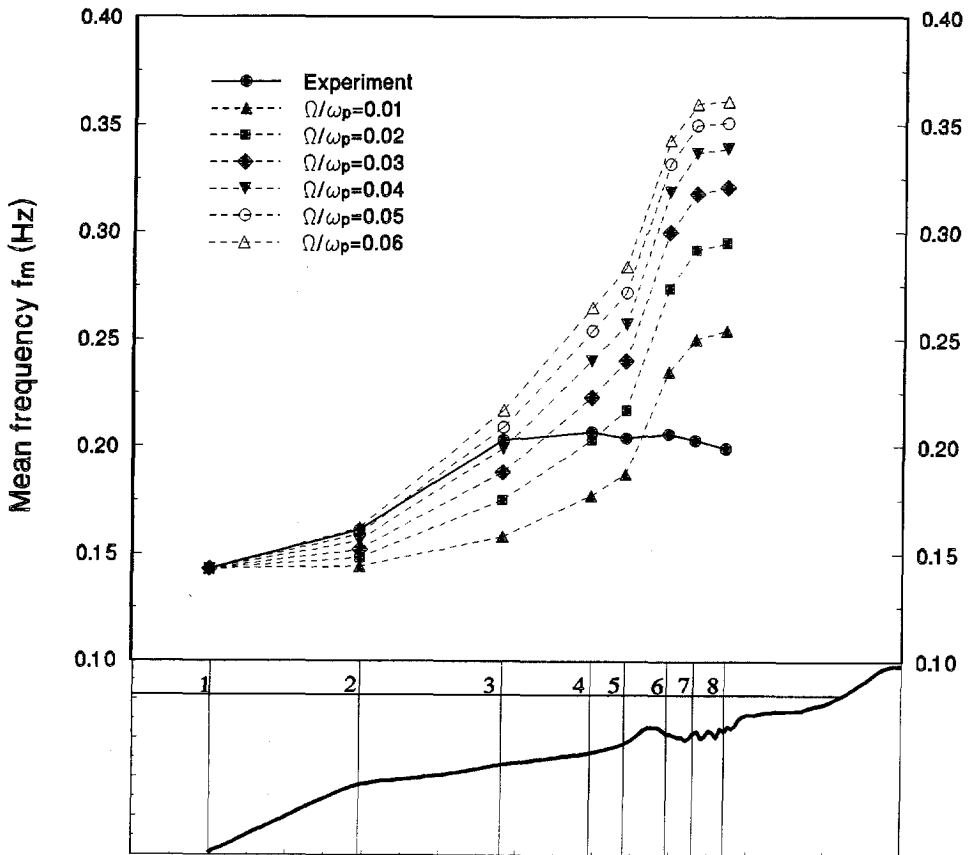


**Figure 6.16** Spatial variation of mean frequency  $f_m$  in waves propagating over a beach profile. Solid line: experiment; Dashed lines: evolution model with conservative approximation using different values for  $\Omega/\omega_p$ .

## 6.5 Discussion

The approach presented in this chapter to include the off-resonant energetic triad interactions represents a modification to the Zakharov kinetic equation for resonant interactions. The modification is done by using  $\mu_{k-1-2}$  in equation (6.1) instead of using the delta function  $\delta(\omega_k - \omega_1 - \omega_2)$  that accounts for the exact resonant triads as in the Zakharov kinetic equation, such that

$$\mu_{k-1-2} = \frac{\Omega}{(\omega_k - \omega_1 - \omega_2)^2 + \Omega^2} \quad (6.38)$$

where  $\Omega$  has the effect of broadening the resonance condition. In this chapter we investigated whether  $\Omega$  can be treated as a constant to be determined empirically. The consequences of such treatment are energy attenuation and unguaranteed spectral evolution.

Holloway (1982) proposed to treat  $\Omega$  as a prognostic variable such that

$$\Omega_{lmn} = \eta_l + \eta_m + \eta_n \quad (6.39)$$

where  $\eta_l$  can be seen as a frequency uncertainty in the mode  $l$  participating in the interaction with  $m$  and  $n$ . Holloway (1982) related  $\eta_l$  to the rate of interaction of component  $l$ . The magnitude of  $\eta_l$  and hence the magnitude of  $\Omega_{lmn}$  increases with increasing wave amplitude. This means that the magnitude of  $\Omega_{lmn}$  for the interaction between  $l$ ,  $m$ , and  $n$  needs to be determined first by solving three equations representing the interaction rates of the three components. These three equations for each possible triad together with the spectral evolution equations represent a closed set of equations guiding the evolution of the energy density spectrum.

In principle the approach of Holloway (1982) sketched above may be applied to provide an estimate for the parameter  $\Omega$ . This may achieve a better prediction of the evolution of the energy spectrum. On the other hand the extensive computational efforts required to resolve the closed set of equations are a concern.

## 6.6 Summary and conclusions

An approach to model the off-resonant triad interactions is presented and investigated. The approach is based on the Zakharov kinetic equation for resonant triad interactions, supplemented with a modification to allow for the off-resonant energetic triad interactions. The present kinetic integral contains a parameter, representing the broadening of the resonant condition, to be determined empirically. The resulting interaction integral has been expressed in nondimensional form and numerically investigated. The results indicated energy flux from the spectral peak region toward the higher harmonics with the following trends:

- NLR depends on the relative depth  $kh$ , with very small intensity in deep water and increasing for decreasing  $kh$  in shallow water.
- NLR is roughly proportional to  $\Omega$ .
- the total NLR (spectrally integrated) departs from zero implying that the present approximation of the nonlinear interactions is not conservative. In intermediate water depth the total energy loss/gain varied within 10-15% of the total energy transfers from the primary peak.

The interaction integral has been cast into an energy source/sink term and implemented in an energy balance equation that describes the evolution of a unidirectional energy spectrum in shoaling regions. The evolution model is verified using observations of waves propagating over a shallow bar as well as over a beach profile. In general the comparisons have shown the ability of the model to generate higher harmonics and a consequent upward shift in the mean frequency. The following drawbacks are found:

- The location of the second spectral peak is at a too low frequency compared with observation. This is ascribed to the fact that triads are considered in wavenumber space such that  $k-k_1-k_2=0$  and not in frequency space.
- The present approximation for the nonlinear triad interactions is non-conservative, implying that the net nonlinear rate of energy transfer (integrated over the spectrum) is not zero, as it should. Such effect is a major problem in

---

describing the evolution of the energy spectrum, in which an artificial energy decay is introduced. An *ad hoc* method is suggested as a remedy to this problem by modifying the computed NLR such that the net energy gain/loss becomes zero.

- The magnitude of the filter bandwidth  $\Omega$  cannot be treated as a constant. It should be related to the rate of interactions as suggested by Holloway (1982). This approach will required extensive additional computational effort.



## Chapter 7

### 7. Parametrized energy formulation for triad interactions

#### 7.1 Introduction

Deterministic evolution equations, based on a Boussinesq model, have been used in chapter 4 to describe harmonic generation in shallow-water waves. For computational efficiency, a phase-averaged approach based on the Zakharov kinetic equation (chapter 5) has been used in chapter 6 to develop an energy formulation for triad interactions. However, this model needs further improvement and investigation. In this chapter, our purpose is to develop a computationally efficient, low cost algorithm to model the effects of triad wave interactions for application in coastal energy-based wave models. Efficiency is achieved by different approximations and parametrizations.

The organization of the chapter is as follows. The deterministic evolution equations for the complex amplitudes, described in chapter 4, are summarized in section 2. Based on these, an evolution equation for the wave energy spectrum is derived in section 3. The evolution of the bispectrum is considered in section 4. In section 5 a simplified energy expression for the triad interactions is presented. Numerical simulations and comparisons are described in section 6. A summary and conclusions are finally given in section 7: (Parts of this chapter have been presented in slightly different form in Eldeberky and Battjes (1995).)

#### 7.2 Evolution equations for the complex amplitudes

Starting with the time-domain Boussinesq equations for a sloping bottom, Madsen and Sørensen (1993) have developed equations which describe the

evolution of a unidirectional wavefield with complex Fourier amplitudes including linear shoaling and triad interactions. They expanded the time ( $t$ ) variation of the surface elevation ( $\zeta$ ) at each location ( $x$ ) in a Fourier series as in

$$\zeta(t; x) = \sum_{p=-\infty}^{\infty} A_p(x) \exp[i(\omega_p t - \psi_p(x))] \quad (7.1)$$

with  $A_p$  denoting a complex amplitude,  $p$  indicating the rank of the harmonic,  $\omega_p = p\omega_1$ , and  $\psi_p$  is the linear contribution of the phase such that  $d\psi_p/dx = k_p$ , the wavenumber corresponding to  $\omega_p$  according to the dispersion equation for the linearized Boussinesq equations. Their evolution equations can be written in abbreviated form as

$$\frac{dA_p}{dx} = -S_p A_p - i \sum_{m=-\infty}^{\infty} R_{(m, p-m)} A_m A_{p-m} \exp[-i(\psi_m + \psi_{p-m} - \psi_p)] \quad (7.2)$$

The first term on the right-hand-side represents linear shoaling, the second the nonlinear quadratic interactions between any three components  $m$ ,  $p-m$ , and  $p$ . Complete expressions for the shoaling coefficient  $S_p$  and the interaction coefficient  $R_{(m, p-m)}$  (real quantities) are given in chapter 4. Introducing the complex Fourier amplitude  $C_p = A_p \exp(-i\psi_p)$  into equation (7.2) and dropping the shoaling term temporarily for brevity, we obtain

$$\frac{dC_p}{dx} = -ik_p C_p - i \sum_{m=-\infty}^{\infty} R_{(m, p-m)} C_m C_{p-m} \quad (7.3)$$

The first term on the right-hand-side represents the linear phase evolution, the second the quadratic interactions. The complex amplitude  $C_p$  in (7.3) can be expressed in terms of its magnitude  $a_p$  and phase  $\phi_p$

$$C_p = a_p \exp(-i\phi_p) \quad (7.4)$$



in which  $\phi_p$  represents total phase due to both linear propagation ( $\psi_p$ ) and nonlinear interactions ( $\theta_p$ ). The evolution equations of the real amplitudes  $a_p$  and phases  $\phi_p$  can be formulated from equation (7.3) as follows

$$\frac{da_p}{dx} = - \sum_{m=-\infty}^{\infty} R_{(m,p-m)} a_m a_{p-m} \sin(\phi_m + \phi_{p-m} - \phi_p) \quad (7.5)$$

$$\frac{d\phi_p}{dx} = k_p + \sum_{m=-\infty}^{\infty} R_{(m,p-m)} \frac{a_m a_{p-m}}{a_p} \cos(\phi_m + \phi_{p-m} - \phi_p) \quad (7.6)$$

The argument of the trigonometric functions in (7.5) and (7.6) represents the relative phase of the interacting triad  $m$ ,  $p-m$ , and  $p$ , the so-called biphas of the frequency-pair  $(m, p-m)$  (see chapter 3, equation 3.11).

It is useful to compare the interaction term in the case of a discrete energy spectrum and a continuous energy density spectrum. Equation (7.5) can be formulated for the continuous case (instead of the discrete one as used above) by introducing the continuous amplitude spectrum  $a(f)$  such that  $a(f) \Delta f = a_p$  where  $f \cong f_p$  and  $\Delta f$  is the frequency bandwidth. The evolution equation for the continuous amplitude spectrum  $a(f)$  becomes

$$\frac{da(f)}{dx} \Big|_{f=f_p} = - \Delta f \sum_{m=-\infty}^{\infty} R_{(m,p-m)} a(f_m) a(f_{p-m}) \sin(\phi_m + \phi_{p-m} - \phi_p) \quad (7.7)$$

Note that the right-hand-side is the discretized representation of a convolution integral over the continuous spectrum. The spectral values of the amplitudes are independent of the choice of the frequency bandwidth  $\Delta f$ , unlike the discrete case (7.5).

Comparison between the interaction term in both cases indicates the following. In the discrete case, decreasing the frequency bandwidth results in an inversely proportional decrease of amplitudes but also in a proportional increase of the

number of interactions in which a discrete component  $p$  participates. Thus the spectral evolution (change in the amplitude  $A_p$ ) is independent of the discretization for infinitesimal value of  $\Delta f$ . In the continuous case, although the spectral densities are independent of discretization, the number of terms in the discrete sum in equation (7.7) increases by decreasing the frequency bandwidth, but this is balanced by the factor  $\Delta f$  ensuring that the spectral evolution is independent of the discretization, as it should.

### 7.3 Evolution equation for the spectral energy

To derive evolution equations for the energy spectrum from (7.3), the relation between the complex amplitude  $C_p$  and the energy density spectrum  $E(f)$  should be given. The mean square sea surface elevation (or variance) can be expressed in terms of Fourier amplitudes as

$$\langle \zeta^2 \rangle = \sum_{p=-\infty}^{\infty} |C_p|^2 = \sum_{p=1}^{\infty} |2C_p|^2 \quad (7.8)$$

where  $\langle . \rangle$  is the expected value, or average, operator. In terms of the continuous energy spectrum  $E(f)$ , the surface elevation variance is given by

$$\langle \zeta^2 \rangle = \int_{-\infty}^{\infty} E(f) df = 2 \int_0^{\infty} E(f) df \quad (7.9)$$

The relation between the complex amplitude and the energy density spectrum can be found from (7.8) and (7.9)

$$E(f)|_{f=f_p} \Delta f = |C_p|^2, \quad p : [-\infty, \infty] \quad (7.10)$$

or

$$E(f)|_{f=f_p} \Delta f = 2 |C_p|^2, \quad p > 0 \quad (7.11)$$

The evolution equation of the discrete spectral energy  $E_p = \langle C_p C_p^* \rangle$  can be obtained as follows. Multiplying equation (7.3) with the conjugate amplitude  $C_p^*$ , the conjugate of equation (7.3) with the amplitude  $C_p$ , and adding the former to the latter, gives

$$\frac{d}{dx}(C_p C_p^*) = -i \sum_{m=-\infty}^{\infty} R_{(m,p-m)} [C_m C_{p-m} C_p^* - C_m^* C_{p-m}^* C_p] \quad (7.12)$$

Using the fact that the second term between the brackets is the complex conjugate of the first term, equation (7.12) becomes

$$\frac{d}{dx}(C_p C_p^*) = 2 \sum_{m=-\infty}^{\infty} R_{(m,p-m)} \text{Im} [C_m C_{p-m} C_p^*] \quad (7.13)$$

The evolution equation of the energy spectrum can be obtained by taking the statistical average of equation (7.13).

$$\frac{dE_p}{dx} = 2 \sum_{m=-\infty}^{\infty} R_{(m,p-m)} \text{Im} [B_{m,p-m}] \quad (7.14)$$

in which  $E_p = \langle C_p C_p^* \rangle$  is the energy spectrum, and  $B_{m,p-m} = \langle C_m C_{p-m} C_p^* \rangle$  is the bispectrum (described in detail in chapter 3). The right-hand-side represents the average effect of triad wave interactions. Equation (7.14) can be rewritten to separate the sum and difference triad interactions as follows:

$$\frac{dE_p}{dx} = 2 \sum_{m=1}^{p-1} R_+ |B_{m,p-m}| \sin(\beta_{m,p-m}) - 4 \sum_{m=1}^{\infty} R_- |B_{m,p}| \sin(\beta_{m,p}) \quad (7.15)$$

Here  $\beta$  is the biphase and  $R_+$  and  $R_-$  are the interaction coefficients for the sum and difference interaction respectively. The first sum in the right-hand-side represents the triad sum interactions, the second the difference interactions.

### 7.4 Evolution equation for the bispectrum

This section deals with a closure hypothesis for the evolution of the bispectrum, which is needed for the integration of (7.15). The approach is aimed at a computationally efficient formulation. This is achieved by parametrizing the complete expressions. This refers both to a lumped representation of the theoretical energy exchange due to triad interactions (as opposed to a frequency-distributed function) and to a parametrization of biphases based on observations.

An evolution equation for the bispectrum  $B_{n,q} = \langle C_n C_q C_p^* \rangle$ , where  $p = n + q$ , can be obtained as follows.

$$\frac{d}{dx} B_{n,q} = \langle C_n C_q \frac{dC_p^*}{dx} \rangle + \langle C_n C_p^* \frac{dC_q}{dx} \rangle + \langle C_q C_p^* \frac{dC_n}{dx} \rangle \quad (7.16)$$

Substitution of equation (7.3) for  $dC/dx$  in equation (7.16) yields the following evolution equation for the bispectrum due to quadratic couplings

$$\begin{aligned} \frac{d}{dx} B_{n,q} = & i(k_p - k_n - k_q) B_{n,q} \\ & + i \sum_{m=-\infty}^{\infty} \left[ R_{(m,p-m)} T_{n,q,-p} - R_{(m,q-m)} T_{n,-p,q} - R_{(m,n-m)} T_{q,-p,n} \right] \end{aligned} \quad (7.17)$$

Here  $T_{n,q,-p} = \langle C_n C_q C_m^* C_{p-m}^* \rangle$ , the fourth-order average amplitude product or the so-called trispectrum. The zero-fourth-order-cumulants hypothesis permits the fourth-order averages to be expressed in terms of second-order averages, retaining only products of terms with opposite-signed phases. Since the subscripts  $p$ ,  $n$ , and  $q$  denote dummy variables of summation, they can be interchanged and after some algebraic manipulations and simplifications we get

$$\frac{d}{dx} B_{m,p-m} = i(k_p - k_m - k_{p-m}) B_{m,p-m} + 2i R_{(m,p-m)} N_{p,m,p-m} \quad (7.18)$$

where

$$N_{l,m,n} = E_m E_n - E_l E_m - E_l E_n \quad (7.19)$$

To determine the bispectrum, we need to spatially integrate equation (7.18). The procedure here is similar to the one used in the derivation of the Zakharov equation, presented in chapter 5. We assume that the third-order average is initially zero and we neglect the space dependence of  $E_p$ , i.e., set the second term on the right-hand-side equal to constant. Integrating (7.18) from 0 to  $x$ , we then obtain

$$B_{m,p-m} = 2i R_{(m,p-m)} N_{p,m,p-m} \left[ \frac{\exp[-i(\psi_p - \psi_m - \psi_{p-m})] - 1}{-i(k_p - k_m - k_{p-m})} \right] \quad (7.20)$$

This expression for the bispectrum is similar to that given in chapter 5 by equation (5.42), except that the present expression is obtained for the spatially varying amplitudes rather than the temporally varying amplitudes. The term between brackets contains two kinds of contributions. First a fast oscillating function; its contribution vanishes after summing over the spectrum in (7.15) due the phase-mixing effect. Second, a term representing a steady contribution. Thus after neglecting the contribution of the fast oscillating function the evolution equation of the discrete spectral energy  $E_p$  can be obtained by substituting the absolute value of the bispectrum in (7.15):

$$\begin{aligned} \frac{dE_p}{dx} = & 4 \sum_{m=1}^{p-1} \frac{R_+^2}{k_p - k_m - k_{p-m}} N_{p,m,p-m} \sin(\beta_{m,p-m}) \\ & - 8 \sum_{m=1}^{\infty} \frac{R_-^2}{k_{p+m} - k_m - k_p} N_{p+m,m,p} \sin(\beta_{m,p}) \end{aligned} \quad (7.21)$$

For application in the case of a continuous energy density spectrum  $E(f)$ , the discrete energy  $E_p$  in (7.21) can be replaced by  $E(f)\Delta f$ . The evolution equation of spectral energy density becomes

$$\begin{aligned} \frac{dE(f)}{dx} \Big|_{f=f_p} = & 4 \sum_{m=1}^{p-1} \left[ \frac{\Delta f}{k_p - k_m - k_{p-m}} \right] R_+^2 \dot{N}_{p,m,p-m} \sin(\beta_{m,p-m}) \\ & - 8 \sum_{m=1}^{\infty} \left[ \frac{\Delta f}{k_{m+p} - k_m - k_p} \right] R_-^2 \dot{N}_{p+m,p} \sin(\beta_{m,p}) \end{aligned} \quad (7.22)$$

Here  $\dot{N}_{l,m,n}$  has the same form as in (7.19) except that it is expressed in terms of the energy density  $E(f)$ .

To reduce the computational effort we introduce an approximation which consists of lumping the contributions to the sums in the right-hand-side of (7.22). Both sums are the discrete representation of a convolution integral over the spectrum, i.e.,  $\int \dots df = \sum \dots \Delta f$ , in which  $\dots$  is the integrand and  $\Delta f$  is an arbitrary (infinitesimal) discretization value. This interaction integral (or sum) is approximated by replacing it with the product of a representative value of the integrand, for which we take the value corresponding to the self-interactions ( $m=p/2$  in the first summation and  $m=p$  in the second summation), and an effective interaction bandwidth  $\delta f$ . This gives

$$\begin{aligned} \frac{dE(f)}{dx} \Big|_{f=f_p} = & 4 \left[ \frac{\delta f}{k_p - 2k_{p/2}} \right] R_{p/2,p/2}^2 \dot{N}_{p,p/2,p/2} \sin(\beta_{p/2,p/2}) \\ & - 8 \left[ \frac{\delta f}{k_{2p} - 2k_p} \right] R_{p,p}^2 \dot{N}_{2p,p,p} \sin(\beta_{p,p}) \end{aligned} \quad (7.23)$$

We now assume that the effective interaction bandwidth  $\delta f$  and the wavenumber mismatch in (7.23) scale with  $f_p$  and  $k_p$  respectively, or that the ratio between brackets scales with the phase speed  $c_p$ , and obtain

$$\begin{aligned} \frac{dE(f)}{dx} \Big|_{f=f_p} = & \alpha c_p R_+^2 \sin |\beta_{p/2,p/2}| [E^2(f_{p/2}) - 2E(f_p)E(f_{p/2})] \\ & - 2\alpha c_{2p} R_-^2 \sin |\beta_{p,p}| [E^2(f_p) - 2E(f_{2p})E(f_p)] \end{aligned} \quad (7.24)$$

in which  $\alpha$  is a tuning parameter.

For application in an energy balance equation, the spatial variation of the energy flux  $c_g(f)E(f)$  due to triad interactions, the so-called triad source term  $S_{ml}$  is needed, which can be obtained by multiplying (7.24) with the corresponding group velocity.

The expression (7.24) for the evolution of the spectral energy density due to the self interaction has two contributions. The first represents a positive contribution of the self interaction at frequency  $f_{p/2}$  (contributing to  $E(f_p)$ ). The second represents a negative contribution of the self interaction at frequency  $f_p$  (taking away from  $E(f_p)$ ). Notice that the positive contribution to  $E(f_p)$  equals one-half the negative one from  $E(f_{p/2})$ . This fact can be used to reduce the computations. Thus the net source term due to triad interactions can be expressed as follows

$$\begin{aligned} S_{ml}(f_p) &= S_{ml}^+(f_p) + S_{ml}^-(f_p) \\ S_{ml}^+(f_p) &= \alpha c_p c_{g,p} R_{(p/2,p/2)}^2 \sin |\beta_{p/2,p/2}| [E^2(f_{p/2}) - 2E(f_p)E(f_{p/2})] \\ S_{ml}^-(f_p) &= -2S_{ml}^+(f_{2p}) \end{aligned} \quad (7.25)$$

The biphase  $\beta$  is given by equation (3.19) in terms of Ursell number. The Ursell number is computed according to (3.18), in which the mean wave period  $T_m$  is used to allow for the influence of harmonic generation. The interaction coefficient  $R$  is taken from the evolution equation of Boussinesq model (chapter 4). For the self interaction it can be expressed as

$$R_{p/2,p/2} = \frac{k_{p/2}^2 (gh + 2c_{p/2}^2)}{k_p h (gh + \frac{2}{15}gh^3k_p^2 - \frac{2}{5}\omega_p^2h^2)} \quad (7.26)$$

Note that  $S_{ml}^+$  represents the positive contribution to the first harmonic, and thus it should not be allowed to be negative. Negative values for  $S_{ml}^+$  are set to zero.

This closes the formulation for the evolution of the energy density due to triad interactions. The expression given by (7.25) is hereafter referred to as the *Lumped Triad Approximation (LTA)*. It has the advantage of considerably reducing the computational effort needed to simulate the generation of high-frequency energy in energy-based wave models compared with the complete expression.

## 7.5 Model to data comparisons

### 7.5.1 Evolution model

Assessment of the triad parametrization presented in this chapter requires verification with observations. Various observations that manifest harmonic generation have been used throughout this study and will be used here to verify the present triad parametrization.

For numerical simulation of the experiments, we need to develop a spatial evolution model for the energy spectrum with a source/sink term representing the effect of triad wave interactions. Since the experiments used here are for a unidirectional wavefield, a one-dimensional evolution model is required for the simulations.

For one-dimensional propagation in  $x$ -direction and steady state solution ( $t$ -independent), the simplified energy balance equation is

$$\frac{\partial}{\partial x} [c_g(f) E(f)] = S \quad (7.27)$$

Here  $E(f)$  is the frequency energy density,  $c_g$  is the linear group velocity of frequency  $f$  and  $S$  is the net source/sink term representing the total effect of generation, dissipation and nonlinear cross-spectral energy transfers.



To examine the validity of the triad parametrization, numerical simulations have been performed for the evolution of the energy spectrum in shallow water. The LTA algorithm (7.25) has been implemented as a source term in the energy balance equation (7.27) to simulate the effect of triad wave interactions. A fourth-order Runge Kutta method is used to numerically integrate the energy balance equation.

### 7.5.2 Numerical simulations and comparisons

Numerical simulations for the evolution of the energy spectrum in shallow water have been carried out for different bottom topographies. The results of the LTA model have been compared against laboratory observations.

#### *Simulations over a submerged bar*

Measurements of Beji and Battjes (1993), already used in chapters 3 and 4, are used here to verify the LTA model for propagation of nonbreaking waves over a submerged bar. The still-water depth is 0.10 m over the bar crest and 0.40 m on either side of it. The upwave and downwave bottom slopes are 1:20 and 1:10 respectively. At the upwave boundary, a narrow-banded spectrum is used with peak frequency  $f_p = 0.5$  Hz and significant wave height  $H_s = 0.020$  m. Comparisons between the measured spectra and those computed by the LTA model are given in Fig. 7.1. The computations are performed using different values of the tuning parameter  $\alpha$ . The results show energy transfers from the primary spectral peak into the harmonics. Results with  $\alpha = 1$  are in reasonable agreement with the observed spectra.

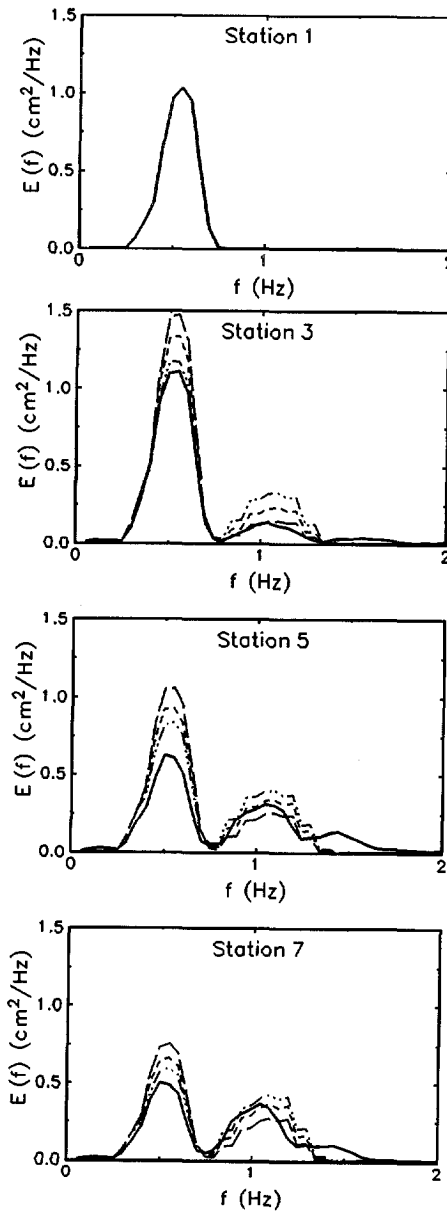


**Figure 7.1** *Energy spectra for waves propagating over a bar; experiments (solid lines) and LTA model:  $\alpha=0.25$  (long-dashed lines);  $\alpha=0.50$  (short-dashed lines);  $\alpha=1.00$  (dot-dashed lines).*

*Simulations over a beach profile*

The large scale laboratory measurements reported by Arcilla et al. (1994) for random wave propagation over a barred beach (described in detail in chapter 3) are used to verify the LTA model for breaking waves. Here the effects of wave breaking are included using the spectral energy source term described in chapter 4 and given by equation (4.45).

At the upwave boundary, a narrow-banded spectrum is used with peak frequency  $f_p=0.125$  Hz and significant wave height  $H_s=0.58$  m. The bottom profile and measurement locations are indicated in Fig. 3.1 (chapter 3).

Comparisons between the observed spectra and those computed by the LTA model are given in Fig. 7.2. The results show that the LTA is capable of transferring energy from the primary spectral peak into the harmonics. The energy dissipation due to wave breaking is well simulated.

The numerical simulations were done on a 486-DX2 personal computer with 66 MHz processor. In the numerical discretization, the frequency resolution is 0.01 Hz (60 frequencies in the range 0.01-0.60 Hz), and the spatial resolution is 0.5 m (269 steps in the range 20-154 m). The CPU time required for the complete simulation (over the bottom profile) of a single case (fixed  $\alpha$ ) using the LTA model is 13 s. However, using the complete deterministic spectral Boussinesq model given in chapter 4, the calculation of the energy spectrum from an average over 20 realizations with different initial sets of random phases takes about 2400 s.

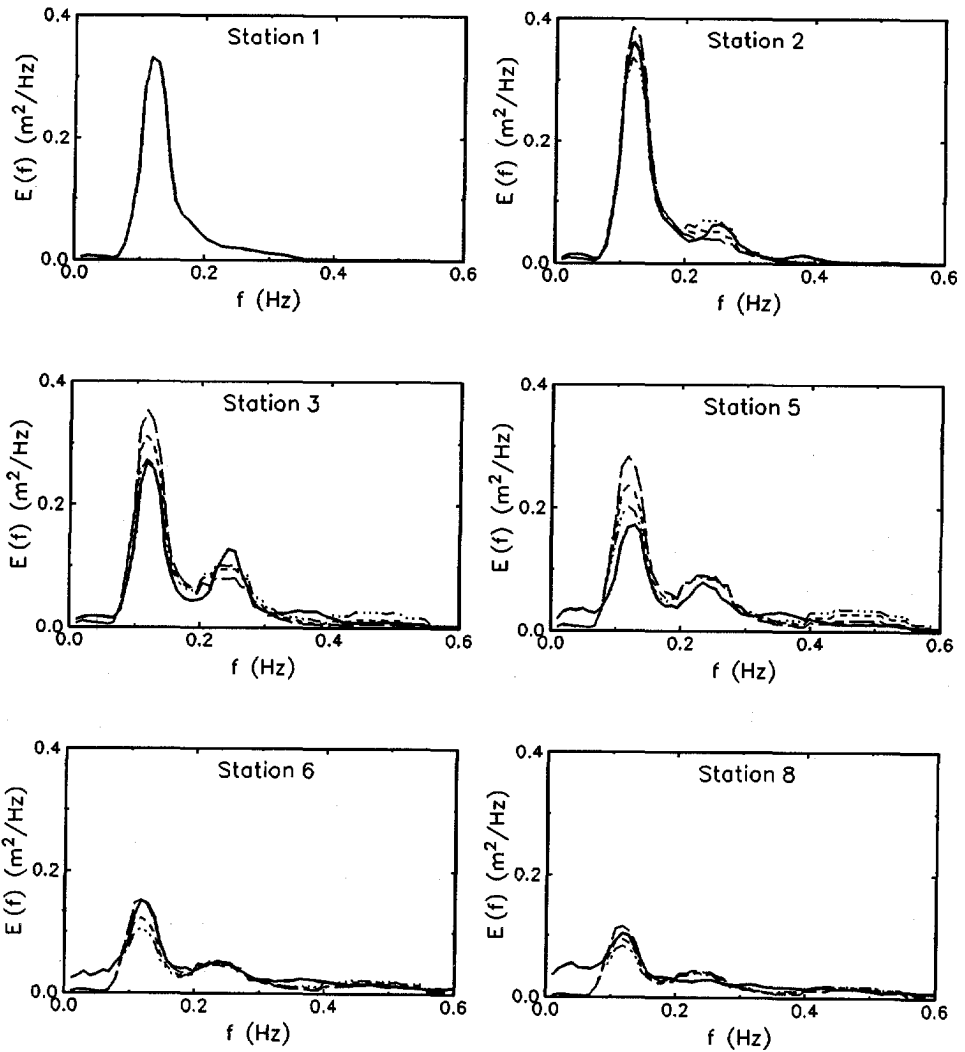


**Figure 7.2** Energy spectra for waves propagating over a beach profile; experiments (solid lines) and LTA model:  $\alpha=0.25$  (long-dashed lines);  $\alpha=0.50$  (short-dashed lines);  $\alpha=1.00$  (dot-dashed lines) .

*Simulations over a horizontal bottom*

The long-term evolution of the wave spectrum in shallow water, computed with the LTA model, is investigated here. To this end, the long-distance propagation of random waves is computed over a horizontal bottom. A narrowband spectrum with peak frequency  $f_p = 0.5$  Hz and significant wave height  $H_s = 0.02$  m is used as initial value. A constant water depth of 0.10 m is used in the simulation. The computation is carried out for nearly 10 wavelengths (20 m). The tuning parameter  $\alpha$  was set to 1. The computed spectra with the LTA are shown in Fig. 7.3.

Initially the results of the LTA model show energy transfers from the primary spectral peak into the first harmonics. The energy levels at the second peak increase up to a distance of about two wavelengths (station 3). Farther downwave the spectra do not evolve further. This implies that the LTA model has a self-stabilizing feature, which is considered a useful property in applications because it implies a certain robustness of the formulation.

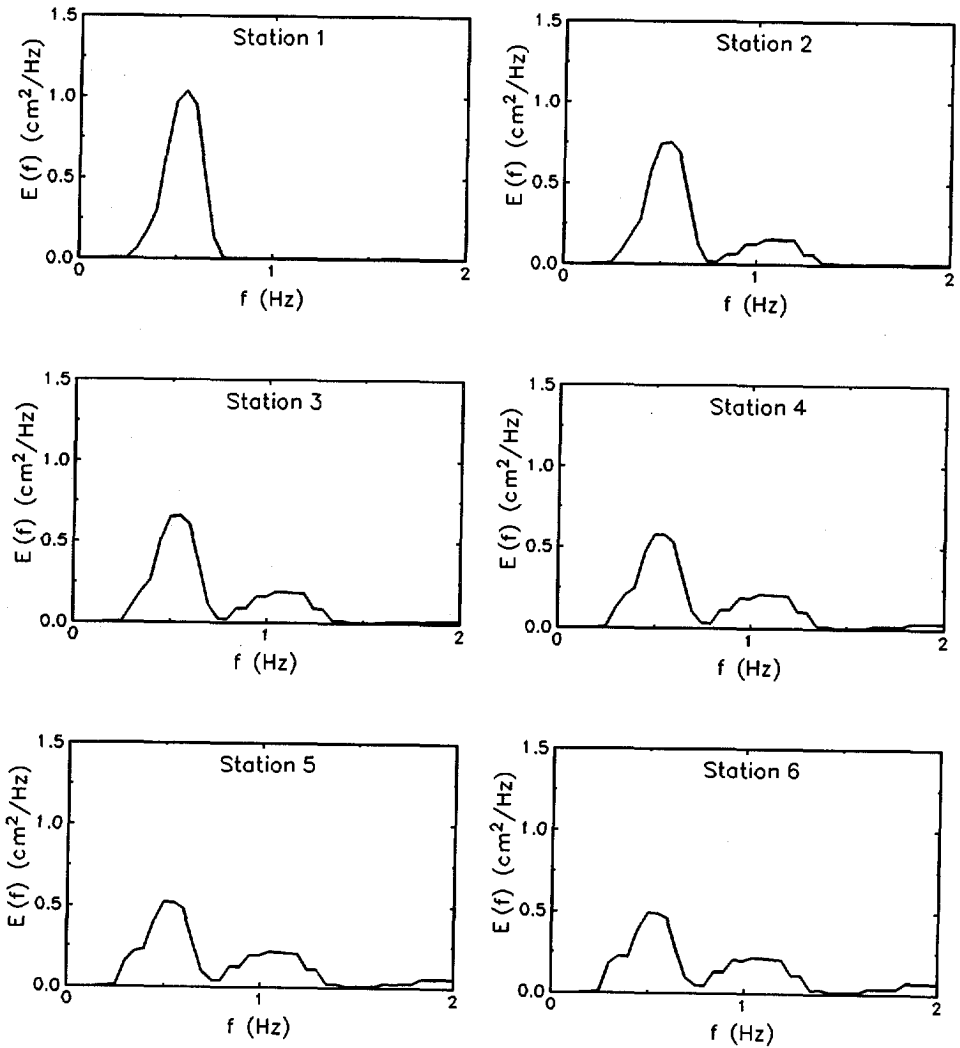


**Figure 7.3** Energy spectra computed with the LTA model with  $\alpha=1$  for waves over a horizontal bottom. Station 1 at the boundary, station 2 at 1 wavelength, station 3 at 2 wavelengths, station 4 at 4 wavelengths, station 5 at 7 wavelengths, station 6 at 10 wavelengths.

## 7.6 Summary and conclusions

A parametrized approach to model the phase-average effect of triad wave interactions is presented. A spectral Boussinesq model is used to derive an energy formulation representing triad wave interactions in random waves, supplemented with an empirical parametrization for the biphase evolution and a lumped presentation of the interaction integral, in which the values of the integrand are scaled with those of the self-interactions. This *Lumpe Triad Approximation (LTA)* model is implemented in a one-dimensional energy balance equation to compute the evolution of the energy spectrum in shallow water. The model is computationally very efficient compared to deterministic models for harmonic generation.

Despite the crudeness of the approximations, the model results are encouraging compared with observations. Numerical simulations for nonlinear shoaling of random waves with and without breaking have shown the ability of the LTA model to simulate the effect of triad wave interactions and the consequent energy transfers to higher harmonics. Additional numerical simulation for long-distance propagation of random waves over a horizontal bottom has shown that the LTA model has a self-stabilizing feature.

The applicability of the LTA model in wind wave models for coastal regions needs further investigation through comparisons with field observations.





## Chapter 8

### 8. Conclusions and recommendations

#### 8.1 General

This study was undertaken with the aim of increasing the knowledge of the nonlinear dynamics in the transformation of wave spectra in the shallow nearshore region, and developing modeling capabilities for these processes.

Observations of shoaling wavefields indicate that waves evolve from a slightly peaked, nearly sinusoidal shape in deep water to a shape characterized by sharp crests, flat troughs and relatively steep shoreward faces. These profile distortions, that occur just before wave breaking, are typical manifestation of the nonlinear effects in the nearshore region. These nonlinear effects together with dissipation of wave energy by breaking represent the dominant physical mechanisms in the evolution of waves in the nearshore. The influence of these transformations on the wave spectrum is considered in this study from both physical and modeling point of view.

Observations of shallow-water waves have been extensively analyzed using bispectral analyses. It has long been established that the bispectrum can be used to examine nonlinearity in shoaling waves. Nonlinear couplings between spectral wave components have been investigated in shoaling breaking waves and in waves passing over a shallow bar.

In the present study, nonlinear shallow-water waves are modeled using two spectral approaches, namely a deterministic, phase-resolving approach and a statistical, phase-averaged approach. In the phase resolving approach, Boussinesq equations are used to establish evolution equations for the wave amplitudes and phases simulating harmonic generation. For computational

efficiency in case of random wave propagation in extensive areas, the phase-averaged approach is preferred, in which the average effect of triad wave interactions is modeled using a statistical description.

The main conclusions of this study are summarized below. Distinctions are made between various approaches used during the course of this study. Suggestions for future research are finally given.

## 8.2 Bispectral analysis

Bispectral analysis is used to elucidate aspects of nonlinear dynamics of shallow-water waves. Analyses of laboratory observations of nonlinear shoaling and breaking waves over a beach profile as well as over a shallow bar have yielded the following conclusions:

- Harmonic generation in shallow water is ascribed to nonlinear triad wave interactions. The generation of the second spectral peak results from the sum interactions between pairs of waves at the primary spectral peak. On the other hand the generation of the low-frequency waves is due to the difference interactions between pairs of waves at the primary spectral peak.
- Wave breaking tends to weaken the strength of the nonlinear couplings between various wave components. It is found that the intensity of the bispectral levels are reduced in regions of strong wave breaking as well as the skewness and asymmetry values.
- In the initial shoaling region, weak nonlinearity leads to increase in the skewness-values only but not in those of the asymmetry, whereas strong nonlinearity in the region just before wave breaking leads to a significant increase in the asymmetry-values.
- The biphasic evolution in shallow water can be crudely parametrized in terms of Ursell number. A simple algebraic relation is formulated, expressing a gradual variation of zero biphasic for  $Ur < 0.1$  (deep water) to a limit value of  $-\pi/2$  in very shallow water ( $Ur \sim 10$ ).
- Nonlinear couplings induced by a bar region in a random wavefield vanish in the deepening region beyond the bar due to decreasing nonlinearity. There is

no memory of phase locks which existed over the bar. The wavefield on the downwave side is statistically homogeneous and can be fully described by the energy density spectrum, without the need for additional, site-dependent phase information.

Standard models for forecasting or hindcasting of random waves are based on phase-averaged energy formulations. In principle a nonlinear phase-resolving (Boussinesq) model can be used locally, e.g. in a bar region, the results of which can be phase-averaged afterwards to estimate energy spectra with which the computations can proceed using a phase-averaged (energy balance) model. The preceding result imply that these models are suitable also on the downwave side of a shallow (bar) region with significant harmonic generation.

### **8.3 Deterministic modeling of nonlinear shallow-water waves**

Deterministic evolution equations for the slowly varying complex Fourier amplitudes, based on a Boussinesq model with improved dispersion characteristics, are used to describe the evolution of nonlinear shallow-water waves. The Boussinesq evolution equations are extended into the surf zone by incorporating the effect of energy dissipation due to depth induced wave breaking. The model is validated using laboratory observations of nonlinear shoaling and breaking waves. The following conclusions can be drawn:

- The Boussinesq evolution equations with improved dispersion characteristics are able to describe harmonic generation in shallow-water waves. The phase mismatch between spectral wave components is of utmost importance for the description of this phenomenon.
- The model predicts nonlinear correction to the phase speeds of various wave components due to nonlinear interactions, leading to virtually nondispersive propagation in shallow water despite the presence of (weak) frequency dispersion.
- Energy dissipation due to depth-induced wave breaking is formulated in a spectral form, both for energy-density models and complex amplitude models, based on the total rate of energy dissipation by breaking. Based on previous

observations, the spectral dissipation term is chosen such that it reduces the total (spectrally integrated) energy without affecting the spectral shape.

- The Boussinesq evolution equations for random breaking waves have yielded realistic predictions of the spectral evolution in the shoaling region and inside the surf zone. This validation supports previous observational results in which wave breaking dissipation appeared to be proportional to the spectral energy level, without other dependence on the frequency.
- The model results are also compared to measured surface elevation for breaking waves. The model is found to yield realistic predictions of the wave profile in the shoaling region and the outer surf zone. The model-data comparisons do not support the need of a phase shift induced by breaking.
- The nonlinearly generated low-frequency waves are significantly damped in the surf zone. The model proposed here for the higher-frequency range seems to predict the low-frequency energy reasonably well in comparison with experimental results, but that may be fortuitous. This problem deserves further study.

#### 8.4 Statistical modeling of nonlinear shallow-water waves

Two approaches have been used in this study to model the average effect of triad wave interactions. The first approach is based on the Zakharov kinetic equation for resonant triad interactions, supplemented with a modification to the frequency mismatch term (Holloway, 1982; 1986). A narrow frequency filter is used to allow for off-resonant energetic triad interactions. In Holloway (1982), the filter bandwidth is taken as a prognostic variable. Here, as suggested by Polnikov (1995), we take it as a constant to be determined empirically.

The interaction integral is calculated to examine the nonlinear rate (NLR) of energy transfers in a Jonswap-type spectrum. The following conclusions can be drawn:

- The nonlinear rate of transfer (NLR) has the property of transferring energy from the primary spectral region toward the higher harmonics.

- The magnitude of NLR increases by decreasing the relative depth  $kh$  and increasing the value of the filter bandwidth  $\Omega$ .
- In case of a directionally bimodal spectrum, the NLR results in secondary peaks that are directionally aligned with the primary peaks due to colinear interactions. The NLR does not show the expected peak at the vector sum of the primary peaks that are observed experimentally (Nwogu, 1994).

The interaction integral has been cast in an energy source/sink term and implemented in the energy balance equation that describes the evolution of a unidirectional energy density spectrum in shoaling regions. The evolution model is verified using observations of waves propagating over a shallow bar as well as over a beach profile. The following conclusions can be drawn:

- The intensity of energy transfers and the consequent generation of higher harmonics are dependent on the chosen value for the frequency broadening parameter. A constant value for the frequency broadening parameter results in unguaranteed spectral evolution.
- The model produces a second spectral peak in the frequency energy spectrum at frequencies less than the first harmonic  $2f_p$  (the second spectral peak appears at the first harmonic in wavenumber spectrum). This is ascribed to the fact that in the present formulation space periodicity is assumed in expanding the canonical variables, resulting in a formulation in wavenumber space.
- The present formulation is not energy conserving, implying that the net nonlinear rate of energy transfers (integrated over the spectrum) departs from zero. Such effect is a problem in describing the evolution of the energy spectrum.
- An *ad hoc* approach is suggested to remedy the present formulation to ensure energy conservation, in which the total energy loss or gain resulting from the original NLR is used to proportionally rescale the negative or positive lobe respectively of the transfer function.

The second approach to model the phase-averaged effect of triad wave interactions is aimed at a computationally efficient algorithm. It is based on an energy formulation derived from the Boussinesq evolution equations supplemented with an empirical parametrization of the biphase evolution and a

lumped presentation of the interaction integral, of which the intensities are scaled with those of the self-interactions. Despite the crudeness of the approximations, this *Lumped Triad Approximation* (LTA) model provides realistic estimates for the spectral evolution in shallow water at low cost.

The LTA model can be applied to two-dimensional problems if the interactions are assumed to be colinear, i.e., directionally decoupled. Colinear interactions result in energy exchanges only among wave components that propagate in the same direction. In this approximation, the nonlinear interactions among various frequency components along each direction can be treated independently from the other directional components.

### 8.5 Recommendations for future research

For future research the following suggestions are made:

- The applicability of the LTA in random-wave models for coastal regions needs further investigation through comparisons with field observations. The present formulation is essentially one-dimensional and can be applied to two-dimensional problem accounting only for the colinear interactions. In principle the parametrization of the biphase can be used with two-dimensional deterministic evolution equations to obtain a two-dimensional energy formulation for the effect of triad wave interactions.
- If the filter bandwidth, in the triad formulation based on the Zakharov kinetic equation is taken as a constant the result is energy attenuation and unguaranteed spectral evolution. We suggest to use the filter bandwidth  $\Omega$  as a prognostic variable. Its value should be related to the rate of growth of individual harmonics as in Holloway (1982).
- In deriving the triad formulation based on the Zakharov kinetic equation, the waves are assumed to be periodic in space. This assumption is violated in the nearshore, in which the waves are rapidly varying in space. A formulation in

---

which time-periodicity is assumed rather than the spatial periodicity is desired.

- In describing the nonlinear triad wave interactions in shallow water, we focussed on the transition from the deterministic description in terms of amplitude and phase to a statistical one in terms of the energy density spectrum, for reasons of computational efficiency. Future research is required to infer the third-order nonlinear statistics of the wavefield such as the skewness and asymmetry from the energy spectrum.





## References

- Abreu, M., A. Larraza, and E.B. Thornton, 1992, Nonlinear transformation of directional wave spectra in shallow water, *J. Geophys. Res.*, 97, pp. 15579-15589.
- Agnon, Y., A. Sheremet, J. Gonsalves, and M. Stiassnie, 1993, Nonlinear evolution of a unidirectional shoaling wave field, *Coastal Eng.*, 20, pp. 29-58.
- Arcilla, A.S., J.A. Roelvink, B.A. O'Connor, A.J.H.M. Reniers, and J.A. Jimenez, 1994, The Delta flume '93 experiment, *Proc. Coastal Dynamics Conf. '94*, Barcelona, Spain, pp. 488-502.
- Armstrong, J.A., N. Bloembergen, J. Ducuing, and P.S. Pershan, 1962, Interactions between light waves in a nonlinear dielectric, *Phys. Rev.*, 127, pp. 1918-1939.
- Banner, M.L., and O.M. Phillips, 1974, On small scale breaking waves, *J. Fluid Mech.*, 65, pp. 647-657.
- Battjes, J.A., and J.P.F.M. Janssen, 1978, Energy loss and set-up due to breaking of random waves, *Proc. Coastal Eng. Conf.*, 16th, pp. 569-587.
- Battjes, J.A., and M.J.F. Stive, 1985, Calibration and verification of a dissipation model for random breaking waves, *J. Geophys. Res.*, 90(C5), pp. 9159-9167.
- Battjes, J.A., and S. Beji, 1992, Breaking waves propagating over a shoal, *Proc. Coastal Eng. Conf.*, 23rd, pp. 42-50.

- Beji, S., and J.A. Battjes, 1993, Experimental investigation of wave propagation over a bar, *Coastal Eng.*, 19, pp. 151-162.
- Beji, S., and J.A. Battjes, 1994, Numerical simulation of nonlinear waves propagating over a bar, *Coastal Eng.*, 23, pp. 1-16.
- Bosboom, J., 1995, Boussinesq modelling of wave-induced particle velocities, *Rep. H2056*, 71 pp., Delft Hydraulics, Delft, Netherlands.
- Boussinesq, J., 1872, Theory of waves and swell propagated in a long horizontal rectangular canal, and imparting to the liquid contained in this canal approximately equal velocities from the surface to the bottom, *J. de Mathematiques Pures et Appliquees*, 17.
- Bryant, P.J., 1973, Periodic waves in shallow water, *J. Fluid Mech.*, 59, pp. 457-480.
- Büsching, F., 1978, Anomalous dispersion of Fourier components of surface gravity wave records, *Proc. Coastal Eng. Conf.*, 16th, pp. 247-267.
- Byrne, R.J., 1969, Field occurrences of induced multiple gravity waves, *J. Geophys. Res.*, 74(10), pp. 2590- 2596.
- Dally, W.R., R.G. Dean, and R.A. Dalrymple, 1985, Wave height variation across beaches of arbitrary profile, *J. Geophys. Res.*, 90(C6), pp. 11917-11927.
- Dattatri, J., H. Raman, and N. Jothi Shankar, 1978, Performance characteristics of submerged breakwaters, *Proc Coastal Eng. Conf.*, 16th, pp. 2153-2171.

- Dingemans, M.W., 1989, Shift in characteristics wave frequency; some spectra in wave basin and in Haringvliet region, *Tech. Rep. Part II*, 56 pp., Delft Hydraulics, Delft, Netherlands.
- Doering, J.R.C., and A.J. Bowen, 1995, Parametrization of orbital velocity asymmetries of shoaling and breaking waves using bispectral analysis, *Coastal Eng.*, 26, pp. 15-33.
- Eldeberky, Y., and J.A. Battjes, 1994a, Phase lock in waves passing over a bar. *Proc. Int. Sym. Waves-Physical and Numerical Modelling*, Vancouver, pp. 1086-1095.
- Eldeberky, Y., and J.A. Battjes, 1994b, Nonlinear coupling in waves passing over a bar, *Proc. Coastal Eng. Conf.*, 24th, pp. 157-167.
- Eldeberky, Y., 1995, Modelling triad wave interactions using a statistical description, *Int. Rep.*, 3-95, 19 pp., Delft University, Delft, Netherlands
- Eldeberky, Y., and J.A. Battjes, 1995, Parameterisation of triad interactions in wave energy models, *Proc. Coastal Dynamics Conf. '95.*, Gdansk, Poland, pp. 140-148.
- Eldeberky, Y., and J.A. Battjes, 1996, Spectral modeling of wave breaking: Application to Boussinesq equations, *J. Geophys. Res.*, 101(C1), pp. 1253-1264.
- Elgar, S., and R.T. Guza, 1985a, Shoaling gravity waves: comparisons between field observations, linear theory, and a nonlinear model, *J. Fluid Mech.*, 158, pp. 47-70.
- Elgar, S., and R.T. Guza, 1985b, Observations of bispectra of shoaling surface gravity waves, *J. Fluid Mech.*, 161, pp. 425-448.

- Elgar, S., and R.T. Guza, 1986, Nonlinear model predictions of bispectra of shoaling surface gravity waves, *J. Fluid Mech.*, 167, pp. 1-18.
- Elgar, S., M.H. Freilich, and R.T. Guza, 1990, Model-data comparisons of moments of nonbreaking shoaling surface gravity waves, *J. Geophys. Res.*, 95, pp. 16055-16063.
- Elgar, S., R.T. Guza, M.H. Freilich, and M.J. Briggs, 1992, Laboratory simulations of directionally spread shoaling waves, *J. Waterw. Port Coastal Ocean Div. Am. Soc. Civ. Eng.*, 118(1), pp. 87-103.
- Flick, R.E., R.T. Guza, and D.L. Inman, 1981, Elevation and velocity measurements of laboratory shoaling waves, *J. Geophys. Res.*, 86, pp. 4149-4160.
- Freilich, M.H., and R.T. Guza, 1984, Nonlinear effects on shoaling surface gravity waves, *Philos. Trans. R. Soc. London.*, A 311, pp. 1-41.
- Freilich, M.H., S. Elgar, and R.T. Guza, 1990, Observations of nonlinear effects in directional spectra of shoaling surface gravity waves, *J. Geophys. Res.*, 95, pp. 9645-9656.
- Hasselmann, K., 1962, On the non-linear energy transfer in a gravity wave spectrum, Part 1. General theory, *J. Fluid Mech.*, 12, pp. 481-500.
- Hasselmann, K., W. Munk, and G. McDonald, 1963, Bispectra of ocean waves, in *Time Series Analysis*, edited by M. Rosenblatt, pp. 125-139, Wiley, New York.
- Haubrich, R.A., 1965, Earth noises, 5 to 500 millicycles per second, *J. Geophys. Res.*, 70, pp. 1415-1427.

- Herbers, T.H.C., and R.T. Guza, 1992, Wind-wave nonlinearity observed at the sea floor. Part II. Wavenumbers and third order statistics, *J. Phys. Oceanogr.*, 22, pp. 489-504.
- Herbers, T.H.C., R.L. Lowe, and R.T. Guza, 1992, Field observations of orbital velocities and pressure in weakly nonlinear surface gravity waves, *J. Fluid Mech.*, 245, pp. 413-435.
- Holthuijsen, L.H., N. Booij, and R.C. Ris, 1993, A spectral wave model for the coastal zone, in *Ocean Wave Measurement and Analysis*, edited by O.T. Magoon and J.M. Hemsley, pp. 613-641, Am. Soc. Civ. Eng., New York.
- Huntley, D.A., and A.J. Bowen, 1975, Comparison of the hydrodynamics of steep and shallow beaches, *Proc. Symposium on nearshore sediment dynamics and sedimentation*, edited by J.R. Hails and A. Carr., Wiley, London, pp. 69-109.
- Johnson, J.W., R.A. Fuchs, and J.R. Morison, 1951, The damping action of submerged breakwaters, *Trans. Amer. Geophys. Union*, 32(5), pp. 704-718.
- Jolas, P., 1960, Passage de la houle sur un seuil, *Houille Blanche*, 2, pp. 148-152.
- Kaihatu, J.M., and J.T. Kirby, 1995, Nonlinear transformation of waves in finite water depth, *Phys. Fluids*, 7(8), pp. 1903-1914.
- Kim, Y.C., and E.J. Powers, 1979, Digital bispectral analysis and its application to the non-linear wave interactions, *IEEE Trans. on Plasma Sc.*, 1, pp. 120-131.

- Kim, Y.C., J.M. Beall, E.J. Powers, and R.W. Miksad, 1980, Bispectrum and nonlinear wave coupling., *Phys. Fluids*, 23, pp. 258-263.
- Kirby, J.T., J.M. Kaihatu, and H. Mase, 1992, Shoaling and breaking of random wave trains: Spectral approaches, *Proc. Eng. Mech. Div. Am. Soc. Civ. Eng. Specialty Conf.*, 9th, pp. 71-74.
- Kojima, H., T. Ijima, and A. Yoshida, 1990, Decomposition and interception of long waves by a submerged horizontal plate, *Proc. Coastal Eng. Conf.*, 22th, pp. 1228-1241.
- Komen, G.J., L. Cavaleri, M. Donelan, K. Hasselmann, S. Hasselmann, and P.A.E.M. Janssen, 1994, *Dynamics and modelling of ocean waves*, Cambridge University Press, London.
- Korteweg, D.J., and G. de Vries, 1895, On the change of form of long waves advancing in a rectangular canal and on a new type of long stationary waves, *Phil. Mag.*, 5, pp. 422-443.
- Liu P.L.-F., S.B. Yoon, and J.T. Kirby, 1985, Nonlinear refraction-diffraction of waves in shallow water, *J. Fluid Mech.*, 153, pp. 185-201.
- Liu, P.L.-F., 1990, Wave transformation, in *Ocean Engineering Science; The Sea*, vol. 9(A), edited by B. Le Méhauté and D.M. Hanes, pp. 27-63, John Wiley, New York.
- Longuet-Higgins, M.S., and N.D. Smith, 1966, An experiment on third-order resonant wave interactions, *J. Fluid Mech.*, 25, pp. 417-435.
- Longuet-Higgins, M.S., and R.W. Stewart, 1962, Radiation stress and mass transport in gravity waves, with application to "surf beats", *J. Fluid Mech.*, 13, pp. 481-504.

- Longuet-Higgins, M.S., and R.W. Stewart, 1964, Radiation stress in water waves; a physical discussion with applications, *Deep-Sea Res.*, 11, pp. 529-562.
- Luth, H.R., G. Klopman, and N. Kitou, 1993, Kinematics of waves breaking partially on an offshore bar, *Rep. H1573*, 13 pp., Delft Hydraulics, Delft, Netherlands.
- Madsen, P.A., R. Murray, and O.R. Sørensen, 1991, A new form of the Boussinesq equations with improved linear dispersion characteristics, *Coastal Eng.*, 15, pp. 371-388.
- Madsen, P.A., and O.R. Sørensen, 1992, A new form of the Boussinesq equations with improved linear dispersion characteristics. Part 2: a slowly-varying bathymetry, *Coastal Eng.*, 18, pp. 183-205.
- Madsen, P.A., and O.R. Sørensen, 1993, Bound waves and triad interactions in shallow water, *J. Ocean Engng.*, 20(4), pp. 359-388.
- Mase, H., and Y. Iwagaki, 1982, Wave height distribution and wave grouping in the surf zone, *Proc. Coastal Eng. Conf.*, 18th, pp. 58-76.
- Mase, H., and J.T. Kirby, 1992, Hybrid frequency-domain KdV equation for random wave transformation, *Proc. Coastal Eng. Conf.*, 23rd, pp. 474-487.
- Masuda, A., and Y. Kuo, 1981a, Note on the imaginary part of the bispectrum, *Deep-Sea Res.*, 28A, pp. 213-222.
- Masuda, A., and Y. Kuo, 1981b, Bispectra for the surface displacement of random gravity waves in deep water, *Deep-Sea Res.*, 28A, pp. 223-237.

- Mei, C.C., 1989, *The applied dynamics of ocean surface waves*, World Scientific, Singapore.
- Merckelbach, L.M., 1995, Boussinesq modelling with higher order dispersion; derivation and numerical modelling, *MSc. thesis*, Delft University of Technology, Delft, Netherlands.
- Monin, A.S. and A.M. Yaglom, 1979, *Statistical Fluid Mechanics: Mechanics of Turbulence*, 1, MIT Press, Cambridge.
- Newell, A.C., and P.J. Aucoin, 1971, Semidispersive wave systems, *J. Fluid Mech.*, 49(3), pp. 593-609.
- Nwogu, O., 1993, Alternative form of Boussinesq equations for nearshore wave propagation, *J. Waterw. Port Coastal Ocean Eng.* ASCE, 119(6), pp. 618-638.
- Nwogu, O., 1994, Nonlinear evolution of directional wave spectra in shallow water, *Proc. Coastal Eng. Conf*, 24th, pp. 467-481.
- Ochi, M.K., and W.C. Wang, 1984, Non-Gaussian characteristics of coastal waves, *Proc. Coastal Eng. Conf.*, 19th, pp. 516-531
- Peregrine, D.H., 1967, Long waves on a beach, *J. Fluid Mech*, 27, pp. 815-827.
- Phillips, O.M., 1960, On the dynamics of unsteady gravity waves of finite amplitude. Part 1, *J. Fluid Mech.*, 9, pp. 193-217.
- Phillips, O.M., 1967, Theoretical and experimental studies of gravity wave interactions, *Proc. R. Soc. Lond.*, A299., pp. 104-119.



- Polnikov, V., 1995, *personal communication*, while he was a visiting researcher at Delft University of Technology, Netherlands, Dec 1995.
- Resio, D.T., 1988, A steady-state wave model for coastal applications, *Proc. Coastal Eng. Conf.*, 21st, pp. 929-940.
- Rey, V., M. Belrous, and E. Guaselli, 1992, Propagation of surface gravity waves over a rectangular submerged bar, *J. Fluid Mech.*, 235, pp. 453-479.
- Roelvink, J.A., and A.J.H.M. Reniers, 1995, LIP 11D Delta Flume Experiments, *Rep. H2130*, 23 pp., Delft Hydraulics, Delft, Netherlands.
- Schäffer, H.A., R. Deigaard, and P.A. Madsen, 1993, A Boussinesq model for waves breaking in shallow water, *Coastal Eng.*, 20, pp. 185-202.
- Schäffer, H.A., and P.A. Madsen, 1995, Further enhancements of Boussinesq-type equations, *Coastal Eng.*, 26, pp. 1-14.
- Smith, J.M., and C.L. Vincent, 1992, Shoaling and decay of two wave trains on beach, *J. Waterw. Port Coastal Ocean Div. Am. Soc. Civ. Eng.*, 118(5), pp. 517-533.
- Stiassnie M., and L. Shemer, 1984, On modifications of the Zakharov equation for surface gravity waves, *J. Fluid Mech.*, 143, pp. 47-67.
- Svendsen, I.A., 1976, A direct derivation of the KdV equation for waves on a beach, and discussion of its implications, *Rep.*, 39, ISVA, Technical University of Denmark, Lyngby, Denmark.
- Thornton, E.B., and R.T. Guza, 1983, Transformation of wave height distribution, *J. Geophys. Res.*, 88(C10), pp. 5925-5938.

- Vincent, C.L., J.M. Smith, and J. Davis, 1994, Parameterization of wave breaking in models, *Proc. Int. Sym. Waves-Physical and Numerical Modelling*, pp. 753-762.
- WAM Development and Implementation Group (WAMDIG), 1988, The WAM model - A third generation ocean wave prediction model, *J. Phys. Oceanogr.*, 18, pp. 1775-1810.
- Witting, J.M., 1984, A unified model for the evolution of nonlinear water waves, *J. Comput. Phys.*, 56, pp. 203-236.
- Won, Y.S., and J.A. Battjes, 1992, Spectral Boussinesq modelling of random waves, in Communication on Hydraulic and Geotechnical Engineering, Rep. 93-2, 27 pp., Delft Univ. of Technol., Delft, Netherlands.
- Yefimov, V.V., Y.P. Solov'yev, and G.N. Khristoforov, 1972, Observational determination of the phase velocities of spectral components of wind waves, *Isv. Atmos. Oceanic Phys.*, 8, pp. 435-446.
- Yeh, T.T., and C.W. Van Atta, 1973, Spectral transfer of scales and velocity fields in heated grid turbulence, *J. Fluid Mech.*, 58, pp. 233-261.
- Young, I.R., 1989, Wave transformation over coral reefs, *J. Geophys Res.*, 94, pp. 9779-9789.
- Zakharov, V.E., 1968, Stability of periodic waves of finite amplitude on the surface of a deep water, Engl. trans. *Soviet Physics, J. Appl. Mech. Tech. Phys.*, 4, pp. 86-94.
- Zakharov, V.E., and V.G. Kharitonov, 1970, Instability of monochromatic waves on the surface of arbitrary depth, Engl. trans. *Soviet Physics, J. Appl. Mech. Tech. Phys.*, 11, pp. 747-751.

---

Zakharov, V.E., V.S. L'vov, and G. Falkovich, 1992, *Kolmogorov spectra of turbulence, I. Wave Turbulence*, Springer verlag.



## Curriculum Vitae

Yasser Eldeberky was born on June 12, 1964 in Cairo, Egypt. Graduated at the Faculty of Engineering at Ain Shams University of Cairo (major in Hydraulic Engineering) in 1987 with honour degree. In 1988 he has been appointed as a teaching assistant at the Department of Civil Engineering of Helwan University. In 1990-1991 attended postgraduate course in Coastal Engineering at the International Institute of Hydraulic and Environmental Engineering (IHE) in Delft, The Netherlands and obtained the Diploma of Hydraulic Engineering (Dip HE Delft) with Distinction. In May 1992 obtained Master of Science degree with Distinction at IHE. His MSc-thesis entitled '*Introduction of Wedge Diffraction to a Mathematical Model for Wave Propagation in Harbours*'

From January 1993 until September 1996 he worked as a Research Fellow at the Faculty of Civil Engineering of the Delft University of Technology in Delft, The Netherlands, where he carried out his doctoral research in the subject '*Nonlinear Transformation of Wave Spectra in the Nearshore Zone*'

Presently he works as a Postdoctoral Researcher at the International Research Centre for Computational Hydrodynamics (ICCH), Danish Hydraulic Institute (DHI) in Hørsholm, Denmark. He has published several articles in scientific journals and conference proceedings, and gave presentations in several international conferences, seminars and colloquiums.

### List of Publications

#### *Papers in Scientific Journals and Refereed Conferences*

- [1] Battjes, J.A., Y. Eldeberky, Y.S. Won, 1993, Spectral Boussinesq modelling of breaking waves, in *Ocean Wave Measurements and Analysis*, edited by O.T. Magoon and J.M. Hemsley, pp. 813-820, Am. Soc. Civ. Eng., New York.

- [2] Eldeberky, Y., and J.A. Battjes, 1994, Phase lock in waves passing over a bar, *Proc. Int. Sym. Waves-Physical and Numerical Modelling*, Vancouver, pp. 1086-1095.
- [3] Holthuijsen, L.H., J.G. de Ronde, Y. Eldeberky, H.L. Tolman, N. Booij, E. Bouws, P.G.P. Ferier, and J. Andorka Gal, 1994, Modelling extreme wave conditions in the southern North Sea, *Proc. Int. Sym. Waves-Physical and Numerical Modelling*, Vancouver, pp. 694-703.
- [4] Eldeberky, Y., and J.A. Battjes, 1994, Nonlinear coupling in waves passing over a bar, *Proc. Coastal Eng. Conf.*, 24th, pp. 157-167.
- [5] Holthuijsen, L.H., J.G. de Ronde, Y. Eldeberky, H.L. Tolman, N. Booij, E. Bouws, P.G.P. Ferier, and J. Andorka Gal, 1994, The maximum significant wave height in the southern North Sea, *Proc. Coastal Eng. Conf.*, 24th, pp. 261-271.
- [6] Eldeberky, Y., and J.A. Battjes, 1995, Parameterisation of triad interactions in wave energy models, *Proc. Coastal Dynamics Conf. '95.*, Gdansk, Poland, pp. 140-148.
- [7] Eldeberky, Y., and J.A. Battjes, 1996, Spectral modeling of wave breaking: Application to Boussinesq equations, *J. Geophys. Res.*, 101(C1), pp. 1253-1264.
- [8] Eldeberky, Y., and J.A. Battjes, 1996, Formulation for harmonic generation in coastal wave energy models, Presented at *8th International Biennial Conference on Physics of Estuaries and Coastal Seas*, The Hague, Netherlands.
- [9] Eldeberky, Y., and J.A. Battjes, 1996, Parameterized energy formulation for triad wave interactions, In preparation for *J. Geophys. Res.*

- 
- [10] Eldeberky, Y., V. Polnikov and J.A. Battjes, 1996, A phase-averaged model for triad interactions in dispersive waves, In *Proc. 25th Coastal Eng. Conf.*, Orlando, USA.

### *Reports*

- [1] Eldeberky, Y., 1992, Introduction of Wedge Diffraction to a Mathematical Model for Wave Propagation in Harbours, *MSc-thesis*, International Institute of Hydraulic and Environmental Engineering (IHE), Delft, The Netherlands.
- [2] Dekker, J., N. Booij, Y. Eldeberky, and J. Andorka Gal, 1993, Wave Conditions along the Dutch Coast, *Technical Report*, H1355, Delft Hydraulics, The Netherlands.
- [3] Holthuijsen, L.H., Y. Eldeberky, N. Booij and P.G.P Ferier, 1995, The Maximum Significant Wave Height in the Southern North Sea, *Technical Report*, 14-94, Delft University of Technology, The Netherlands.
- [4] Eldeberky, Y., 1995, Modelling Triad Wave Interactions using a Statistical Description, *Technical Report*, 14-94, Delft University of Technology, The Netherlands.
- [5] Eldeberky, Y., 1996, Nonlinear Transformation of Wave Spectra in the Nearshore Zone, *Communications on Hydraulic and Geotechnical Engineering* ISSN 0169-6548, Report no. 96-4 , Delft University of Technology, The Netherlands.